uOttawa

L'Université canadienne
Canada's university

FACULTÉ DES ÉTUDES SUPÉRIEURES ET POSTOCTORALES

uOttawa

L'Université canadienne
Canada's university

FACULTY OF GRADUATE AND POSDOCTORAL STUDIES

Christopher Smelser

AUTEUR DE LA THÈSE / AUTHOR OF THESIS

Ph.D. (Physics)

GRADE / DEGREE

Department of Physics

FACULTÉ, ÉCOLE, DÉPARTEMENT / FACULTY, SCHOOL, DEPARTMENT

Ultrafast Infrared Laser Fabrication of Fiber Bragg Gratings with a Phase Mask

TITRE DE LA THÈSE / TITLE OF THESIS

Stephen Mihailov

DIRECTEUR (DIRECTRICE) DE LA THÈSE / THESIS SUPERVISOR

CO-DIRECTEUR (CO-DIRECTRICE) DE LA THÈSE / THESIS CO-SUPERVISOR

EXAMINATEURS (EXAMINATRICES) DE LA THÈSE / THESIS EXAMINERS

J. Armitage

R. Kashyap

R. Bhardwaj

P. Corkum (absent)

Gary W. Slater

Le Doyen de la Faculté des études supérieures et postdoctorales / Dean of the Faculty of Graduate and Postdoctoral Studies

Ultrafast Infrared Laser Fabrication of Fibre Bragg Gratings with a Phase Mask

By

Christopher W. Smelser

Thesis submitted to

the Faculty of Graduate and Postdoctoral Studies

in partial fulfillment of the requirements for the Degree of

DOCTOR OF PHILOSOPHY

Ottawa-Carleton Institute for Physics

University of Ottawa

Ottawa, Canada

September 2006

Your file Votre référence
ISBN: 978-0-494-32420-2
Our file Notre référence
ISBN: 978-0-494-32420-2

Abstract

This thesis details the first successful phase mask assisted inscription of a retro-reflecting fiber Bragg grating (FBG) with an ultrafast laser source. Ultrafast FBG fabrication is demonstrated in the traditional Ge-doped silica fiber, pure silica fiber, and sapphire crystal fiber. Successful grating fabrication in pure silica and sapphire indicates that, unlike with traditional UV sources, a wide range of materials can be modified with ultrafast laser radiation.

A multiple beam interference model is developed that can accurately simulate the femtosecond and picosecond pulse induced interference patterns in the cladding and core regions of the Ge-doped silica fiber. The model is then extended to simulate pulse propagation through the phase mask and investigate the overlap of the diffracted orders. It is found that at extended distances from the phase mask the diffracted orders no longer overlap, resulting in a pure two-beam interference pattern as the ± 1 orders contain most of the incident energy. These predictions are then compared with experimental observations.

Hydrogen loading of standard Ge-doped SMF-28 fiber is shown to reduce the grating formation threshold significantly. The existence of two ultrafast induced grating types is demonstrated and their annealing and scaling behavior is investigated.

As the index change profile of phase mask assisted ultrafast gratings differs from their UV induced counterparts a Rouard's method model is developed to model the spectral response of these gratings. The spectral response is shown to be consistent with the higher nonlinear intensity dependence of the induced index change. In addition a saturable growth rate is demonstrated and the impact of the incomplete overlap of the induced index change with the core region of the fiber is considered.

Acknowledgements

I would like to thank my family and friends for all the years of support. I would also like to thank Stephen Mihailov and Dan Grobnic and the rest of the group at CRC.

Articles related to this Thesis

Journal publications (submitted, accepted, published)

1. **C. W. Smelser**, S. J. Mihailov and D. Grobnic, "Rouard's method modeling of Type I-IR fiber Bragg gratings made using an ultrafast IR laser and a phase mask" accepted for publication in the Journal of the Optical Society of America B (2006)
2. D. Grobnic, S.J. Mihailov, **C.W. Smelser**, M. Becker and M.W. Rothhardt, "Femtosecond laser fabrication of Bragg Gratings in Borosilicate Ion-Exchange Waveguides" accepted for publication in Photonics Technology Letters (2006)
3. D Grobnic, S J Mihailov, H Ding, F Bilodeau and **C W Smelser**, "Single and low order mode interrogation of a multimode sapphire fibre Bragg grating sensor with tapered fibres" Measurement Science and Technology **17** (5), p. 980-984 (2006)
4. D. Grobnic, **C. W. Smelser**, S. J. Mihailov and R. B. Walker, "Long-term thermal stability tests at 1000 °C of silica fiber Bragg gratings made with ultrafast laser radiation" accepted for publication in Measurement Science and Technology **17** (5) p. 1009-1013 (2006)
5. D. Grobnic, S. J. Mihailov, H. Ding, and **C. W. Smelser**, "Bragg Grating Evanescent Field Sensor Made in Biconical Tapered Fiber with Femtosecond IR Radiation" Photonics Technology Letters **18** (1), 160-162 (2006).
6. **C. W. Smelser**, Stephen. J. Mihailov, and Dan Grobnic, "Formation of Type I-IR and Type II-IR gratings with an ultrafast IR laser and a phase mask", Optics Express **13** (14), p.5377-5386 (2005)
7. D. Grobnic, S. J. Mihailov, **C. W. Smelser**, F. Génèreux, G. Baldenberger and R. Vallée "Bragg Gratings made in Reverse Proton Exchange Lithium Niobate Waveguides with a Femtosecond IR Laser and a Phase Mask" Photonics Technology Letters **17** (7), p. 1453-1455 (2005)
8. **C.W. Smelser**, S. J. Mihailov, D. Grobnic: "*Hydrogen Loading for Fiber Grating Writing with a Femtosecond Laser and a Phase Mask*" Optics Letters **29** (18), p.2127-2129 (2004).
9. D. Grobnic, S. J. Mihailov, **C. W. Smelser**, H. Ding: "*Sapphire Fiber Bragg Grating Sensor Made Using Femtosecond Laser Radiation for Ultra High Temperature Applications*" Photonics Technology Letters **16** (11), p. 2505-2507 (2004).
10. D. Grobnic, **C. W. Smelser**, S. J. Mihailov, R. B. Walker and P. Lu: "*Fiber Bragg Gratings with Suppressed Cladding Modes Made in SMF-28 with a Femtosecond IR Laser and a Phase Mask*" Photonics Technology Letters **16** (8), p. 1864-1866 (2004).
11. **C.W. Smelser**, D. Grobnic, S. J. Mihailov: "*Generation of Pure Two beam Interference Grating Structures in an Optical Fiber With a Femtosecond IR Source and a Phase Mask*" Optics Letters **29** (15), p.1730-1732 (2004).
12. **C.W. Smelser**, S. J. Mihailov, D. Grobnic, P. Lu, R. B. Walker, H. Ding and X. Dai: "*Multiple Beam Interference Patterns in Optical Fiber Generated with Ultrafast Pulses and a Phase Mask*" Optics Letters **29** (13), p.1458-1460 (2004).
13. S.J. Mihailov, **C. W. Smelser**, D. Grobnic, R. B. Walker, P. Lu, H. Ding and J. Unruh: "*Bragg Gratings Written in All-SiO_2 and Ge-doped Core Fibers with 800 nm Femtosecond Radiation and a Phase Mask* "Journal of Lightwave Technology **22** (1), p. 94-100 (2004)
14. S.J. Mihailov, **C.W. Smelser**, P. Lu, R.B. Walker, H. Ding, D. Grobnic, G. Henderson and J. Unruh: "*Fiber Bragg gratings made with a phase mask and 800 nm femtosecond radiation*" Optics Letters **28** (12), p. 995-997 (2003).

Conference publications:

1. D. Grobnic, H. Ding, S. J. Mihailov, **C. W. Smelser**, P. Lu, *"Low Order Mode Excitation of Bragg Gratings made with Ultrafast IR Radiation in Large Core Area Multimode Fibres"*, European Conference on Optical Communications (ECOC), Sept. 24-28, Cannes, France (2006), paper We3.P.35.
2. S. J. Mihailov, D. Grobnic, H. Ding, **C. W. Smelser**, P. Lu, J. Broeng, *"Femtosecond IR Laser Inscription of Bragg Gratings in Photonic Crystal Fibre Tapers"*, European Conference on Optical Communications (ECOC), Sept. 24-28, Cannes, France (2006), paper Th3.3.3.
3. D. Grobnic, S. J. Mihailov, C. W. Smelser, P. Lu, *"Bragg Gratings written in Un-doped Fluoride Glass Fibres Using Ultrafast 800nm Radiation"*, European Conference on Optical Communications (ECOC), Sept. 24-28, Cannes, France (2006), paper Th3.3.7.
4. **C.W. Smelser**, S. J. Mihailov, D. Grobnic. *"Dependence of grating profile on incident intensity during the formation of Type I-IR ultrafast fiber Bragg gratings"*, presented at CLEO/QELS 2006 Long Beach California, May 21-26 2006, paper CTtuY4.
5. S.J. Mihailov, D. Grobnic, **C.W. Smelser**, R. B. Walker, H. Ding, *"Ultrafast Laser Fabrication of Bragg Grating Devices"*, invited talk presented at the Bragg Grating, Photosensitivity and Poling Topical Meeting (BGPP 2005), Sydney Australia, July 4-6, 2005.
6. **C. W. Smelser**, S. J. Mihailov, D. Grobnic, *"Type I-IR and type II-IR fiber Bragg grating formation with an ultrafast infrared source and a phase mask"* accepted to the Bragg Grating, Photosensitivity and Poling Topical Meeting (BGPP 2005), Sydney Australia, July 4-6, 2005.
7. **C. W. Smelser**, S. J. Mihailov, D. Grobnic, *"Intensity dependence of the index modulation growth rate of type I-IR ultrafast fiber Bragg gratings"* accepted to to the Bragg Grating, Photosensitivity and Poling Topical Meeting (BGPP 2005), Sydney Australia, July 4-6, 2005
8. D. Grobnic, S. J. Mihailov, **C. W. Smelser,** *"High Order Spectral Response Characteristics of Fiber Bragg Gratings made with Ultrafast IR Radiation and Phase Mask"*, accepted to the Bragg Grating, Photosensitivity and Poling Topical Meeting (BGPP 2005), Sydney Australia, July 4-6, 2005.
9. D. Grobnic, H. Ding, S.J. Mihailov, and **C.W. Smelser**, *"Retro-reflective evanescent field sensors based on Bragg Gratings made in biconical tapered fiber with femtosecond IR radiation"* International Conference on Optical Fibre Sensors OFS-17, Bruges, Belgium May 23-27, 2005, post deadline paper.
10. D. Grobnic, S.J. Mihailov, H. Ding, F. Bilodeau and **C.W. Smelser**, *"Single and low order mode interrogation of a multimode Sapphire fiber Bragg grating sensor with tapered fibers"* International Conference on Optical Fibre Sensors OFS-17, Bruges, Belgium May 23-27, 2005, paper P2-42
11. D. Grobnic, **C. W. Smelser**, S. J. Mihailov, R. B. Walker, *"Long-term thermal stability tests at 1000 °C of silica fiber Bragg grating made with ultrafast laser radiation"* International Conference on Optical Fibre Sensors OFS-17, Bruges, Belgium May 23-27, 2005, paper We1-5.
12. **C. W. Smelser**, D. Grobnic, S. J. Mihailov, *"Self Focusing Behaviour in the Fabrication of Fiber Bragg Gratings with an Ultrafast Laser and a Phase Mask"* CLEO 2005 May 23-26, 2005 Baltimore, Maryland, USA, paper JWB16.
13. W. J. Reichman, D. M. Krol, **C. W. Smelser** and S. J. Mihailov, *"Fluorescence spectroscopy of fiber gratings written with an ultrafast infrared laser and a phase mask"* presented at CLEO 2005 May 23-26, 2005 Baltimore, Maryland, USA, paper CTuAA3.
14. S.J. Mihailov, **C.W. Smelser**, D. Grobnic, R.B. Walker, H. Ding, P. Lu, *"Femtosecond Laser Fabrication of Photonic Devices"*, invited talk presented at the Optical Fiber Communications Conference, Los Angeles CA, March 6-11, 2005.
15. **C. W. Smelser**, D. Grobnic, P. Lu, S.J Mihailov, R. B. Walker, X. Dai, H. Ding *"Characterization of fiber Bragg gratings written using a remote writing technique and a coherent CW UV source"*, Photonics North Conference 2004, Ottawa, ON, Sept. 26-29 paper 5577-32.

16. D. Grobnic, **C.W. Smelser**, S.J. Mihailov and R. B. Walker *"Isothermal Behavior of Fiber Bragg Gratings Made with Ultrafast Radiation at Temperatures Above 1000 °C"*, 30th European Conference on Optical Communication, September 5-9, 2004 - Stockholm, Sweden, paper Tu1.3.5.
17. D. Grobnic, S.J. Mihailov, **C.W. Smelser** and H. Ding, *"Ultra High Temperature FBG Sensor Made in Sapphire Fiber Using Femtosecond Laser Radiation"*, 30th European Conference on Optical Communication, September 5-9, 2004 - Stockholm, Sweden, paper Tu1.3.4.
18. D. Grobnic, **C.W. Smelser**, S.J. Mihailov, R.B. Walker and P. Lu. *"Suppression of Cladding Modes in Fibre Gratings made with an Ultrafast Laser and a Phase Mask"*, 30th European Conference on Optical Communication, September 5-9, 2004 - Stockholm, Sweden, paper Tu1.3.3.
19. **C.W.Smelser**, S.J. Mihailov, D.Grobnic, R. B.Walker, P. Lu, and H. Ding: *"Impact of hydrogen loading on the fabrication of fiber Bragg gratings with ultrafast 800 nm laser radiation"*, in Proc. Bragg Gratings, Photosensitivity, and Poling in Glass Waveguides, Monterey, CA, 2003, Paper PDP3.
20. S.J. Mihailov, **C.W. Smelser** and D. Grobnic: *"Fabrication of fiber Bragg gratings (FBG) in all-SiO_2 and Ge-doped core fibers with 800 nm picosecond radiation,"* in Proc. Bragg Gratings, Photosensitivity, and Poling in Glass Waveguides, Monterey, CA, 2003, Paper TuB2.
21. S.J. Mihailov, **C.W. Smelser**, P. Lu, R.B. Walker, D. Grobnic, H. Ding and J. Unruh, *"Fiber Bragg Gratings (FBG) made with a phase mask and 800 nm femtosecond radiation"*, Optical Fiber Communications Conference (OFC 2003), Atlanta, GA, 2003, Paper PD30.

Patents

1. Stephen J. Mihailov, **Christopher W. Smelser**, Ping Lu, Robert B. Walker, Dan Grobnic, Huimin Ding, George Henderson, Xiaoli Dai, US. Patent no: 6,993,221 B2

2. Stephen J. Mihailov, Dan Grobnic, **Christopher Smelser**, Robert Walker, Ping Lu, Huimin Ding, George Henderson, Xiaoli Dai, US. Patent no: 7,031,571 B2

Table of contents

List of Figures

List of Tables

Chapter 1: Introduction

1.1 Introductory comments

This thesis begins with an introductory section that outlines some of the concepts that will be covered in the articles. This section is intended to provide some background for the reader and highlight some of the unique properties of ultrafast gratings.

1.2. Photosensitivity and UV fiber Bragg gratings

1.2.1. The Discovery of Photosensitivity

The field of fiber Bragg gratings was born with the discovery of photosensitivity by K. O. Hill in 1978 [1]. The breakthrough occurred when 488 nm light from an Argon-ion laser was coupled into a germanium doped silica fiber. The experimental setup [2] is shown in Fig. 1.

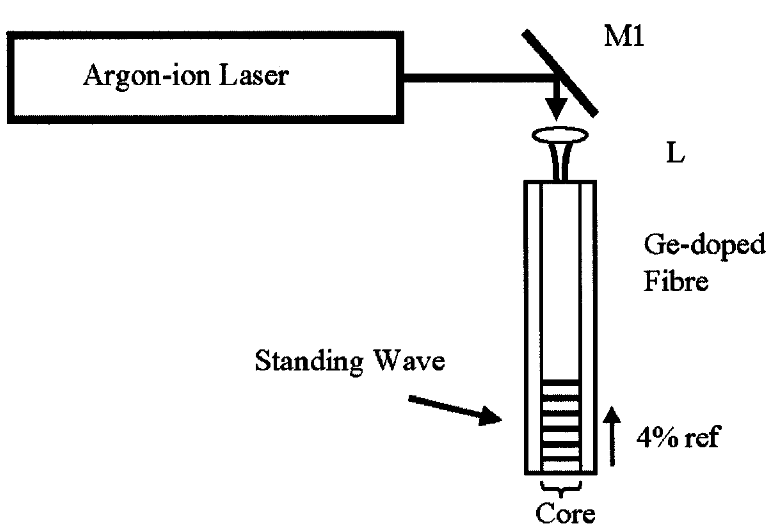

Fig. 1. Apparatus used by Hill to produce fiber gratings. An Argon-ion laser operating at 488 nm is coupled into a Ge-doped fiber and the small reflection from the cleaved end up the fiber sets up s standing wave. M1 is a mirror and a Lens L couples light into the fiber.

It was observed that the loss in the fiber increased over time until all the incident light was back reflected from the fiber. Hill proposed that the intense peaks of the standing wave, set up with the 4 % back reflection from the end face of the fiber, must change the index of refraction of the Ge-doped core of the material periodically according to:

$$d = \frac{\lambda}{2n_{eff}} \qquad (1).$$

Here d is the periodicity of the standing wave, λ is the 488 nm wavelength of the Argon-ion laser, and n_{eff} is the effective core mode index.

The periodicity of the index modulation in the fiber resulted in a reflection peak centered at the wavelength of the laser inscribing the grating. The reflected wavelength could be modified with tension or heat but the applicability of such a grating was clearly limited. The mechanism responsible for the index change in the material was not understood at the time.

1.2.2. Two-Photon Dependence and Interferometric Grating Fabrication

Three years later Lam and Garside [3] demonstrated that the index change in these gratings resulted from the absorption of two photons. This indicated that the mechanism responsible for the index change was not absorption at the Argon-ion wavelength of 488 nm but rather at the second harmonic of 244 nm. This important discovery prompted Meltz [4] to attempt to produce fiber Bragg gratings with a frequency-doubled excimer pumped dye laser with an output wavelength of ~244 nm. In this study a unique interferometric apparatus, shown in Fig. 2., was used to write gratings with periodicities that would reflect wavelengths other than that of the writing laser.

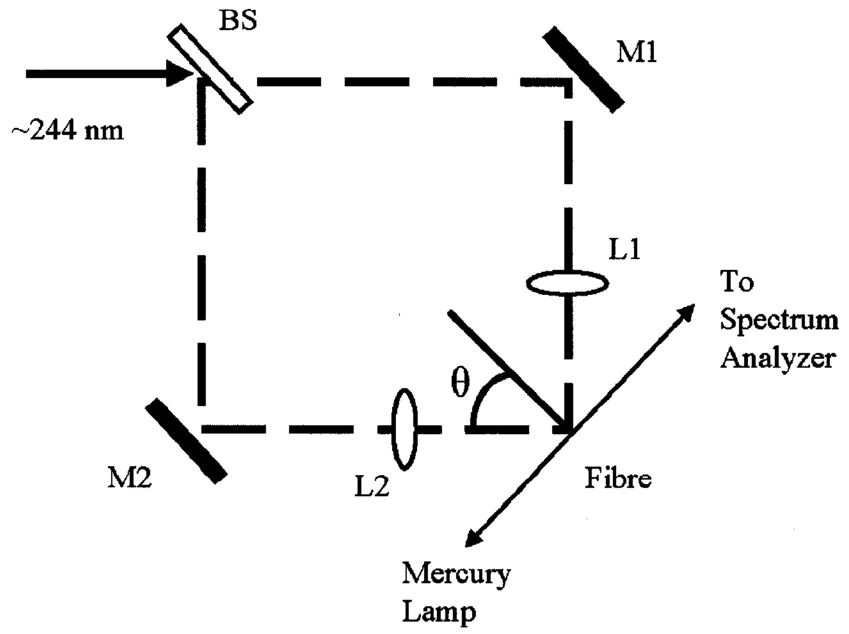

Fig. 2. The interferometric apparatus used by Meltz to inscribe fiber Bragg gratings at visible wavelengths. A 244 nm beam is split into two and recombined at the fiber. The spectrum was monitored with a mercury lamp and an optical spectrum analyzer. BS is a beam splitter, L1/L2 are cylindrical lenses, and M1/M2 are turning mirrors.

The reflected signal will depend on both the wavelength of the laser source and the angle of the incident beams.

$$\lambda_{Bragg} = \frac{n_{eff}\lambda_{uv}}{\sin(\theta)} \tag{2}$$

Here n_{eff} is the effective index of the core mode in the fiber, λ_{uv} is the writing beam wavelength, and θ is the angle of the interfering beams from the normal to the fiber. This represented an important step forward as now gratings could be fabricated at wavelengths that would be useful for telecommunications and sensor applications.

1.2.3. Phase Mask Assisted Fabrication of Fiber Bragg Gratings

Fiber Bragg grating fabrication was further simplified with the introduction of a transmissive phase mask into the grating fabrication apparatus [5]. As shown in Fig. 3 when UV light passes through a silica phase mask (which is transmissive at 248 nm) the various phase mask orders combine in such a way as to produce an interference pattern.

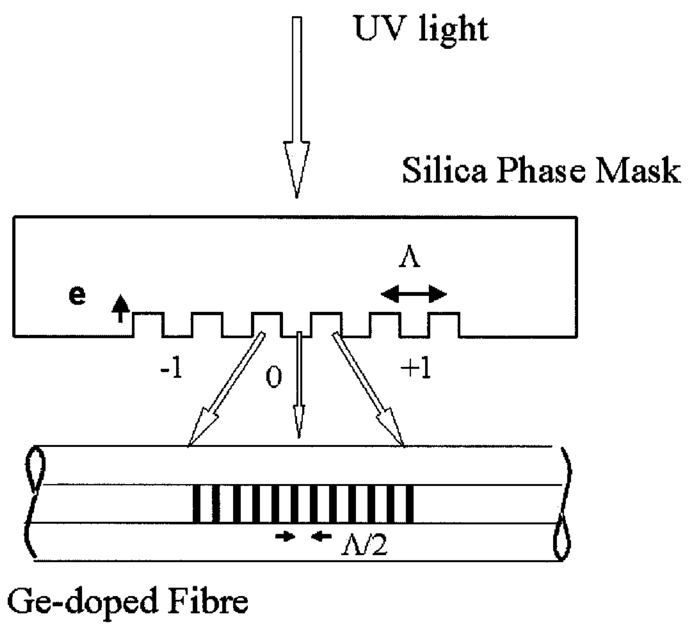

Fig. 3. A transmissive phase mask diffracts the incident UV beam into several different orders. These beams combine to produce an interference pattern behind the phase mask. This interference pattern is imprinted onto the fiber core. The etch depth e determines the relative magnitudes of the orders, and the pitch Λ determines the order angles. If the ± 1 orders dominate the interference pattern then the grating has a pitch of $\Lambda/2$.

If the phase mask could be designed to minimize the impact of the zeroth order on the interference pattern while maximizing the ± 1 orders then it would be possible to produce a two-beam interference pattern with a periodicity of $\Lambda/2$. This pattern would impinge on the Ge-doped fiber core and produce a grating structure. The resonant wavelength of such a structure would be:

$$\lambda_{Bragg} = \Lambda n_{eff} \tag{3}$$

where Λ is the pitch of the transmissive phase mask and n_{eff} is the effective index of the core mode of the fiber.

1.2.4. The Color Center Model for Index Change

Significant progress had been made in the fabrication of fiber Bragg gratings but the fundamental mechanisms responsible for the index change in the material were still not fully understood. It seemed, with the gratings produced by Meltz [4] and Lam and Garside [3], that the presence of absorption in Ge-doped silica at ~244 nm was related to the resulting index change. Silica glass is a very complex material where oxygen and silicon combine in tetrahedral units to produce a wide variety of structures. When doped with Ge the germanium atom replaces silicon in the structure. The resulting material can contain defects that introduce absorption bands at energies less than the band gap of pure silica. A 242 nm absorption band exists which results from Germanium Oxygen Deficient Color Centers. Specifically, there are two Germanium Oxygen Deficient Centers that are thought to be responsible for the 242 nm absorption peak in Ge-doped silica [6,7]. The first, referred to as the Neutral Oxygen Vacancy results from an oxygen vacancy where a Ge-Ge, Si-Ge, or Si-Si bond had been formed in its place. The second, the Germanium Lone Pair Center is a doubly ionized Ge atom bonded to two oxygen atoms. Both of these defects are depicted in Fig. 4.

The color center model of index change is based on the dissociation of these defects to produced new species within the Ge-doped core of the fiber. There will be a resulting transformation in the absorption spectrum, which alters the index of refraction via Kramers-Kronig relations. The Kramers-Kronig equations relate the structure of the absorption spectrum to the magnitude of the index of refraction [8]. A number of studies have been performed that utilized both spectral absorption and electron spin resonance to determine the by-products of the interaction of these two defects with the incident UV radiation [9-12].

There are generally three major defects that result from the irradiation of Neutral Oxygen Vacancies. It is believed that upon exposure to UV radiation Neutral Oxygen Vacancies dissociate to form Germanium-electron Centers or GeE' centers.

The Germanium-electron Center defects are a Ge atom bound to four oxygen atoms with a trapped electron, as shown in Fig. 4. These defects are labeled as Ge (I) and Ge (II) and have characteristic absorptions at 4.4 eV (270 nm) and 5.8 eV (215nm), respectively [11]. It is not clear what underlying difference there is between the two defects [9]. It has been shown that the Ge (I,II) defects can transform into GeE' defects when irradiated with strong UV radiation [12]. GeE' defects are composed of a dangling electron at a Ge atom bound to three oxygen atoms [9]. GeE' centers have a characteristic absorption at 6.3 eV (200 nm) [10].

The Germanium Lone Pair Centers are known to fluoresce at 3.1 eV (~400 nm) and 4.28 eV (290 nm) when exposed to UV radiation [13]. There is also some evidence relating their depletion and the increase of GeE' centers [11].

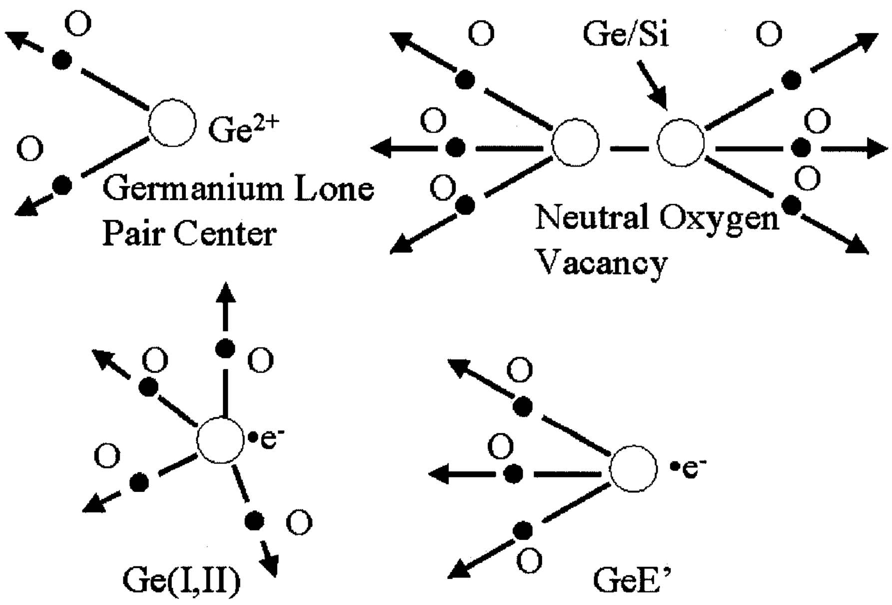

Fig. 4. Here are a few of the defects that are commonly found in Ge-doped silica. The top two are responsible for the 242 nm color center absorption peak. The Ge(I,II) and GeE' are commonly formed upon irradiation of Ge-doped silica with a UV laser source. The arrows indicate that the oxygen atoms are bonded to the rest of the silica latice.

Whatever the pathway through which these defects are created, they are likely responsible for the index change observed in the original study by Hill. Kramers-Kronig relations indicate that these defects can account for index changes of 5×10^{-5} [14].

Aside from the inadequacy of the color center model to explain the commonly observed index change of $>10^{-3}$ there have been some observations that challenge the color center model as the main route to index change. It has been demonstrated that the ArF excimer laser, operating at 193 nm, induces a much larger index change than the KrF laser at 248 nm [11]. This result is puzzling as the KrF laser is much more efficient at producing color centers, likely because of its proximity to the 242 nm absorption band. It has also been shown that it is possible to produce significant index changes in all-silica core fiber with an ArF laser, perhaps through another mechanism [15].

1.2.5. Hydrogen Loading and Flame Brushing for Increasing Photosensitivity

As mentioned previously it has been demonstrated both theoretically and in practice that the color centers can only account for index changes on the order of 5×10^{-5} [6,14]. Typically higher index changes are desirable for telecommunications applications. As a consequence it is important to find a means to further 'sensitize' the fiber. A solution to this problem was found through cold, high pressure, hydrogen loading of Ge-doped silica fiber [16] and hydrogen flame brushing [17].

Through the hydrogen 'loading' process, molecular hydrogen was incorporated into the glass matrix. Once irradiated with a UV laser a chemical reaction ensued that could produce index changes as high as 5×10^{-3}. One would naively think that the molecular hydrogen had reacted with the color centers to produce defects that contributed much more significantly to the index change. This, however, was not supported by the fact that the wavelength dependence of the index change seemed to suggest that it was an absorption at a wavelength below 200 nm that was responsible for triggering the process, not the 242 nm absorption peak [18]. Furthermore, the ArF laser operating at 193 nm seemed to be much more efficient in producing index change in hydrogen loaded fiber [19].

The fiber could also be sensitized through the method of flame brushing [17]. This method involved the brief exposure of Ge-doped fiber to a hot hydrogen flame resulting in both an increase in effective index in the fiber core and increase core photosensitivity.

1.2.6. Densification

As silica glass is an amorphous material made up of a large variety of structures it is possible to rearrange the molecules in such a way as to produce a more dense material without creating cracks or voids in the material. Some researchers have come to believe that it is compaction of the glass matrix in the irradiated zones that results in the most significant contribution to the observed index change [20,21]. Measurements have been made that indicate that the densification of silica can account for an induced index change of 1×10^{-3} [21].

1.2.7. UV Grating Types

Grating structures have been categorized into different types depending on the mechanism responsible for their growth. Two UV grating types seem to have much in common with gratings fabricated with ultrafast lasers [22].

Type I gratings

Gratings that are formed through what is thought to be color center formation or densification are referred to as Type I gratings [23]. There are a few defining characteristics. First, these gratings exhibit temperature stability up to about 500 °C before they are rapidly annealed out. It has been suggested that this is a consequence of the instability of color centers at elevated temperatures [24]. Spectral changes upon UV irradiation have also been shown to be reversible. It is also possible that the compacted material relaxes into its original state at these temperatures [25]. These gratings typically grow monotonically and allow for a high degree of control over the index change profile in the fiber. These gratings also have a relatively low birefringence, which is particularly desirable in telecommunications applications [26]. Gratings formed with ultrafast infrared radiation with similar physical properties have been referred to as Type I-IR fiber Bragg gratings [22].

Type II gratings

With pulsed UV laser sources such as an excimer laser it is possible to increase the intensity until the fiber is catastrophically damaged through an ionization mechanism to produce a Type II damage grating [23]. These gratings typically exhibit high background loss due to scattering from the damage induced in the glass. Gratings are also typically formed in one pulse, with subsequent pulses destroying the grating. These gratings, unlike Type I gratings, are stable at temperatures in excess of 1000 °C making them ideally suited for high temperature sensor applications. Ultrafast infrared laser induced gratings with similar properties have been referred to as Type II-IR gratings [22].

1.3. Ultrafast modification of dielectrics and interference properties

1.3.1. A brief description of ultrafast lasers

Modification of dielectrics with 800 nm infrared radiation requires intensities on the order of 10^{13} W/cm^2. As Ti:sapphire lasers cannot produce pulse energies high enough to achieve these intensities it is necessary to further amplify the pulses. This introduces a problem though as direct amplification of femtosecond pulses quickly results in peak powers that destroys the amplifying medium through self-focusing [27]. Increasing the pulse duration prior to amplification would eliminate this problem.

The amplified Ti:sapphire laser system employs a technique called chirped pulse amplification to amplify ultrafast laser pulses [28]. This system is composed of several stages: the main oscillator, the stretcher, the amplifier and the compressor. The overall layout of the scheme is shown in Fig. 5.

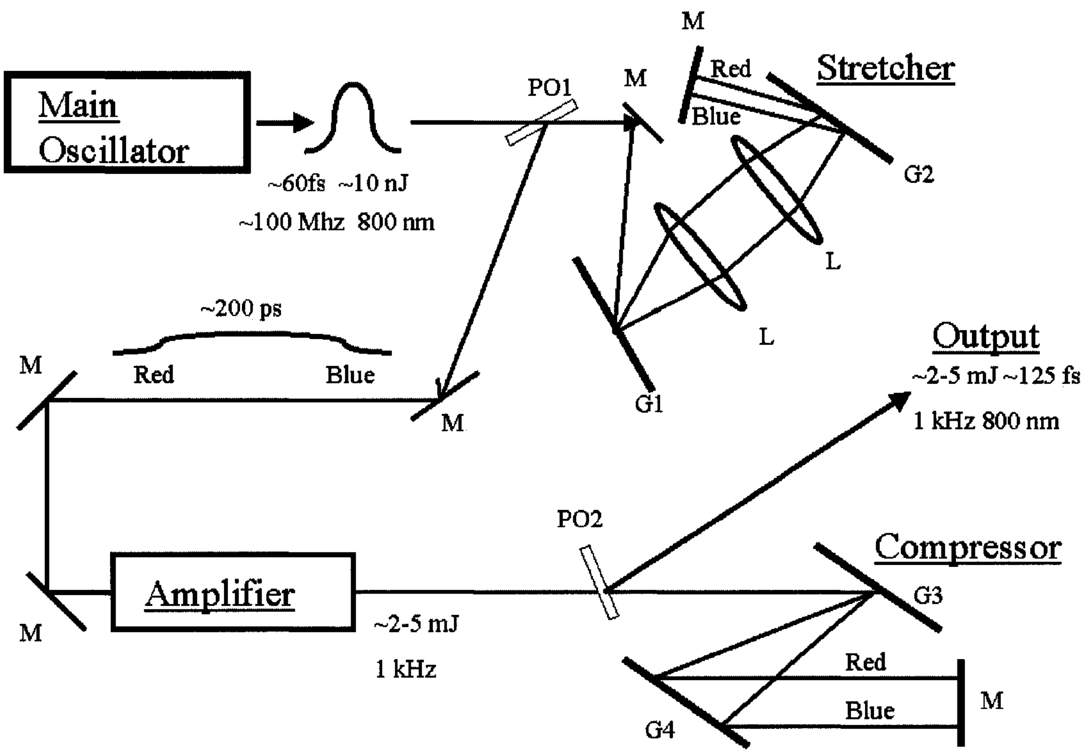

Fig. 5. Layout of the chirped pulse amplification scheme. Pulses produced in the main oscillator are expanded in the stretcher, are amplified and recompressed in the compressor. Here M is a mirror, L is a lens, G is a grating, and PO is a pick-off mirror. This scheme amplifies the pulses by 5-6 orders of magnitude.

The main oscillator provides a pulse train of 800 nm pulses of ~60 fs duration and ~10 nJ pulse energy at a repetition rate of 100 MHz. This pulse train passes into the stretcher stage consisting of a grating pair separated by a telescope [29, 30]. In this configuration it is possible to arrange the gratings G1 and G2 such that the optical path length of longer wavelength light (Red), for a double pass through the stretcher, is larger than that of shorter wavelength light (Blue). This will result in positive group velocity dispersion (GVD). Pulses can be typically stretched as much as three orders of magnitude for ~100 fs input pulses. After a double pass through the stretcher the light is picked off at PO1 and directed into the amplifier stage. As the pulse is now a few orders of magnitude longer, with no increase in energy, the peak power will now be low enough that the amplifying medium will not be damaged by the seed pulse. As the temporal pulse length is still very long the pulse must be compressed back down to femtosecond time scales. A grating pair, such as G3 and G4 in Fig. 5 can be used to recompress the pulse [29, 30]. In the configuration shown the optical path length is now smaller for shorter wavelengths, introducing negative GVD that can counteract the positive GVD introduced in the stretcher stage and in the amplifying medium. After a double pass through the compressor the pulse is picked off at PO2. The output of the amplified laser system is typically 2-5 mJ pulses at 800 nm, with pulse durations of ~125 fs at a repetition rate of 1 kHz. Intensities on the order of 10^{13} W/cm^2 can be readily achieved with pulses of this energy and duration. The pulse duration can be modified by adjusting the separation between the grating pair in the compressor stage.

1.3.2. Modification of Dielectrics with intense ultrafast laser pulses

Since the advent of Chirped Pulse Amplification, peak intensities on the order of 10^{13} W/cm^2 have been readily achievable with a Ti:sapphire solid state amplifier [28]. At such high peak intensities it has been demonstrated that it is possible to directly modify transparent dielectric materials such as silica [31, 32]. Intense pulses have been used to produce such fundamental devices as waveguides and splitters in bulk silica [33, 34]. The mechanisms responsible for this material modification have long been thought to be the nonlinear ionization process described in Fig. 6.

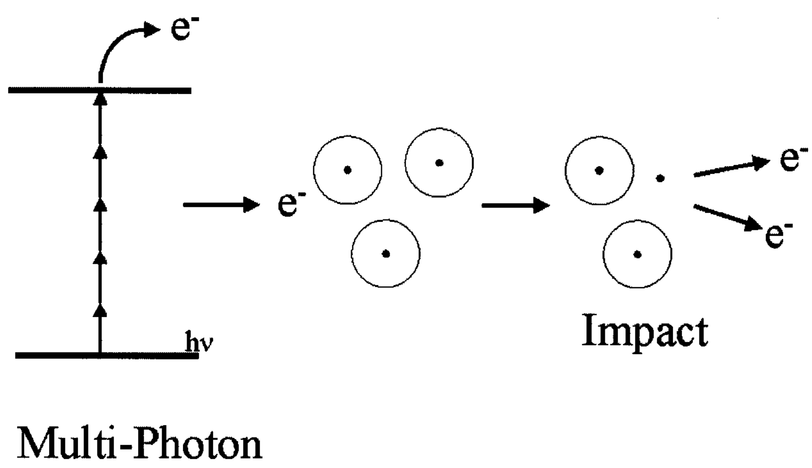

Fig. 6. An electron is multiphoton ionized out of a molecule. It is then accelerated in the electric field to sufficient energies to impact with another atom and free an additional electron. This creates an avalanche of free electrons in the medium.

First free electrons are created through a multi-photon ionization process. In dielectric materials there is little linear absorption in the visible region of the spectrum. Therefore the absorption of several photons is required to produce a free electron. The ionization rate is $P = \sigma^k I^k$, where σ^k is the multi-photon ionization cross section and I is the intensity of the laser [35]. The number k represents the fewest number of photons that will bridge the band gap in the dielectric material. In the case of silica, and absorption of five to six 800 nm photons (with photon energies of 1.55eV) is required to bridge the band gap of which is estimated to be between 7.6 and 9.3 eV [36, 37]. As the ionization rate depends on I^k, the creation of free electrons will depend in a highly nonlinear fashion on the incident intensity. After free electrons are produced, it is believed that these electrons are further heated in the electric field to sufficiently high energies that they can further ionize the medium through impact ionization creating an avalanche of electrons [38]. Once the free electron population reaches densities on the order of 10^{21} cm^{-3} the dielectric medium becomes strongly absorbing and the material is destroyed [38].

For long pulse ionization (such as with nanosecond excimer lasers) it is believed that seed electrons are required to initiate the avalanche ionization process as the intensity is too low for significant multi-photon ionization. This renders the process highly probabilistic with a poorly defined threshold. Due to the very high peak intensities of ultrafast laser sources, multi-photon ionization processes can provide the seed electrons for the process to take place, resulting in a very highly deterministic intensity threshold at which the medium is strongly ionized [31,38].

The above processes relate to the formation of ultrafast fiber Bragg gratings in two important ways. First, it appears that the formation of Type I-IR ultrafast fiber Bragg gratings depends in a highly nonlinear fashion on the interference field intensity [22]. It is possible that these gratings are formed through an intermediate level of free electron generation, below that necessary to strongly ionize the medium. The resulting index change has been shown to have temperature stability similar to that of traditional type I UV written gratings [22]. Second, at higher intensities ($\sim 4.5\times10^{13}$ W/cm^2) there is a sharp transition into a regime where the material modification appears to result from a damage process similar to what would be expected from a highly ionized absorbing medium. These gratings have been shown to possess very high temperature stability, similar to that observed with type II UV gratings [22].

The type I and II-IR grating formation regimes have similar morphology to the 'smooth' and 'rough' modification regimes that have been investigated with ultrafast waveguide fabrication [39-41]. It is very likely that the mechanisms responsible for 'smooth' and 'rough' modification are identical to those involved in type I-IR and type II-IR grating formation.

1.3.3 Spatial Coherence and the phase mask

Coherence is a measure of degree of correlation of electric field components that are separated in time and/or space [42]. This can be measured with the Young's double slit apparatus shown in Fig. 7.

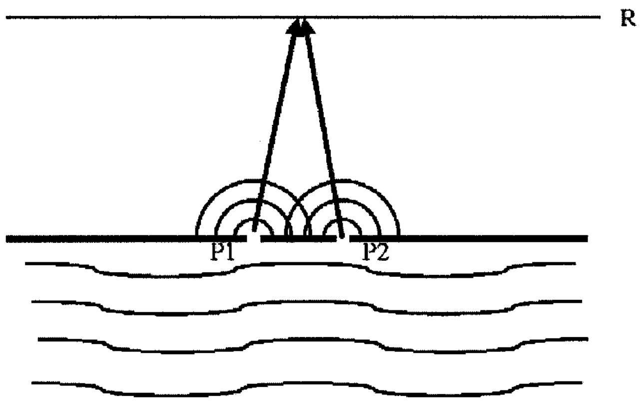

Fig. 7. Young's double slit apparatus. The impinging field components at P1 and P2 interfere at the plane R. If these field components are correlated an interference pattern will result.

A wave impinges on two slits at P1 and P2. Only the field components at P1 and P2 are allowed to interfere at R as the rest of the barrier is opaque. The field components at P1 and P2 will exhibit an interference pattern if there is some degree of correlation between these fields at R. For a source with a high degree of temporal coherence, spatial coherence will dominate the degree of coherence. For some separation between the slits, referred to as the spatial coherence size [43], no interference pattern will be present at R.

Interference patterns produced with a phase mask have a similar property. For an incident beam at normal incidence to the phase mask, the path lengths of a particular order pair (for example ±1) are automatically matched. As the phase mask-fiber separation is increased, the strongly interfering field components become increasingly separated on the phase mask, as shown in Fig. 8. For a source with small spatial coherence, a target fiber can only be moved a small distance from the phase mask before the field components are separated by a distance, *s*, that is larger than the spatial coherence size.

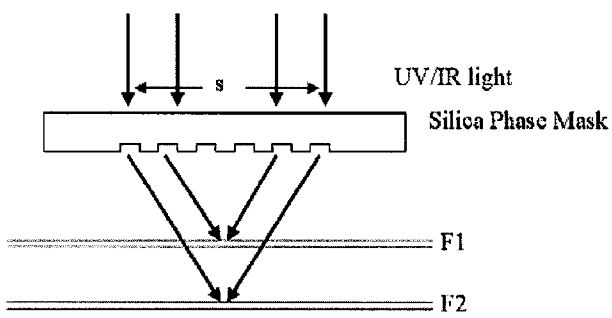

Fig. 8. The interference of diffracted field components through a phase mask. As the fiber position (F1 and F2) is moved away from the phase mask the interfering field components are further toward the edge of the incident beam.

An excimer laser typically has a spatial coherence size as small as <300 μm [43, 44]. The small spatial coherence of an excimer laser significantly limits the allowable separation between the phase mask and fiber during grating fabrication as at extended distances from the mask the interference pattern visibility is greatly reduced. The maximum allowable phase mask fiber separation, before the visibility drops significantly, can be estimated by [43]:

$$D_{pm/f} = \frac{L_{coh}}{2\tan\left(\theta/2\right)} \tag{4}$$

Here L_{coh} is the spatial coherence size and θ is the angle between the ±1 phase mask orders. For an excimer laser operating at 248 nm (KrF), with a phase mask pitch of 1.07 μm the angle between the ±1 orders is ~26.8°. This results in a maximum phase mask-fiber separation of ~600 μm.

Ultrafast lasers possess much greater spatial coherence than excimer lasers [45]. For an ultrafast 800 nm laser with a 3.21 μm phase mask the angle between the ±1 orders is ~28.8°. This value is comparable with that of the excimer and a 1.07 μm phase mask. Ultrafast fiber gratings written with a 3.21 μm mask are routinely written with a phase mask fiber separation in excess of 6 mm, an increase ten fold over the maximum separation for efficient writing with an excimer [46, 47]. The 1/e intensity diameter of this laser was ~4.9 mm. A phase mask fiber separation of 6 mm suggests, based on Eq. 4, a spatial coherence size of ~3 mm. This means that the spatial coherence size of the ultrafast source is almost the entire width of the laser beam. As it is possible to write gratings at distances even further than 6 mm it is likely that it is the finite transverse beam width and not spatial coherence that limits the interference pattern visibility with the ultrafast laser.

The region in which the visibility of the phase mask interference pattern will be significant with both laser sources is compared in Fig. 9.

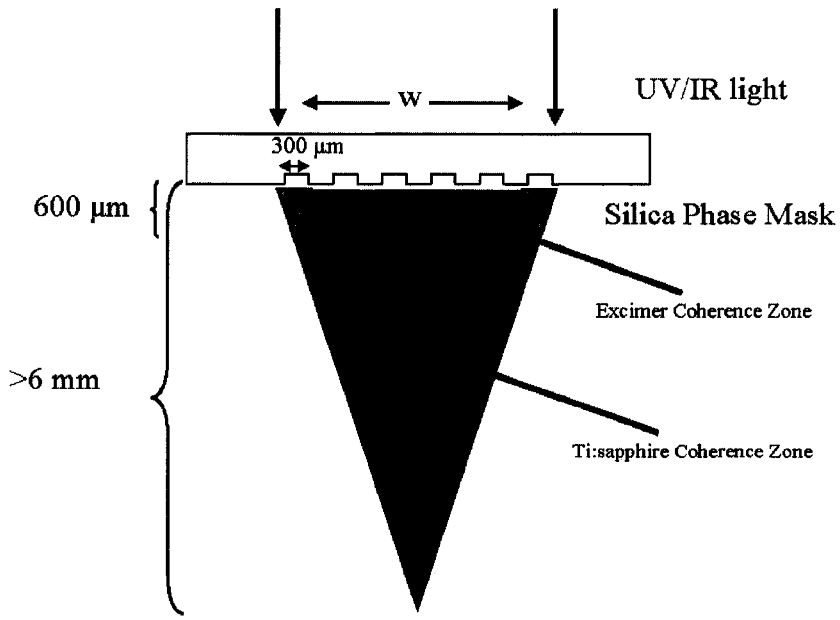

Fig. 9. Illustrates the region for which the interference pattern will have a significant visibility for the both the excimer and the ultrafast laser. This region is limited by the spatial coherence size of the laser source. In the case of the excimer laser this region is quite small, as the coherence length is only 300 μm.

For an equal incident beam width we see from Fig. 9 that the region in which the excimer laser will be coherent, referred to as a coherence zone, is confined to a small region near the phase mask. The Ti:sapphire coherence zone is much larger due to its high spatial coherence. The interference pattern produced with such a laser will have a high visibility several mm from the phase mask.

1.3.4. Multiple beam interference and Order Walk-off

The ultrafast laser induced modification of Ge-doped optical fiber is not confined to the core region of the fiber and extends into the cladding layer. Because of the high index changes the grating can be directly observed under an optical microscope. As shown in Fig. 10 the patterns in the core and cladding appear as if they result from the interference of a large number of phase mask orders [48].

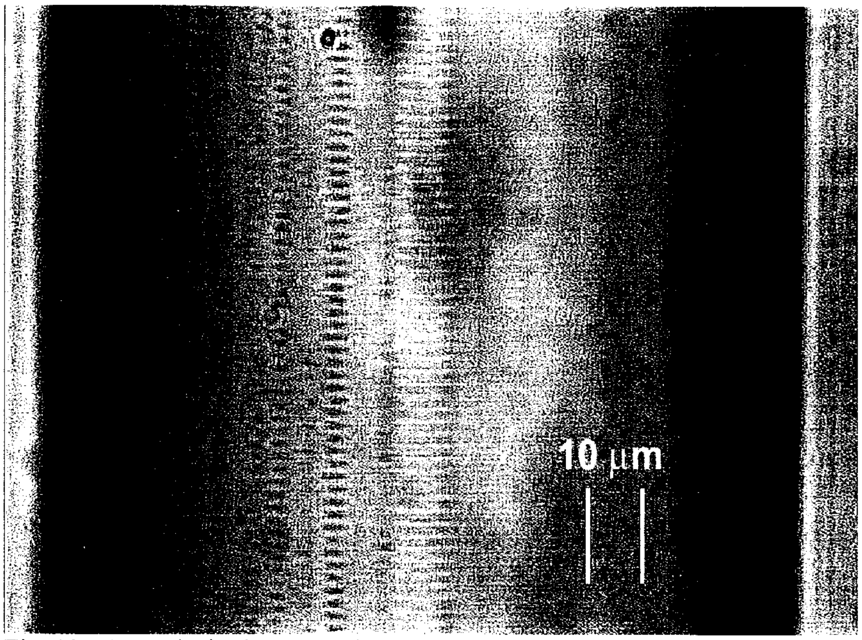

Fig. 10. An optical microscope image of a fiber demonstrates that the pattern produce in the fiber is complex and may result from the interference of several phase mask orders. (ref. [48])

Due to the high spatial and temporal coherence of the laser source it should be possible to develop a simple phase mask order interference model where the electric fields of the various phase mask orders are combined to produce the interference field. The induced index change would then be related to the intensity of the field. This is slightly different than models that were developed for UV grating fabrication as the reduced coherence of the excimer laser prohibited the use of a coherent superposition of plane waves in the model. This interference model was the subject of two of the articles in this thesis [46, 49]. In order to model the types of grating patterns shown in Fig.10 it was also assumed that near the center of the grating it would be a good approximation that the interference pattern was composed of plane waves with magnitudes determined by the energy contained in each phase mask order. There was no consideration of the transverse beam amplitude in the calculation.

$$|E(x,y,t)|^2 = \left|\sum_{\lambda}\sum_{i} a_{\lambda} a_i \exp\left[-i\omega t + ikx\sin(\theta_i) + ky\cos(\theta_i)\right]\right|^2 \quad (5)$$

Here a_λ and a_i are the amplitudes of the spectral components and diffracted orders respectively. ω is the angular frequency and k is the magnitude of the wave vector. The x axis is parallel to the phase mask while the y axis is normal to the phase mask. The order amplitudes were set by measurements of the order energy. For the CW laser model a_λ is set to 1. The angles θ_i are calculated by the grating equation $\sin\theta_i = i\lambda/d$, where d is the mask pitch and λ is the wavelength in the medium. The measured percentage of energies contained in each order for a 4.28 μm pitch phase mask are shown in Table 1.

Mask Pitch	4.28 μm
Energy in 0 Order	2.5%
±1 Orders	39.6%
±2 Orders	1.5%
±3 Orders	4.1%
±4 Orders	2%
±5 Orders	1.5%

Table 1- Percentage of energy associated with the allowed orders for a phase mask with a pitch of 4.28 μm and an laser wavelength of 800 nm. (Ref. [49])

The measured interference patterns and the modeled profiles for a 4.28 μm phase mask are shown in Fig. 11. Fig.11 (a) illustrates the pattern created by a 1.6 ps pulse in the fiber. Fig.11 (b) illustrates the modeled profile where all 11 allowed orders have been used in the calculation. The agreement between the modeled profile and the measurement is excellent. Fig. 11 (c) illustrates the pattern created with the same phase mask but a 125 fs laser pulse. The pattern is clearly different than that shown in Fig. 11

(a). As shown in Fig. 11 (d) this profile can be modeled by reducing the number of interfering orders to five.

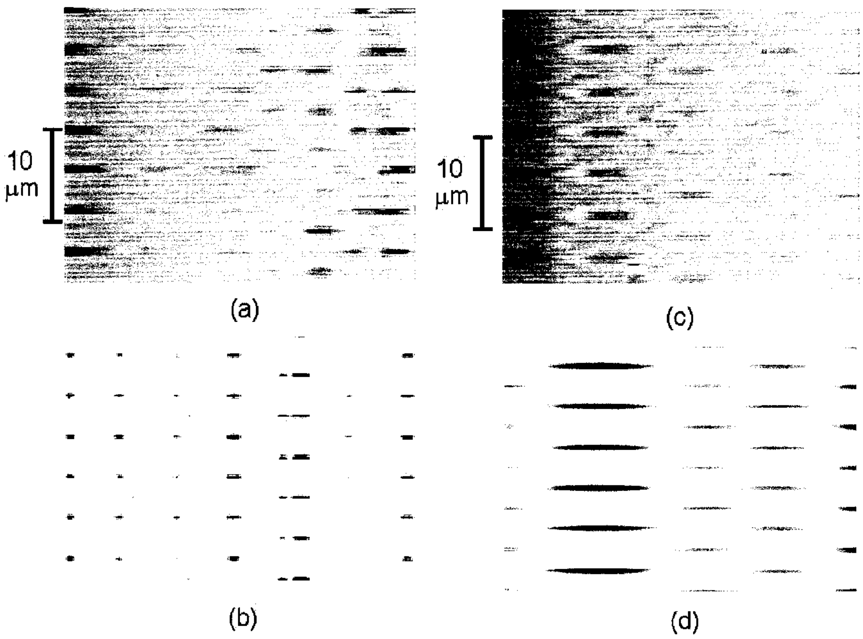

Fig. 11. (a) is the microscope image of the fiber cladding after being irradiated with 1.6 ps pulses and (b) is the modeled 11-beam interference pattern resulting from a 4.28 μm pitch mask. (c) is the image of the cladding after irradiation with 125 fs pulses and (d) is the modeled result including only 5 beams. (Ref. [49])

To explain why the pattern changes simply by reducing the temporal length of the incident laser pulse, one needs to consider the spatial extent of the ultrafast pulse envelope. Typically there is some small separation between the fiber and the phase mask during grating inscription. The high spatial coherence of the ultrafast laser source would allow for larger separations. As a 125 fs ultrafast pulse only occupies ~45 μm of space it is possible that the order of magnitude reduction in pulse length may alter the interference pattern. If the bandwidth of the plane wave interference model is increased by modifying a_λ so that it adequately represents a 125 fs pulse (~8 nm FWHM Gaussian) the model may adequately explain the reduction in interfering orders. Fig. 12 (a) illustrates the interference pattern produced with a 125 fs pulse when the fiber is placed 100 μm from a 2.14 μm pitch phase mask[49]. The various phase mask orders interfere to produce a complex pattern. The leading edge of the 125 fs pulse seems to produce a slightly less complex pattern. Fig. 12 (b) demonstrates the resulting interference pattern when the phase mask-fiber separation is increased to 1 mm.

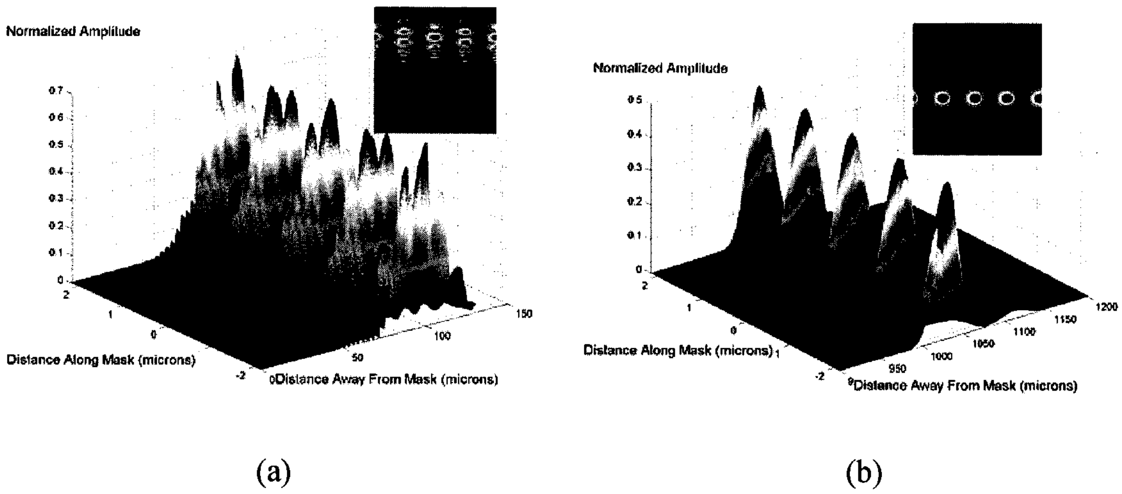

Fig. 12. (a) Illustrates the interference pattern produced by a 125 fs pulse shortly after it passes through a phase mask with a pitch of 2.14 μm (seen 100 μm from the mask). (b) After propagating 1mm the orders no longer overlap and a two beam interference pattern is produced. (Ref. [49])

We see that shortly after passage through the mask, fewer phase mask orders interfere due to the short spatial extent of the pulse until, at large enough distances from the mask, only the ±1 phase mask orders strongly interfere. This model explains the reduction of interfering orders for femtosecond pulses compared to picosecond pulses. For even small distances from the phase mask as in Fig. 12 (a), the short spatial extent of the femtosecond pulses results in a significant reduction in the number of interfering orders.. The model further suggests that for a femtosecond pulse it should be possible to move the target fiber away from the phase mask and create a two-beam interference pattern as in Fig. 12 (b). Fig. 13 compares the 5, 3 and 2 beam interference patterns in (a), (b) and (c) to gratings fabricated with a 4.28 μm pitch phase mask in (d), (e) and (f) at distances of 200, 500 and 5000 μm, respectively [46]. The reduction in the number of interfering phase mask orders is evident.

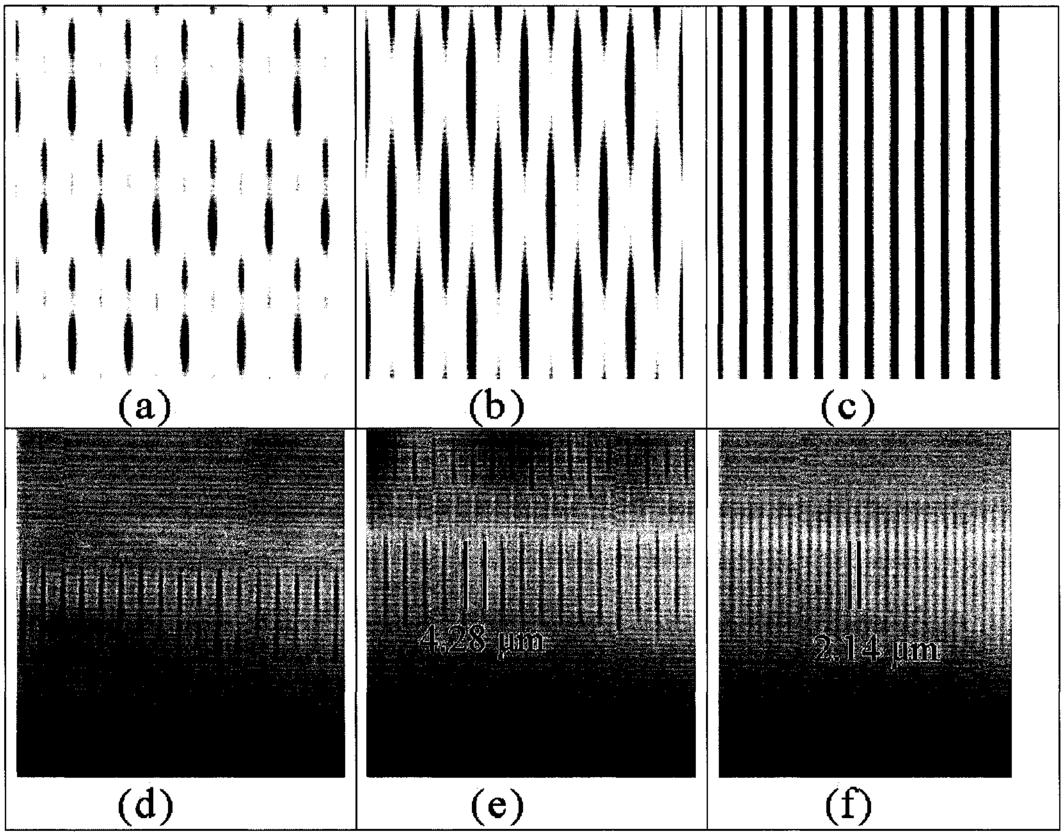

Fig. 13. Illustrates a comparison of the modeled 5, 3 and 2 beam interference patterns with the observed structure in the fiber at progressively larger distances from the phase mask. (a)-(c) depicts the modeled 5, 3, and 2 beam interference patterns. For comparison, (d)-(f) depicts the observed grating structures at 200, 500, and 5000 μm. At 5000 μm only two beam interference is present. (Ref. [46])

This method for producing two-beam interference is unique to ultrafast gratings and happens both as a consequence of the high spatial and temporal coherence of the laser source and its small temporal pulse length.

1.3.5. Limitations of grating fabrication with ultrafast lasers

The ultrafast laser-based fiber Bragg grating apparatus is similar to that for UV laser inscription of gratings depicted in section 1.2.3. where light is focused through a phase mask onto a fiber sample. Two significant differences between UV laser and ultrafast laser fabrication of gratings are related to the effects described in sections 1.3.2 and 1.3.4.

The first significant difference results from the high intensities that are required for the modification of the material with the ultrafast IR pulse. With UV laser sources it is not necessary to place the fiber directly at the focus as the index change results from linear absorption requiring smaller intensities to modify the material. As high intensities are required in the ultrafast IR case, the beam must be focused near the core of the fiber. Positioning of the beam at the core of the fiber is, consequently, critical for the proper fabrication of ultrafast gratings. A vertical scanning scheme has been used successfully to ensure that the ultrafast beam impinges on the core of the fiber [47].

Secondly, the phase mask and fiber are both made of silica. When the fiber is placed in close contact with the phase mask there is danger of phase mask damage. Fortunately, due to the coherent nature of the ultafast source and phase mask order walk-off, there can be a significant phase mask-fiber separation. As the focus of the beam will remain at the fiber core, any separation of the phase mask and fiber will greatly reduce the intensity at the phase mask.

1.4. Coupled mode Theory and Rouard's Method

This section will be concerned with topics related to modeling UV inscribed gratings. More specifically it will deal with coupled mode theory [50-52], complications arising from apodization [53-55] and Rouard's method [56-58]. Unique grating properties possessed by ultrafast IR gratings such as intrinsic higher order resonances [59-61] and cladding mode suppression [47, 63] will also be introduced.

1.4.1. The index change profile and Fourier series

As mentioned in section 1.2.3., a fiber Bragg grating is typically formed when two UV beams are interfered to produce an interference pattern along the length of the fiber. If these beams are uniform the resulting pattern will be the same as that shown in Fig. 14. These beams will induce a small index modulation in the fiber core that has the same pattern.

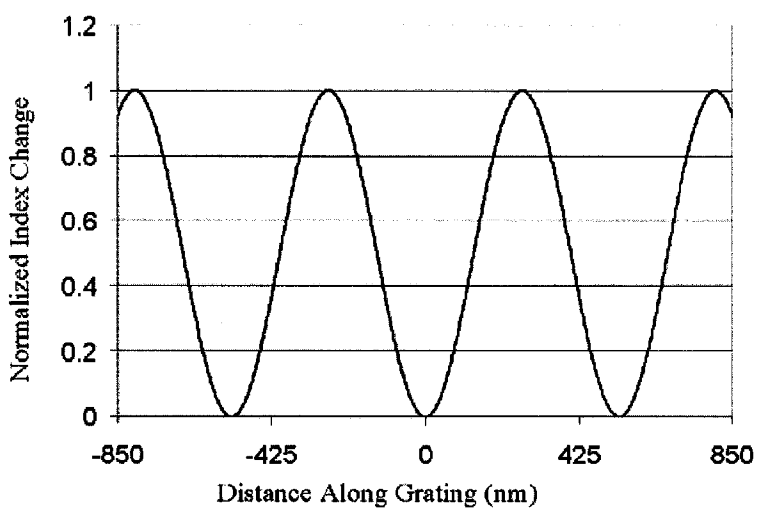

Fig. 14. Sinusoidal index change profile induced with a UV laser. The index change pattern follows the interference profile intensity.

This index modulation profile can be represented as a Fourier series. The constant term of the Fourier series and the first order term are the Δn_o and Δn_1.

$$\Delta n_o = \Delta n_1 = \frac{\Delta n_{peak}}{2} \tag{6}$$

1.4.2. Coupled Mode Equations and The overlap Integral

The most commonly used modeling method for fiber Bragg gratings is coupled mode theory. The equations that describe the coupling of a forward propagating core mode to a backward propagating core mode with a fiber Bragg grating are [50, 52]:

$$\frac{dR}{dz} = i\sigma R(z) + i\kappa S(z) \tag{7}$$

$$\frac{dS}{dz} = -i\sigma S(z) - i\kappa R(z) \tag{8}$$

Here R is the amplitude of the forward propagating core mode and S is the amplitude of the back ward propagating core mode.

σ and κ are known as the "dc" and "ac" coupling coefficients:

$$\sigma = \frac{2\pi}{\lambda}\Delta n_{0,core} + \beta_{core} - \frac{\pi}{\Lambda} \tag{9}$$

$$\kappa = \frac{2\pi}{\lambda}\Delta n_{1,core} \tag{10}$$

where β_{core} is the propagation constant of the core mode, Λ is the period of the grating, and

$$\Delta n_{0,1,core} = \Delta n_{0,1} \iint_{core} dxdy\varepsilon_{core}(x,y)\varepsilon_{core}(x,y)^* = \Delta n_{0,1}\Gamma . \tag{11}$$

$\Delta n_{0,1}$ are the constant and first order terms in the Fourier series of the index modulation, and ε_{core} is the transverse electric field amplitude of the core mode. The integral is the confinement factor [52] of the grating and typically has a value of Γ=0.73 for standard single mode fiber at 1550 nm. The integral is only over the core region of the fiber as the induced index change is negligible in the cladding.

1.4.3. Solution For a Uniform Sinusoidal Grating

Once the Fourier coefficients of the induced index change are known then equations (7) and (8) can be solved analytically [50, 52]. Typically the boundary conditions that are used are $R(0)$=1 and $S(L)$=0. This means that the reflected signal vanishes at the end of the grating and the incident amplitude is normalized to one.

A solution for the amplitude of the reflected signal at the Bragg resonance is:

$$\rho = \frac{S(0)}{R(0)} = \frac{-\kappa \sinh(\delta L)}{\sigma \sinh(\delta L) + i\delta \cosh(\delta L)} \tag{12}$$

where,

$$\delta = \sqrt{\kappa^2 - \sigma^2} \tag{13}$$

The reflected power is related to $|\rho|^2$.

$$|\rho|^2 = \frac{\kappa^2 \sinh^2(\delta L)}{\kappa^2 \cosh^2(\delta L) - \sigma^2} \tag{14}$$

The modeled reflection and transmission spectrum for an ~2 mm long uniform grating with a grating period of 535 nm and an index change of $\Delta n_{1,eff} \sim 2.5 \times 10^{-3}$ is shown in Fig. 15.

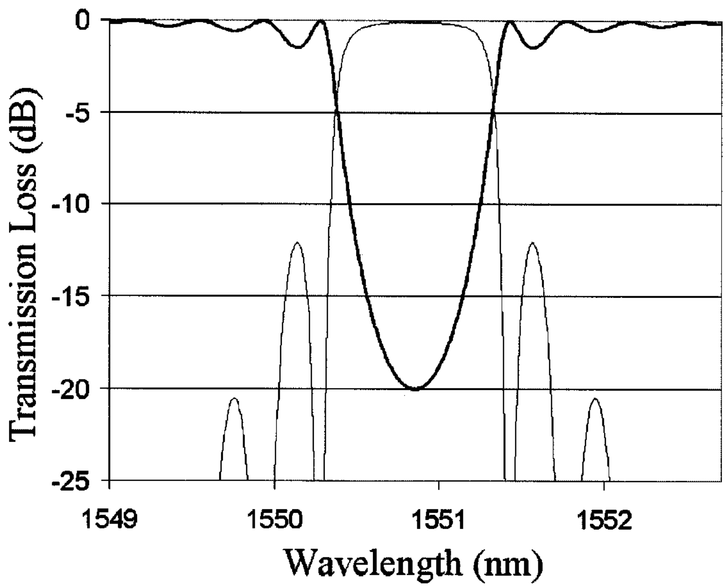

Fig. 15. Calculated transmission (black) and reflection (grey) spectra for an ~2 mm long uniform fiber Bragg grating with a grating period of 535 nm and an index change of $\Delta n_{1,eff}$~2.5×10^{-3} from Eq. 14.

At the Bragg resonance (ie. $\sigma = 0$) then equation (11) simplifies to,

$$\rho = -i \tanh(\kappa L) \tag{15}$$

And the reflected power is:

$$r = \tanh^2(\kappa L) \tag{16}$$

<u>1.4.4. Non-uniform amplitude periodic gratings : Apodization</u>

Careful tailoring of the amplitude profile of a grating has been shown to be useful in a number of applications [53]. A uniform profile is often undesirable due to large side bands that are introduced in the grating spectrum, as seen in Fig. 15. A technique, referred to as apodization, is often used to eliminate this unwanted loss. If the dc component of the grating is constant throughout the whole fiber length as shown in Fig. 16 (a) the side band loss can be significantly reduced as in Fig. 16 (b), when compared to

Fig. 15. The term 'apodization profile' is often used to describe the varying amplitude profile of a grating.

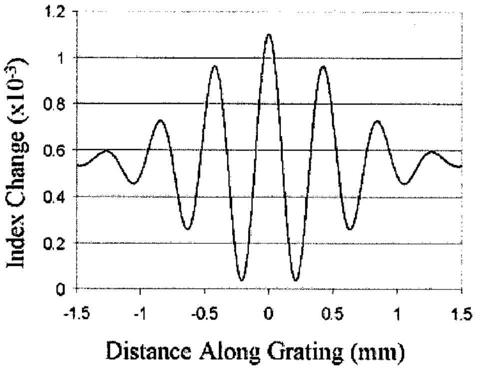

(a)

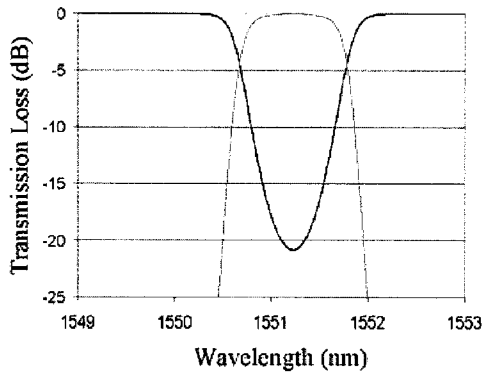

(b)

Fig. 16. (a) The grating profile (periodicity is exaggerated for clarity) of an apodized grating. The 1/e length of this grating is 0.8 mm, the peak index change is 1.1×10^{-3} and the grating periodicity was set at 535 nm. (b) Clearly, when the dc component of the index change is constant throughout the grating the side bands are suppressed.

As with apodization the resulting grating spectrum often depends on the index change profile. For instance a UV grating written with a Gaussian beam with a 1/e intensity spot size of ~2 mm typically has the profile shown in Fig. 17 (a) (when the index of refraction is far below the saturation level).

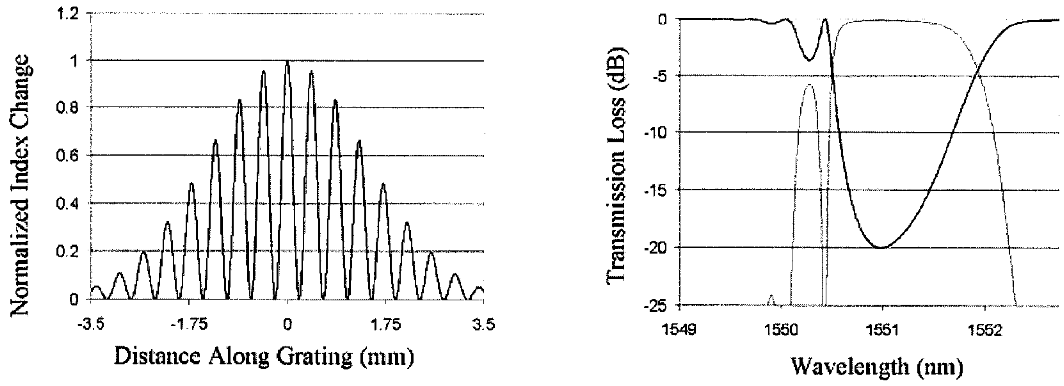

(a) (b)

Fig. 17. (a) is the index change profile for a grating written directly with a beam with a 1/e spot size of ~2 mm. The pitch is exaggerated for clarity. (b) the grating spectrum for the profile shown in (a). The sideband structure and symmetry of the grating are clearly different than that shown in Fig. 15.

Here the periodicity of the grating has been exaggerated for clarity. The varying amplitude along the grating has a significant impact on both the magnitude and the wavelength of the reflected light at each point within the grating structure. As shown in Fig. 17 (b) this affects the spectral profile significantly. In this case, the central portion of the grating is red shifted relative to the edges of the grating. This sets up an effective Fabry-Perot cavity for the wavelengths on the short wavelength side of the spectrum. As a consequence the side bands are much more pronounced on this side of the spectrum.

In the ultrafast studies presented in this thesis, the incident beam was measured by the knife edge technique to have a ~3.2 mm 1/e intensity spot size. For each study the gratings possessed the Gaussian profile shown in Fig. 17 (a). Due to the nonlinear dependence of the index change on the intensity, the gratings induced in the fiber are much narrower in length, in some cases appearing as if they were made with a Gaussian beam with a 1/e spot size of 1.4 mm [22].

As the amplitude and wavelength of the reflected light can vary along the length of the grating a more sophisticated approach must be employed in order to accurately model the gratings spectral response. The most common approach is the use of a transfer matrix method [54, 55].

1.4.5. The Transfer matrix Method

Assuming that the variation in amplitude of the grating along the length of the fiber is not too rapid it is possible to subdivide the grating into a series of smaller gratings as shown in Fig. 18.

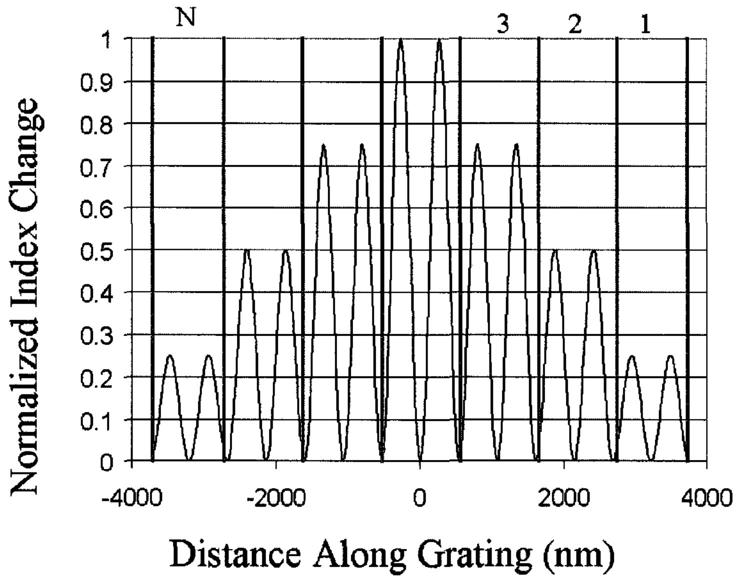

Fig. 18. A grating can be treated as a series of concatenated gratings. The total grating response can then be determined through matrix multiplication.

The reflection and transmission of the total grating can be described using the matrix equation:

$$\begin{bmatrix} R(0) \\ S(0) \end{bmatrix} = T \begin{bmatrix} R(L) \\ S(L) \end{bmatrix} = T^{N} \ldots T^{2} T^{1} \begin{bmatrix} R(L) \\ S(L) \end{bmatrix}. \qquad (17)$$

where T^i is a matrix that describes the coupled mode solution of each grating segment. For the boundary conditions $R(0)=1$ and $S(L)=0$ it is then possible to determine the reflectivity for the entire grating. The transfer matrix method will work well with periodic gratings but complications arise when a completely arbitrary index structure is investigated. In these cases it is best to resort to a thin film method such as Rouard's method.

1.4.6. Rouard's Method

Rouard's method involves subdividing an index change profile into a large number of segments in a similar manner as the transfer matrix method [56-58]. The difference is that the structure is divided into a series of Fresnel reflections. A series of three thin films are shown in Fig. 19.

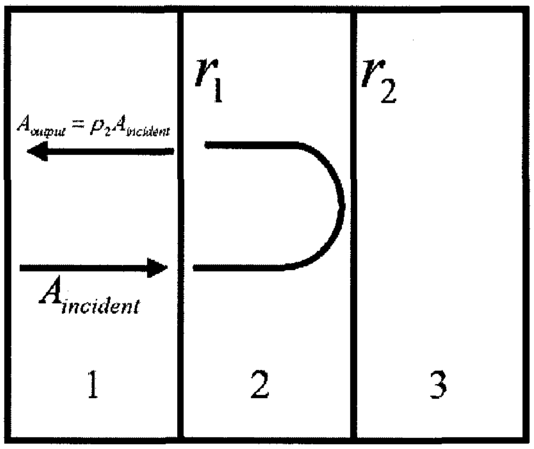

Fig. 19. Reflection from three planes. The incident amplitude A_{inc} undergoes reflections from the surfaces r_1 and r_2. These two reflections can be treated as one reflection with a complex reflectivity ρ_2.

The complex reflectivity from a series of three adjacent films can be determined from:

$$\rho_2 = \frac{r_1 + r_2 \exp(-i\delta)}{1 + r_1 r_2 \exp(-i\delta)} \tag{18}$$

Here ρ_2 is a complex reflectivity, and r_1 and r_2 are the Fresnel reflection coefficients of the first and second interfaces. δ is the accumulated phase by a double pass through layer 2.

$$\delta = |\vec{k}| 2d = \frac{4\pi n_2}{\lambda_o} d \qquad (19)$$

where n_2 is the index of refraction of layer 2, λ_o is the free space wavelength and d is the thickness of layer 2. As shown in Fig. 20 a grating can be divided into a long series of i segments.

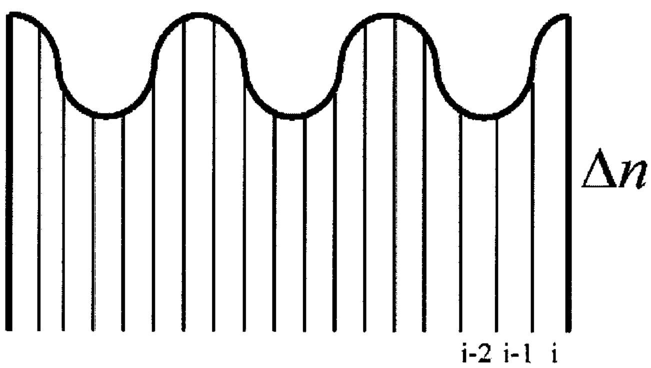

Fig. 20. A grating can be subdivided into a series of Fresnel reflections. The total complex reflectivity can be determined through an iterative process.

Starting at the extreme end of a series of thin films the complex reflectivity can be determined for the last three segments.

$$\rho_{i-1} = \frac{r_{i-2} + r_{i-1}\exp(-i\delta)}{1 + r_{i-2} r_{i-1}\exp(-i\delta)} \qquad (20)$$

The reflectivity is then calculated for the layers i-3, i-2, and i-1 where the reflectivity between the i-1 and i-2 segments is the complex reflectivity ρ_{i-1}. The index of refraction can be taken as the average within the segment. This iterative procedure can be carried out for the entire series of segments to determine the reflectivity for the entire grating.

Rouard's method is not, however, without it's limitations. Each Fresnel zone is required to be much narrower than that required for the transfer matrix approach. In the case of modeling Type I-IR ultrafast lasers it was found that each Fresnel zone had to be as small as 50 nm to adequate model the grating spectra [59]. A Fresnel zone of 50 nm is roughly an order of magnitude smaller than is usually required for the transfer matrix approach. As a consequence Rouard's method tends to require more computation time. Another disadvantage is that Rouard's method does tend to misrepresent the actual index change in the medium when the grating forms in the cladding as well as the core, as is the case with ultrafast gratings. Because the model only considers index change and not the coupling coefficient an increase in overlap of the grating with the core mode will be misinterpreted as an increase in index change [59].

1.5. Some Unique Properties of Ultrafast Gratings

1.5.1. Intrinsic Higher Order Resonances

Any uniform periodic grating structure can be modeled with the use of Coupled Mode Theory. One need only decompose the grating structure in terms of its Fourier series components. For a grating structure that is not purely sinusoidal, higher order grating resonances result from the higher order Fourier components. The amplitude of the reflected signal at the fundamental pitch is governed by the magnitude of the Fourier component at that wavelength [60].

Typically, UV gratings do not exhibit higher order resonances until the induced index change in the material begins to saturate [61] as shown in Fig. 21. As the index change saturates, the profile becomes nonsinusoidal and will begin to exhibit Bragg resonances at λ_{Bragg}/n where $n = 2,3,4,\ldots$

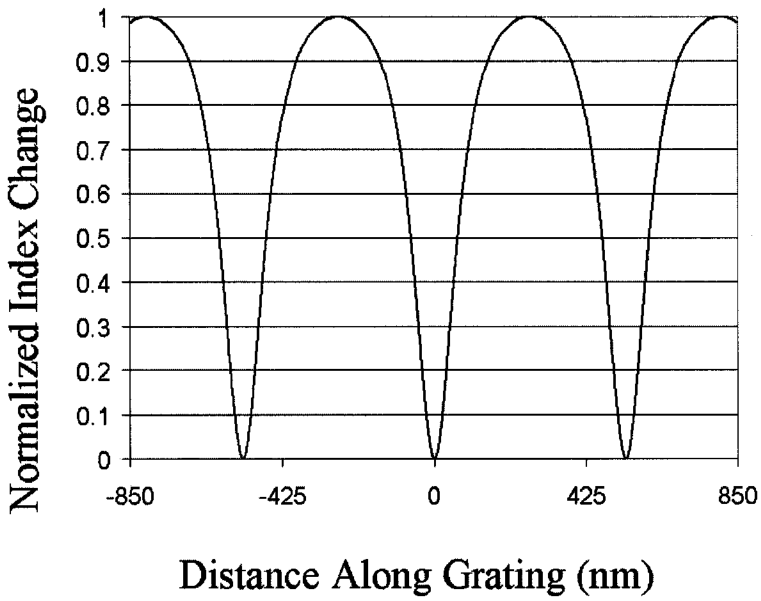

Fig. 21. Saturated index change profile for a uniform UV grating. As the grating is not purely sinusoidal the spectral response will exhibit higher order resonances.

Gratings induced with an ultrafast IR laser have been shown to depend nonlinearly on the incident laser intensity [22]. The observed fifth order dependence of the index change on the input interference pattern intensity means that the modeled grating profile will have the shape shown in Fig. 22.

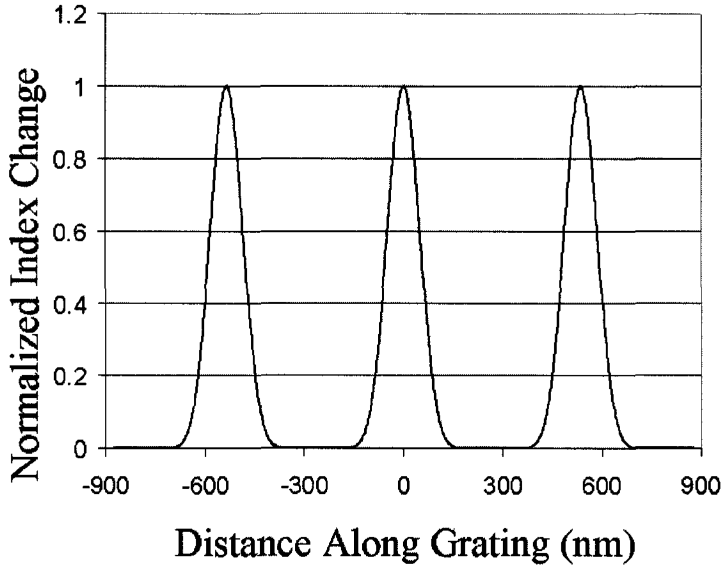

Fig. 22. The index change profile for a grating that depends nonlinearly on the incident interference intensity. This profile also deviates from a pure sinusoid and this grating will exhibit an intrinsic higher order response. This profile is a modeled result.

When this profile is decomposed there are total of 5 harmonics and a contribution to the effective (the dc component) index approximately 0.5 times that of UV induced gratings. This means that ultrafast gratings possess intrinsic higher order resonances at index changes far below that needed for saturation of the index change. Gratings produced with an ultrafast laser source have been shown to exhibit higher order gratings [62] as illustrated in Fig. 23 for a grating with a pitch of 2.14 μm (phase mask with a pitch of 4.28 μm) . The resonances depicted in the figure are the 4^{th} and 5^{th} order peaks at 1550 nm and 1240 nm, respectively. This spectrum is measured with a broadband white light source and a spectrum analyzer set to a resolution of 1 nm, therefore, the transmission loss does not appear as large as it is in reality.

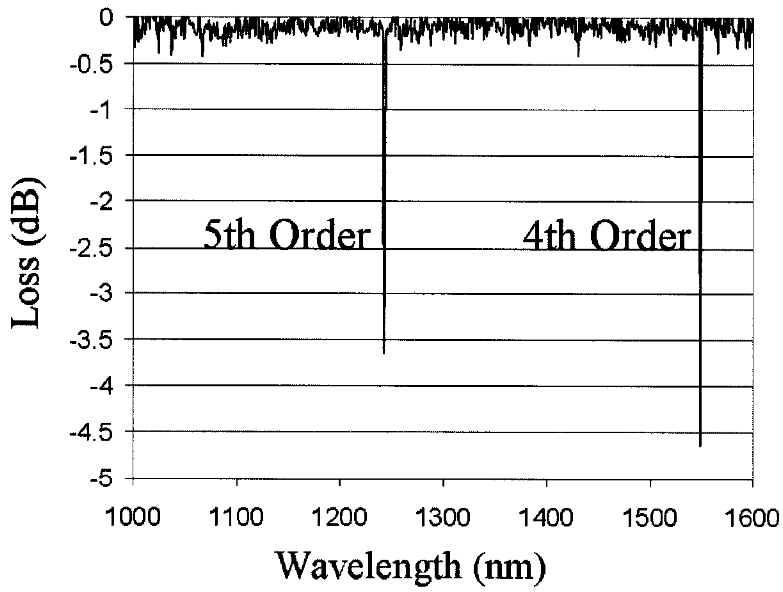

Fig. 23. Measurement of higher order grating responses in a grating fabricated with an ultrafast laser.

It is possible to model ultrafast gratings with coupled mode theory. The perceived index change will then simply be the Fourier component of the grating profile at the Bragg resonance. This is not a measure of the true index change in the material however, as the true grating structure is composed of a number of higher order components. Rouard's method is attractive for modeling ultrafast written gratings as higher order resonances are taken into consideration in the calculation and the modeled index change is perhaps a more true measure of the actual index change in the medium.

The presence of higher order resonances may also present some complications for reliable fabrication of apodized gratings. The ac and dc Fourier components of UV induced grating are equal as in Eq. (6). With equal ac and dc components tailoring the spectral profile of a fiber Bragg grating is a straightforward process [53]. However, as ultrafast gratings possess higher order spectral components it is no longer accurate to assume equal ac and dc Fourier components. Knowledge of the relative magnitude of the

Fourier components in ultrafast gratings would be critical for the reliable fabrication of spectrally tailored gratings.

1.5.2. Cladding Mode Suppression and the overlap integral

Coupling of light from the core mode of the fiber to cladding modes is governed by the coupling coefficient:

$$\kappa_{core,clad} = \frac{2\pi}{\lambda} \iint dxdy \Delta n_1 \varepsilon_{core}(x,y) \varepsilon_{clad}(x,y)^* \tag{21}$$

λ is the free space wavelength, Δn_1 is the first order term in the index change Fourier series and ε are the transverse fiber mode profiles. If it is possible produce a similar grating in both the core and cladding region then, by virtue of the orthogonality of the fiber modes, this coupling vanishes. It has been demonstrated that ultrafast lasers modify both the core and cladding region of the fiber [47]. As a consequence of this it is possible to create a quasi-uniform index change throughout both the core and cladding region. This uniform grating structure has been shown to suppress the coupling of the core mode to the cladding modes. Suppression of coupling to cladding modes normally requires specially designed fiber that contains Ge doping in both the core and cladding region [63]. As shown in Fig. 24 ultrafast lasers have been used to suppress cladding modes in standard SMF-28 fiber.

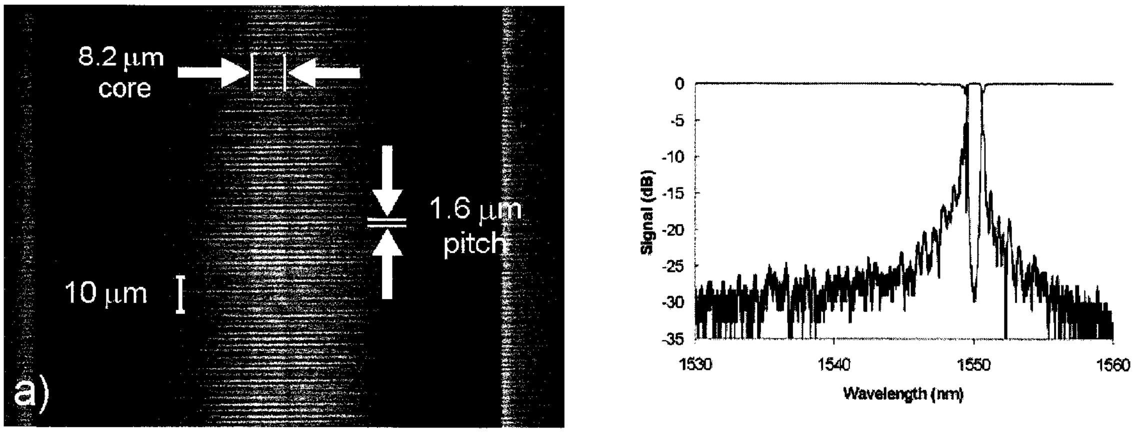

(b)

Fig. 24. (a) Optical microscope image of an ultrafast gratings written in standard SMF-28 fiber. Clearly the index modulation is present in both the core and cladding regions of the fiber. (b) The spectral response of the grating exhibits no cladding modes resonances on the blue side of the spectrum (commonly as large as 2-3 dB). (Ref. [47])

1.5.3. Gratings in Novel Materials

One particularly powerful property of ultrafast lasers is that they provide the capability to modify a wide range of materials. This is likely due to the fact that the gratings formation mechanism does not rely on the presence of germanium for photosensitivity. Gratings have been formed in materials as varied as sapphire crystal fiber [64], Lithium Niobate [65], borosilicate glass [66], photonic crystal fiber [67], and Fluoride fiber[68].

1.6. Statement of Contributions

Here I will outline my contribution to the articles presented in this thesis. In a number of these studies I was given free reign to pursue my ideas and Dr. Stephen Mihailov and Dr. Dan Grobnic were both collaborators and advisors. Our approach was, basically, to simultaneously pursue research in both the more 'fundamental' aspects of ultrafast grating fabrication and applications of these gratings. A number of the topics I investigated such as order walk-off, grating types and Rouard's method modeling appear in this thesis. Also appearing is Dr. Grobnic's cladding mode suppression paper and sapphire grating paper, which indicates the potential of ultrafast grating technology and techniques.

Article I

S.J. Mihailov, **C.W. Smelser**, P. Lu, R.B. Walker, H. Ding, D. Grobnic, G. Henderson and J. Unruh: "*Fiber Bragg gratings made with a phase mask and 800 nm femtosecond radiation*" Optics Letters **28** (12), p. 995-997 (2003)

Dr. Stephen Mihailov suggested that we attempt to write a grating using a silica phase mask and an ultrafast laser. He designed the gratings with multiple pitches and I was tasked with setting up and attempting to perform the experiment. After approximately a month of preliminary experiments I succeeded in writing a phase mask assisted ultrafast grating. Since then the research has progressed significantly.

Article II

C.W. Smelser, S. J. Mihailov, D. Grobnic, P. Lu, R. B. Walker, H. Ding and X. Dai: "*Multiple Beam Interference Patterns in Optical Fiber Generated with Ultrafast Pulses and a Phase Mask*" Optics Letters **29** (13), p.1458-1460 (2004).

Dr. Mihailov and Huimin Ding had discovered that the gratings could be viewed under the optical microscope. I took pictures of grating patterns and developed a multiple beam interference model to simulate them. In the process I noticed that the patterns depended on the laser pulse length. I modified my code to accommodate a pulsed source and, in so doing, discovered phase mask order walk-off. In this case I performed the experiment, developed the simulation and wrote the manuscript.

Article III

C.W. Smelser, D. Grobnic, S. J. Mihailov: "*Generation of Pure Two beam Interference Grating Structures in an Optical Fiber With a Femtosecond IR Source and a Phase Mask*" Optics Letters **29** (15), p.1730-1732 (2004).

In order to confirm the order walk-off simulation predictions I went and performed experiments to determine the grating profile as a function of phase mask fiber separation. These results compared very favorably to the expected interference patterns. I was then responsible for writing the manuscript.

Article IV

C.W. Smelser, S. J. Mihailov, D. Grobnic: "*Hydrogen Loading for Fiber Grating Writing with a Femtosecond Laser and a Phase Mask*" Optics Letters **29** (18), p.2127-2129 (2004).

After the initial success in Article I Dr. Mihailov had suggested determining the impact of hydrogen loading on the grating formation threshold. The initial results, published at a conference in 2003, indicated that the grating threshold was lower in the Ge-doped region of SMF-28 fiber. With the aid of the order walk-off technique developed in Article III it was possible to more accurately measure the threshold for grating growth. I performed the experiments and wrote the manuscript.

Article V

D. Grobnic, **C. W. Smelser**, S. J. Mihailov, R. B. Walker and P. Lu: "*Fiber Bragg Gratings with Suppressed Cladding Modes Made in SMF-28 with a Femtosecond IR Laser and a Phase Mask*" Photonics Technology Letters **16** (8), p. 1864-1866 (2004).

Dr. Grobnic introduced vertical scanning of the fiber with a piezo-actuated stage. This made it possible to modify both the core and cladding region of the fiber. Dr. Grobnic suggested that it might be possible to suppress the cladding modes in standard fiber with a combination of order walk-off and vertical scanning. He and I worked on the experiment together. Dr. Mihailov and Dr. Grobnic developed the manuscript.

Article VI

C. W. Smelser, S. J. Mihailov, D. Grobnic, *"Formation of Type I-IR and Type II-IR gratings with an ultrafast IR laser and a phase mask"* Opt. Express **13**, 5377-5386 (2005)

While working on the experiment for Article IV I noticed that a very strange transition was taking place where the normal grating growth would suddenly accelerate resulting in very large index changes. This was usually accompanied by the emergence of white light. After considerable debate between Dr. Mihailov, Dr. Grobnic and myself I went and performed some experiments to determine the thresholds for both grating types with femtosecond pulses and wrote several versions of this manuscript. Dr. Grobnic performed the annealing experiments, and Dr. Mihailov modified some of the content, specifically the annealing section.

Article VII

C. W. Smelser, S. J. Mihailov, and D. Grobnic, "Rouard's method modeling of type I-IR fiber Bragg gratings made using an ultrafast IR laser and a phase mask," J. Opt. Soc. Am. B 23, 2011-2017 (2006)

We collectively agreed that it would be beneficial to attempt to model these gratings using a technique such as Rouard's method. I then wrote the model and compared the type I-IR spectra to the expected nonlinear modeled results. I then developed the manuscript over a number of months, regularly consulting with Dr. Mihailov and Dr. Grobnic.

Article VIII

D. Grobnic, S. J. Mihailov, **C. W. Smelser**, H. Ding: "*Sapphire Fiber Bragg Grating Sensor Made Using Femtosecond Laser Radiation for Ultra High Temperature Applications*" Photonics Technology Letters **16** (11), p. 2505-2507 (2004).

This is the Article that I was least personally involved in. I worked briefly with Dr. Grobnic on the initial sapphire grating but Dr. Grobnic and Dr. Mihailov were far more directly involved in this study than I. It stands as an example of the enormous potential of this technology.

1.7. Overview of Articles

Article I represents the seminal work in the subject of phase mask assisted fabrication of retro-reflecting fiber Bragg gratings with an amplified Ti:sapphire laser source operating at 800 nm. These initial gratings were written in a configuration where the fiber was placed in close proximity to the phase mask in the same manner as the original UV inscribed fiber Bragg gratings.

Inspection of these gratings soon revealed that gratings fabricated with larger phase mask pitches such as 2.14, 3.21 and 4.28 μm could be viewed under an optical microscope. It became clear that, unlike the traditional UV gratings, a grating pattern was inscribed in both the cladding and core layer of the fiber. In **Article II** the patterns produced by large pitch phase masks are compared to a multiple beam interference model. While models had been developed in the past for UV grating fabrication [35] the ability to view these patterns under an optical microscope offered a unique opportunity to directly compare such a model with experiment. In addition to demonstrating the validity of the multiple beam interference model, this article demonstrates that the observed interference pattern seems to be dependent on the pulse length of the laser pulse. It was this observation of pulse length dependence in the generated interference pattern that spawned the concept of phase mask order walk-off.

Article III outlines the phase mask order walk-off experiment. It is shown that, due to the high spatial coherence of the ultrafast laser source and its short pulse nature, it is possible to create two beam interference gratings simply by placing the fiber sample at a distance from the phase mask. This effect would not be possible with the lasers that were traditionally used to fabricate UV gratings as either their spatial coherence was such that the fiber needed to be placed adjacent to the phase mask or the temporal pulse length was long enough that the phase mask orders would always overlap.

The mechanism responsible for the index change in these fibers is still a mystery. Initially it was believed that multiphoton ionization processes were responsible for triggering the index change and that color center formation plays an insignificant role in the grating formation. This conclusion seemed reasonable as the grating inscription was clearly not limited to the core region of the fiber. It seemed reasonable then that enhancement of photosensitivity through hydrogen loading, as it is usually linked the presence of germanium in the fiber core, would not be possible with ultrafast grating fabrication. Interestingly, **Article IV** demonstrates that the grating writing intensity threshold in hydrogen loaded SMF-28 fiber is actually a factor of 3 smaller than in unloaded or all silica core fiber. This result was perhaps the first evidence of the commonalities between low intensity ultrafast grating inscription and UV inscribed gratings.

The discovery of order walk-off and two beam interference described in Article III coupled with the presence of the grating in both the core and cladding region suggested an intriguing application for this remote writing technique. Due to fiber mode orthogonality the coupling of light from the core mode of the fiber to the cladding modes can be eliminated if the grating can be written smoothly throughout the core and cladding region of the fiber. Normally, with UV laser sources, special germanium-boron co-doped fiber is required for this [53]. In these fibers the cladding mode loss has been reduced to as low as 0.1 dB. **Article V** demonstrates that, through the used of the two beam interference technique with an ultrafast laser source, the cladding mode loss can be reduced to ~0.1 dB in standard SMF-28 fiber without special photosensitization.

As was suggested by the hydrogen loading experiment, ultrafast gratings may have more in common with UV gratings than originally believed. The original ultrafast fiber Bragg gratings were fabricated with the fiber placed in close proximity to the phase mask. The hydrogen loading experiment, two-beam interference, and cladding mode suppression experiment were performed with the fiber placed away from the phase mask. The original gratings had been shown to possess high temperature stability in a manner similar to single shot Type II UV written gratings. As outlined in **Article VI** it was now becoming clear that there were two regimes of grating growth, termed Type I-IR and Type II-IR. The gratings written in close proximity to the mask that exhibited abrupt grating growth and were shown to be high temperature stable were referred to as Type II-IR gratings. The gratings that exhibited monotonic growth similar to Type I UV written gratings were referred to as Type I-IR. Type I-IR gratings were also shown to be unstable at high temperatures. As the grating growth in Type I-IR gratings was monotonic and the order walk-off technique offered some control over the grating growth it now became possible to determine how the index change growth rate in the grating depended on the interference field intensity. Naturally, as the 800 nm laser wavelength was far removed from any absorption bands in Ge-doped silica, it seemed reasonable that the index change was related to a nonlinear absorption process. It was demonstrated, at the end of **Article VI**, that the index change could be related to a 5 photon absorption process.

The nonlinear dependence of the index change with the interference field intensity and the presence of absorption in the cladding layer would almost certainly pose some problems for modeling ultrafast fabricated gratings. **Article VII** outlines an attempt to utilize Rouard's grating modeling method to model Type I-IR ultrafast gratings. It is shown that at low intensities the grating profile appears to be nearly consistent with the 5-photon dependence of the grating profile on the input field intensity. However, at higher intensities the resulting spectrum deviates significantly from the models predicted spectrum. It is possible that absorption in the cladding drastically modifies the interference field impinging on the fiber core.

One of the main benefits of grating fabrication with utrafast laser sources is the freedom to modify a large range of materials. One such material, that has very attracted physical properties for high temperature sensor applications, is sapphire crystal fiber. **Article VIII** demonstrates a retro-reflecting multi-mode temperature sensor in sapphire crystal fiber.

Article I

S.J. Mihailov, C.W. Smelser, P. Lu, R.B. Walker, H. Ding, D. Grobnic, G. Henderson and J. Unruh: "*Fiber Bragg gratings made with a phase mask and 800 nm femtosecond radiation*" Optics Letters 28 (12), p. 995-997 (2003)

Fiber Bragg gratings made with a phase mask and 800-nm femtosecond radiation

Stephen J. Mihailov, Christopher W. Smelser, Ping Lu, Robert B. Walker, Dan Grobnic, Huimin Ding, and George Henderson

Communications Research Centre Canada, 3701 Carling Avenue, P.O. Box 11490, Station H, Ottawa, Ontario K2H 8S2, Canada

James Unruh

Photronics, Inc., 601 Millenium Drive, Allen, Texas 75013

Received February 20, 2003

High-quality retroreflecting fiber Bragg gratings were written in standard Ge-doped telecom fiber (Corning SMF-28) after a few minutes exposure with pulsed 800-nm, 120-fs laser radiation by use of a deep-etch silica zero-order nulled phase mask optimized for 800 nm. Induced index modulations of 1.9×10^{-3} were achieved with peak power intensities of 1.2×10^{13} W/cm^2 without any fiber sensitization. The fiber gratings are stable and did not erase after 2 weeks at 300 °C. The primary mechanism of induced index change results from a structural modification to the fiber core. © 2003 Optical Society of America

OCIS codes: 320.7140, 320.2250, 350.3390, 230.1480.

Recently there has been considerable interest in the use of ultrahigh-peak-power femtosecond laser radiation for the induction of index change in dielectric materials to produce waveguide structures.[1,2] In existing waveguide structures, for example, in optical fiber, femtosecond laser systems have been used to fabricate long-period fiber grating structures in a step-and-repeat fashion.[3,4] Fertein *et al.*[4] were able to induce index changes as high as 6×10^{-3} in standard Ge-doped telecom fiber. Traditional fiber Bragg grating (FBG) structures have usually been written by UV exposure of Ge-doped fiber either holographically[5] or through a zero-order nulled phase mask.[6] For femtosecond systems, interferometric setups for holographic exposure are nontrivial to align, since path lengths need to be matched to within the spatial location of the femtosecond pulse.[7] In the case of a 120-fs beam, path lengths would need to be matched to within 36 μm of each other. The phase mask technique has several advantages over the holographic technique in terms of reproducibility and ease of alignment especially in the case of laser sources with low spatial and temporal coherence as path lengths of each interferometric arm are automatically matched. A potential problem with writing gratings that use the phase mask technique and femtosecond pulses is that the spectral content of the femtosecond pulse is large, and when the pulse passes through the phase mask it will be broadly dispersed, and the energy will be spread over a large area.[8] Using phase masks with pitches that are much larger than the wavelength of the incident radiation reduces the effect of the spreading of the large spectral content of the pulse.[9] In this way a zero-order nulled phase mask was successfully used to inscribe high-quality, higher-order Bragg gratings with high index modulation (Δn) in standard telecom fiber.

Ge-doped SMF-28 fiber was exposed to laser pulses of 120-fs duration that were generated by a Ti:sapphire amplifier at a wavelength of 800 nm and up to 1-kHz repetition rate. The Fourier-transform-limited bandwidth of this pulse was ~8 nm. The 2-mm-diameter beam was focused with a cylindrical lens with a focal length of 80 mm through the silica phase mask onto the fiber. The fiber was positioned in close proximity to the phase mask. We selected the short focal length of the lens to produce sufficient intensity in the fiber but avoid supercontinuum generation in the phase mask. Considering Gaussian beam optics, the width of the focal spot size would be $w \approx \lambda f / \pi w_0$, where λ is the wavelength, f is the focal length of the lens, and w_0 is the incident beam diameter. For 300-μJ pulse energies, a peak intensity of 1.2×10^{13} W/cm^2 was produced. The Rayleigh range for the focused beam is $z_R = \pi w^2 / \lambda = 407$ μm.

The phase masks used in this work were precisely etched to produce low zero-order transmission at 800 nm. A series of phase mask patterns were written on a single 12.7-cm-square fused-silica substrate and coated with a thin layer of chromium. A fifth-generation MEBES electron-beam writer was used to produce uniform pitch patterns. After the lithographic exposure of a resist by use of a standard poly(butene-1-sulphone) wet process the grating pattern was transferred into the chrome layer. The exposed quartz on the mask was then etched for optimal zero-order nullification at 800 nm by use of fluorine-based chemistry in an Applied Materials DPS dry-etch tool. Because of the depth requirement of 925 nm, a special etch process was used in which polymer buildup during the reactive-ion etching was controlled. This process allowed a sidewall angle of 85° to be maintained even with an aspect ratio of 1.7:1 at the smallest pitch. After the quartz etch the remaining chrome was removed with a wet-etch process.

At the Bragg resonance λ_0 the pitch of the grating structure in the fiber, Λ, is defined by $m\lambda_0 = 2n_{\text{eff}}\Lambda$,

0146-9592/03/120995-03$15.00/0

where m is the order number and n_{eff} is the effective index of the fiber. With good zero-order nulling, $\Lambda = \Lambda_m/2$, where Λ_m is the mask pitch. Four masks were produced with different pitches such that higher-order Bragg resonances occurred at 1550 nm, namely, 4.284, 3.213, 2.142, and 1.071 μm. Measurements of the diffracted-order transmission of the unfocused beam through the phase masks are shown in Table 1. Better aspect ratios of the grating grooves were achieved for the higher-order phase mask pitches, which resulted in good zero-order nulling (<2%).

When the focused beam was diffracted by the phase mask there was evidence of third-harmonic generation of 266-nm UV photons in the silica substrate. Since the phase mask was fabricated from amorphous fused silica, no second-harmonic generation was expected or observed. The energy level of the UV-diffracted order could not be measured with the powermeter, making the energy of UV-generated photons <1 μJ/pulse.

Gratings were successfully written in fibers with each of the phase masks by use of similar pulse powers and exposure times, namely, 300 μJ/pulse, 1-kHz repetition rate, and 1–2-min exposure times (see Fig. 1). Gratings were measured with an Er^+ white-light source and spectrum analyzer. As can be seen from the figure, the strengths and bandwidths of each of the higher-order gratings are similar to the modeled first-order grating [Fig. 1(a)], implying that at the Bragg resonance the induced index modulation can be inferred from the expression for maximum reflectivity $R = \tanh^2(\kappa L)$, where the coupling coefficient $\kappa = \pi m \Delta n_m / 2 n_{eff} \Lambda_m$, L is the grating length, and Δn_m is the index modulation of the mth order.[10] The simulated grating shown in Fig. 1(a) has a $\Delta n_1 = 8.5 \times 10^{-4}$ for $L = 2$ mm. Out-of-band insertion loss for these weaker gratings was <0.3 dB. The presence of lossy backward-propagating cladding modes in the spectra suggests that the photoinscription is localized to the Ge-doped core region only rather than into the surrounding cladding. This localized photoinscription is similar to UV-induced fiber gratings in which the index perturbation responsible for cladding-mode coupling generally exists only in the core of the fiber.[11] Annealing of the gratings at 300 °C for 2 weeks resulted in no change in the reflectivity, implying that the dominant mechanism of induced index change is different from the UV-induced color-center photosensitivity mechanism involving GeO defect centers.[12] It is possible that the mechanism for photoinduced index change is a multiphoton absorption process that is associated with the Ge doping. At present the contribution of the third-order UV-generated photons in the photoinduced index change is unclear. Power-dependent studies of index change and power density will be presented elsewhere.

The mechanism for index change may be more analogous to the damage-type mechanisms seen in type II FBGs.[13] Unlike typical type II UV-induced single-shot damage gratings, which often have poor-quality spectra and are difficult to reproduce, femtosecond-pulse-induced gratings can be made with multiple-pulse exposures and show linear growth in reflectivity with the number of incident pulses. In Fig. 2 the variation in reflectivity of a grating versus the number of irradiating pulses, along with a shift in λ_0 of the device, was measured with a Er^+ white-light source and spectrum analyzer. After 15,000 pulses the dynamic range of the detection system was reached. The resonance shift corresponds to a change of n_{eff} of 1.8×10^{-4}. In this case the device was written with the 2.142-μm pitch mask at a repetition rate that was reduced from 1 kHz to 10 Hz. After 22,000 pulses the reflectivity of the device was measured with a tunable laser to be −44.5 dB and is shown in Fig. 3. Out-of-band insertion loss of the device was measured

Table 1. Coupling of 800-nm Radiation Into Various Phase Mask Orders

	Transmission (%)	
Mask Pitch Λ_m (μm)	0 order	±1 order
1.071	25.7	36.4
2.142	6.0	36.4
3.213	1.9	38.8
4.284	1.3	39.9

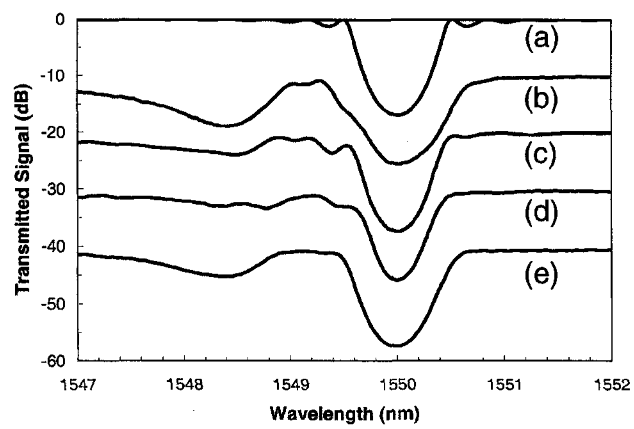

Fig. 1. Spectral responses of FBGs written with the different-order phase masks. Spectra are offset by −10 dB for clarity. (a) Simulated 0.5355-μm pitch grating in fiber, $L = 2$ mm, $\Delta n_1 = 8.5 \times 10^{-4}$. (b), (c), (d), and (e) are gratings written with the 1.071-, 2.142-, 3.213-, and 4.284-μm pitch masks, respectively.

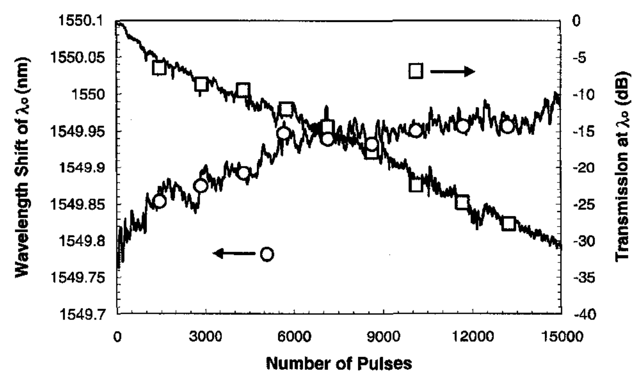

Fig. 2. Variation of reflectivity and resonant wavelength with the number of incident IR pulses, (300 μJ/pulse, 10 Hz). The squares denote reflectivity; circles, wavelength shift.

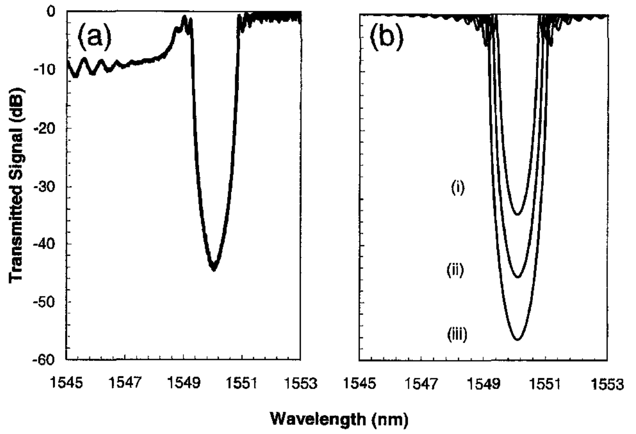

Fig. 3. (a) Reflectivity of a high-order grating written with the 2.142-μm pitch mask. (b) Simulated 0.5355-μm pitch grating in fiber, $L = 2$ mm, with Δn_1 values of (i) $= 1.5 \times 10^{-3}$, (ii) $= 1.9 \times 10^{-3}$, and (iii) $= 2.2 \times 10^{-3}$.

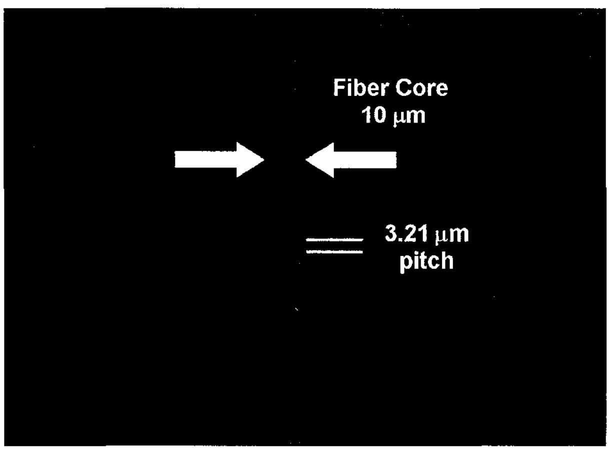

Fig. 4. Photographic image of photoinduced index modulation as seen through an optical microscope. The spacing between lines in the image corresponds to the 3.213-μm period of the phase mask.

with the cutback method to be 0.57 dB, which is lower than ~1-dB loss of strong UV gratings written in hydrogen-sensitized fiber.[14] Modeled responses of a standard grating with a pitch of 0.5355 μm, length of 2 mm, and Δn values of 1.5, 1.9, and 2.2×10^{-3} are shown for comparison. A linear extrapolation of the reflectivity curve in Fig. 2 with the data point in Fig. 3 indicated that index modulation had not as yet saturated. The effective index modulation amplitude is ten times larger than the average index change. The index change that is observed is mainly structural, resulting from compaction or dilation in the bright fringes of the optical pattern and the index modulation amplitude is due to adjacent regions of opposite index change.

By use of an optical microscope, index modulations in the core were directly observed for a strong grating made with 3.212-μm pitch mask (see Fig. 4). Similar to single-shot excimer damage gratings,[15] Λ of the fiber gratings is the same as the phase mask; however, a 90° rotation of the fiber showed that the photoinduced index modulation is not localized to the core–cladding interface but extends across the entire core of the fiber. As well, structural modifications to the air–cladding surface were also observed.[16] Such macroscopic structural modifications of the glass are highly stable at elevated temperatures.

Higher-order retroreflective fiber Bragg gratings were written in standard SMF-28 telecom fiber with 800-nm infrared femtosecond radiation and a zero-order nulled phase mask. The gratings have spectral quality similar to type I, UV-induced FBGs but with the ultrastable temperature characteristics of type II gratings. Observed index modulations in the grating structures were consistent with fundamental-order pitch gratings with index modulation of 1.9×10^{-3}.

The authors thank D. P. Mathurs and Andy Zanzal of Photronics, Inc., for useful discussions as well as the reviewers for their insightful comments. S. J. Mihailov's e-mail address is stephen.mihailov@crc.ca.

References

1. K. M. Davis, K. Miura, N. Sugimoto, and K. Hirao, Opt. Lett. **21,** 1729 (1996).
2. K. Miura, J. Qui, H. Inouye, T. Mitsuyu, and K. Hirao, Appl. Phys. Lett. **71,** 3329 (1997).
3. Y. Kondo, K. Nouchi, T. Mitsuyu, M. Watanabe, P. G. Kazansky, and K. Hirao, Opt. Lett. **24,** 646 (1999).
4. E. Fertein, C. Przygodzki, H. Delbarre, A. Hidayat, M. Douay, and P. Niay, Appl. Opt. **40,** 3506 (2001).
5. G. Meltz, W. W. Morey, and W. H. Glenn, Opt. Lett. **14,** 823 (1989).
6. K. O. Hill, B. Malo, F. Bilodeau, D. C. Johnson, and J. Albert, Appl. Phys. Lett. **62,** 1035 (1993).
7. K.-I. Kawamura, N. Sarukura, M. Hirano, and H. Hosono, Appl. Phys. Lett. **78,** 1038 (2001).
8. G. D. Goodno, G. Dadusc, and R. J. D. Miller, J. Opt. Soc. Am. B **15,** 1791 (1998).
9. P. E. Dyer, R. J. Farley, and R. Giedl, Opt. Commun. **115,** 327 (1995).
10. W. X. Xie, M. Douay, P. Bernage, P. Niay, J. F. Bayon, and T. Georges, Opt. Commun. **101,** 85 (1993).
11. T. Erdogan, J. Opt. Soc. Am. A **14,** 1760 (1997).
12. T. Erdogan, V. Mizrahi, P. J. Lemaire, and D. Monroe, J. Appl. Phys. **76,** 73 (1994).
13. J. L. Archambault, L. Reekie, and P. St. J. Russell, Electron. Lett. **29,** 453 (1993).
14. J. Canning, M. Åslund, and P.-F. Hu, Opt. Lett. **25,** 1621 (2000).
15. B. Malo, D. C. Johnson, F. Bilodeau, J. Albert, and K. O. Hill, Opt. Lett. **18,** 1277 (1993).
16. S. J. Mihailov and M. C. Gower, Electron. Lett. **30,** 707 (1994).

Article II

C.W. Smelser, S. J. Mihailov, D. Grobnic, P. Lu, R. B. Walker, H. Ding and X. Dai: "*Multiple Beam Interference Patterns in Optical Fiber Generated with Ultrafast Pulses and a Phase Mask*" Optics Letters 29 (13), p.1458-1460 (2004).

Multiple-beam interference patterns in optical fiber generated with ultrafast pulses and a phase mask

Christopher W. Smelser, Stephen J. Mihailov, Dan Grobnic, Ping Lu, Robert B. Walker, Huimin Ding, and Xiaoli Dai

Communications Research Centre Canada, 3701 Carling Avenue, P.O. Box 11490, Station H, Ottawa, Ontario, Canada K2H 8S2

Received February 11, 2004

We compare the cladding patterns present in grating structures fabricated with an ultrafast laser and a phase mask with a cw beam interference model. We find that the observed patterns agree well with the model results for picosecond pulses; however, for femtosecond pulses, we show that the full bandwidth and the pulsed nature of the sources must be considered because the pattern can be affected by group-velocity walk-off. An interesting consequence of order walk-off is the possibility of pure two-beam interference generation with a phase mask in the femtosecond pulse regime. © 2004 Optical Society of America

OCIS codes: 320.7140, 230.1480, 320.5390, 320.2250, 350.3390, 050.0050.

Fiber Bragg grating (FBG) technology enjoys a wide range of applications in telecommunications and sensors. One common method for fabricating FBGs is to focus a pulsed or cw UV laser source through a 0th-order nulled phase mask onto a fiber.[1] The beam orders generated by the phase mask then interfere and write a grating pattern into the core of the fiber. Several groups have modeled and directly measured the interference patterns associated with the exposure of 0th-order nulled phase masks with these UV sources.[2–4] Excimer laser sources that are often used to write FBGs have low spatiotemporal coherence and nanosecond pulse durations. The models that were developed to understand the interference phenomenon assumed these laser properties.[2,4] Recently, we demonstrated that it is possible to use an ultrafast femtosecond and picosecond IR source to fabricate gratings in standard SMF-28 and all-silica-core fiber, which can be observed through an optical microscope.[5,6] In these works there was a significant amount of material modification in the cladding layer. The pattern of this modification appears similar to that produced from multiple-beam interference. A model describing ultrafast interference patterns would have to take the larger bandwidth and the coherent properties of the source into consideration.

In this Letter we initially compare the cladding structure observed in gratings written with an ultrafast IR laser to the pattern predicted by a cw interference model. We then include the full bandwidth and discuss the group-velocity walk-off effect that should be observed for femtosecond pulse lengths.

FBGs were fabricated in all-silica-core single-mode fiber with multiple pulses from an ultrafast femtosecond and picosecond source by focusing the 800-nm output of a regeneratively amplified Ti:sapphire laser with an 80-mm cylindrical lens through a silica 0th-order nulled phase mask onto the fiber sample. The pulse energy was set at 600 μJ for both picosecond and femtosecond pulse durations. All-silica-core fiber was chosen because there appears to be increased modification of the cladding in its fluorine-doped cladding. The fibers were placed in near contact with the phase mask. When operating in either femtosecond or picosecond mode, the Fourier-transform-limited pulse duration was 125 fs or 2 ps, respectively, as measured with an autocorrelator. In the femtosecond regime we observed that it was preferable to introduce a chirp into the pulse, which lengthened the pulse to approximately 400 fs. We believe that this is required because of nonlinear effects in the phase mask.[6] Phase masks with pitches of 2.14 and 4.28 μm were used, which produced higher-order Bragg gratings with Bragg resonances at 1550 nm. Any structural modification to the core or cladding could then be viewed under an optical microscope.

An interference model was then developed for comparison with the microscope images and to help understand the effect of the larger bandwidth of the ultrafast source. In generating the model pattern for comparison with the observed cladding structure a cw model was used. The whole bandwidth of the source was necessary to demonstrate the beam walk-off effect. The model coherently superposes plane waves corresponding to the orders of the phase mask. Unlike previous models[2–4] in which it was not necessary to take into account the propagation of the pulse envelope, in this model a time-dependent term in the exponential ensures that the resulting pulse is a traveling wave. The resulting intensity would be proportional to

$$|E(x,y,t)|^2 = \left|\sum_{\lambda}\sum_{i} a_\lambda a_i \exp[-i\omega t + ikx\sin(\theta_i) + ky\cos(\theta_i)]\right|^2 . \quad (1)$$

Here a_λ and a_i are the amplitudes of the spectral components and diffracted orders, respectively. ω is the angular frequency, and k is the magnitude of the wave vector. The x axis is parallel to the phase mask while the y axis is normal to the phase mask. The central wavelength was set at 800 nm, and the bandwidth for the pulsed model was assumed to be Gaussian. The order amplitudes were set by measurements

0146-9592/04/131458-03$15.00/0

of the order energy. Angles θ_i are calculated by the grating equation $\sin \theta_i = i\lambda/d$, where d is the mask pitch and λ is the wavelength in the medium. The polarization of the writing beam was parallel to the phase mask grooves, and the Fresnel reflection of the beam off the surface of the fiber was taken into consideration. The refractive index could be set at 1 or 1.45 for free space or silica, respectively. Neither the material absorption loss nor the finite transverse beam width was included in the model. To display the modeled pattern, a level curve was chosen to simulate the grating threshold.[6]

We begin with a comparison of the cw model to the observed patterns. Table 1 lists the measured power in each of the orders. Figure 1 shows the measured and modeled results for the 4.28-μm mask. Figures 1(a) and 1(b) illustrate the measured picosecond pattern and the modeled result, respectively. All 11 beams were used in the simulation. Figures 1(c) and 1(d) are the measured femtosecond and modeled five-beam interference patterns, respectively. The higher orders were discarded in producing the lower-order pattern. If we note the location of the interference fringe rows and phase shifts between rows, clearly the femtosecond result appears similar to the 5-beam interference case and the picosecond result resembles the 11-beam case. The femtosecond pattern appears to involve fewer orders. Figure 2 further demonstrates that a discrepancy exists between the picosecond and femtosecond results. Figures 2(a) and 2(b) are the measured 2-ps and modeled results with the 2.14-μm mask, respectively. The model here includes all five orders as predicted in Table 1. Figures 2(c) and 2(d) are the measured femtosecond and three-beam interference patterns (0th and $\pm$1st orders), respectively. Again the femtosecond pattern appears to include fewer orders. The cw model, as predicted from the measured orders in Table 1, fails to predict this result.

The discrepancies between the picosecond and femtosecond patterns are explained by group-velocity walk-off of phase mask order pairs. If we include the full bandwidth in the simulation, we see that the interference pattern is traced out by a pulse that propagates through space. The interference pattern is created by the overlap of the diffracted orders. The diffracted orders travel at angles set by the grating equation, and the overlap of the orders can be examined by projecting the pulse onto axes parallel and perpendicular to the phase mask. The transverse beam width of the laser used in our experiments was approximately 5 mm. For a 4.28-μm mask the peaks of the $\pm$5th orders would only be transversely displaced from the 0th order by approximately 250 μm after traveling 100 μm through free space. This displacement is a factor of 20 smaller than the beam width and would not affect the interference pattern. In a direction normal to the phase mask there would be a longitudinal separation of approximately 65 μm between the 0th and $\pm$5th orders when the 0th order reaches 100 μm. Since the spatial extent of a 150-fs pulse is only 45 μm and the strength of the $\pm$5th orders is small, there should be no contribution from the higher orders at these distances. Even if the pulse length was 400 fs, which would extend 120 μm in space, the spatial separation of 65 μm is still large. For a 2-ps pulse, for which the spatial extent of the pulse is 600 μm, a separation of 65 μm represents a

Table 1. Percentage of Energy in Each Order

Mask Pitch	4.28 μm	2.14 μm
Energy in 0th order	2.5%	7.4%
$\pm$1st orders	39.6%	37.8%
$\pm$2nd orders	1.5%	7.9%
$\pm$3rd orders	4.1%	0%
$\pm$4th orders	2%	0%
$\pm$5th orders	1.5%	0%

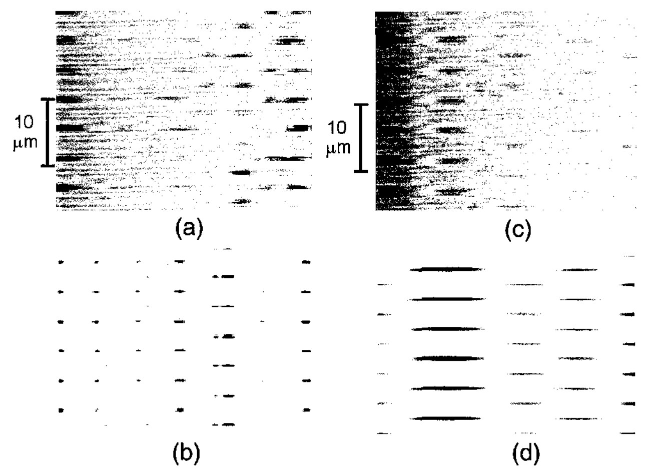

Fig. 1. (a) Microscope image of the all-silica fiber cladding after being irradiated with 2-ps pulses. (b) Modeled 11-beam interference pattern resulting from a 4.28-μm-pitch mask. (c) Image of the cladding after irradiation with 400-fs pulses. (d) Modeled result including only five beams. These images are to scale. The spacing between adjacent interference maxima is the same as the pitch of the mask (4.28 μm).

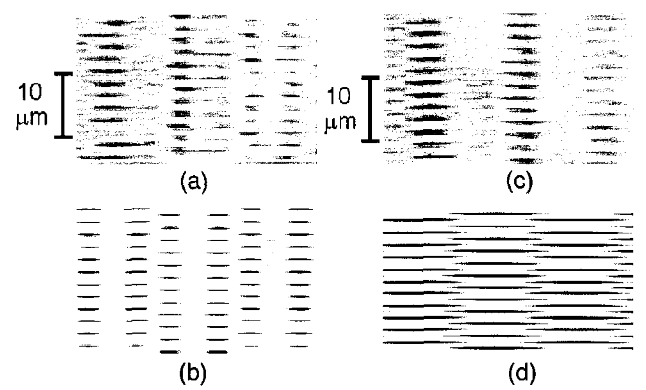

Fig. 2. (a) Microscope image of the all-silica fiber cladding after being irradiated with 2-ps pulses. (b) Modeled five-beam interference pattern resulting from a 2.14-μm-pitch mask. (c) Image of the cladding after irradiation with 400-fs pulses. (d) Modeled result including only three beams. These images are to scale. The spacing between adjacent interference maxima is the same as the pitch of the mask (2.14 μm).

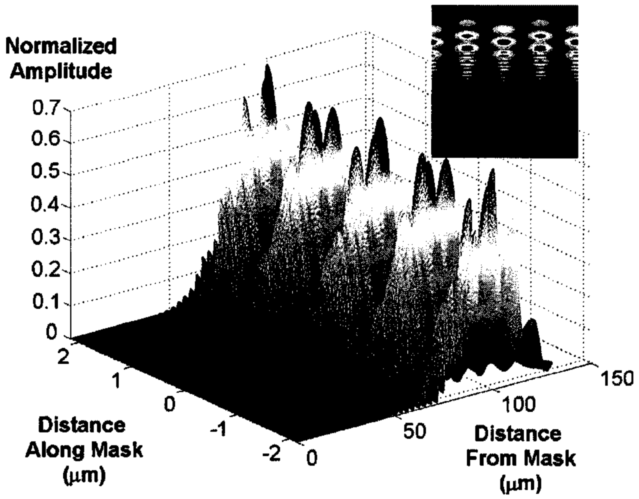

(a)

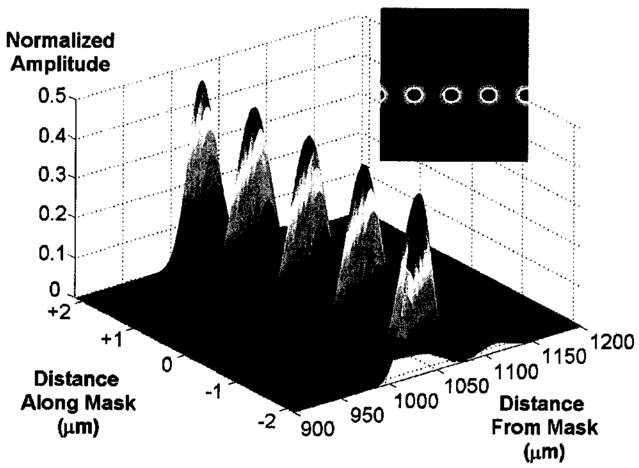

(b)

Fig. 3. (a) 150-fs pulse after it has traveled 100 μm beyond the 2-μm phase mask. Inset, top view of the pulse. (b) 150-fs pulse after it has traveled 1 mm. Inset, top view of the pulse. Near the mask the interference pattern is complicated because it involves a number of orders, whereas at distances far from the mask, the pattern is predominantly two-beam interference.

smaller fraction of the pulse length and we would expect walk-off to be minimized. Each order propagates through space at the speed of light; however, if the pulses are observed along an axis normal to the phase mask, they will appear to travel with different group velocities and the walk-off effect can be thought of as a group-velocity mismatch between the order pairs.

In Fig. 3 we include the full bandwidth in the model to illustrate the effect of the order walk-off. In Fig. 3(a) a 150-fs pulse is propagated 100 μm through free space from a 2.14-μm mask. We see that the $\pm$2nd-order beams lag approximately 30 μm behind the 0th and $\pm$1st orders. The pattern would then appear as if it were generated with only three beams because the $\pm$2nd orders carry little energy. We should not expect to observe this with a picosecond pulse because the pulse length is an order of magnitude longer and the overlap of the orders would be almost complete. At a longer distance of 1000 μm from the phase mask, as shown in Fig. 3(b), the strong $\pm$1st-order overlapping beams are seen to lag 75 μm behind a weak 0th-order beam. The weak $\pm$2nd-order beams lag 370 μm behind the 0th-order beam and are therefore not seen in the figure. One intriguing consequence of the walk-off effect is the possibility of fabricating pure two-beam interference gratings with a phase mask. A pulse that has traveled 1 mm beyond the 2-μm mask exhibits only two-beam interference. This is not strictly possible for long-pulse regimes because 0th-order nulling is not complete.

We have demonstrated that a beam interference model can be used to adequately describe the cladding pattern present after the fabrication of an ultrafast FBG with picosecond IR pulses and a phase mask. In addition to this, we have addressed the issue of the increased bandwidth of the ultrafast source and demonstrated that order walk-off can effectively reduce the number of beams involved in the interference pattern. This explains the difference between cladding patterns produced with picosecond and femtosecond sources. This effect could be exploited to produce pure two-beam interference in the core of the fiber with a phase mask.

C. Smelser's e-mail address is christopher.smelser@crc.ca.

References

1. K. O. Hill, B. Malo, F. Bilodeau, D. C. Johnson, and J. Albert, Appl. Phys. Lett. **62,** 1035 (1993).
2. P. E. Dyer, R. J. Farley, and R. Giedl, Opt. Commun. **115,** 327 (1995).
3. N. M. Dragomir, C. Rollinson, S. A. Wade, A. J. Stevenson, S. F. Collins, G. W. Baxter, P. Farrell, and A. Roberts, Opt. Lett. **28,** 789 (2003).
4. J. D. Mills, C. W. J. Hillman, B. H. Blott, and W. S. Brocklesby, Appl. Opt. **39,** 6128 (2000).
5. S. J. Mihailov, C. W. Smelser, P. Lu, R. B. Walker, D. Grobnic, H. Ding, G. Henderson, and J. Unruh, Opt. Lett. **28,** 995 (2003).
6. S. J. Mihailov, C. W. Smelser, P. Lu, R. B. Walker, D. Grobnic, H. Ding, G. Henderson, and J. Unruh, J. Lightwave Technol. **22,** 94 (2004).

Article III

C.W. Smelser, D. Grobnic, S. J. Mihailov: "*Generation of Pure Two beam Interference Grating Structures in an Optical Fiber With a Femtosecond IR Source and a Phase Mask*" Optics Letters 29 (15), p.1730-1732 (2004).

Generation of pure two-beam interference grating structures in an optical fiber with a femtosecond infrared source and a phase mask

C. W. Smelser, D. Grobnic, and S. J. Mihailov

Communications Research Centre Canada, 3701 Carling Avenue, P.O. Box 11490, Station H, Ottawa, Ontario K2H 8S2, Canada

Received February 23, 2004

Fiber Bragg gratings were fabricated in all-silica core fiber by focusing 125-fs 800-nm pulses with an 80-mm lens through a phase mask with 4.28-μm pitch onto a fiber sample. When the phase-mask–fiber separation was 5 mm the observed structure was clearly the result of two-beam interference between the ± 1 orders. The elimination of the remaining 9 orders is a consequence of the walk-off experienced by the mask orders and the short duration of the femtosecond pulse. This effect is unique to the fabrication of Bragg gratings with femtosecond sources and would not be observed with a longer pulse duration or incoherent UV sources.

OCIS codes: 320.7140, 230.1480, 320.5390, 350.3390, 050.0050.

With the advent of side-written fiber Bragg gratings there has been increased interest in the interference phenomena associated with phase masks. A common approach for inscribing fiber Bragg gratings is to focus a nanosecond UV excimer or cw argon-ion laser source through a zero-order nulled phase mask onto a fiber sample.[1] The interference pattern generated with the mask is inscribed onto the core of the fiber as the Ge-doped core absorbs the UV light to produce defects. A zero-order nulled phase mask is used in an attempt to eliminate the influence of the zero order on the resulting interference pattern. Unfortunately, a small amplitude in the zeroth order significantly affects the interference pattern.[2,3] Recently, retroreflecting fiber Bragg gratings were fabricated in SMF-28 and all-silica-core fiber with an ultrafast 800-nm source.[4,5] The grating structures could be viewed under an optical microscope. With ultrafast sources the interference patterns set up by the phase mask are imprinted in both the fiber cladding and the core. Ultrafast sources have a large bandwidth and can be treated as a coherent source. Interference patterns produced with ultrafast pulses and a phase mask can be described by a plane-wave model that takes the coherence properties and the bandwidth of ultrafast sources into account. A comparison of patterns generated with picosecond and femtosecond pulses revealed a reduction in the number of interfering orders for femtosecond pulses.[6] The interference model suggested that, owing to the short pulse length of the femtosecond source, the diffracted orders failed to overlap away from the phase mask. When the fiber is placed several millimeters from the phase mask this reduction in the number of interfering orders will, in theory, result in the interference of only the ± 1 orders.

This Letter reports the successful production of two-beam interference patterns in all-silica core fiber. First, the order walk-off effect is introduced. Next, a grating written at a phase-mask–fiber separation of 2.5 mm is studied to show that the observed interference pattern can vary along the length of the grating. Finally, grating patterns at distances ranging from 200 to 5000 μm are compared with the expected five-, three-, and two-beam interference patterns generated with a cw interference model. A pure two-beam pattern is observed at a distance of 5000 μm. Two-beam interference of the type shown in this Letter is not strictly possible with UV sources and a zero-order nulled phase mask, as the zero-order nulling is never complete and walk-off along an axis normal to the phase mask cannot occur because of the large spatial dimension of nanosecond or cw sources.

Fiber Bragg gratings were fabricated in all-silica core fiber by focusing the output of a 1000-Hz regeneratively amplified Ti:sapphire ultrafast laser source through a nominally zero-order nulled silica phase mask with an 80-mm lens onto a fiber sample. The fibers were placed at distances from the phase mask that varied from 200 μm to 5 mm. The beam remained focused at the fiber, and only the relative position of the mask was varied. The pulse energy was set at 600 μJ for phase-mask–fiber distances shorter than 2.5 mm and was increased to 800 μJ for larger distances. The pulse duration as measured with an autocorrelator was 125 fs. The measured $1/e$ radius of the beam was 2.45 mm. Each fiber was irradiated for 30 s. All-silica core fiber was used, as the grating structures were more easily fabricated in its fluorine-doped cladding than in the undoped cladding of SMF-28 fiber. A phase mask with a pitch of 4.28 μm was chosen for the experiment, and the ± 1 orders contained 80% of the energy.[6]

A cw beam interference model is used to compare the measured grating structures with the patterns expected from multiple-beam interference. This involves the coherent superposition of plane waves with angles set by the grating equation, $\sin \theta_m = m\lambda/d$. The resulting interference field would have the form

0146-9592/04/151730-03$15.00/0

$$|E(x,y)|^2 = \left| \sum_m a_m \exp[ikx \sin(\theta_m) + iky \cos(\theta_m)] \right|^2 .$$

Here a_m is the amplitude of the diffracted orders, d is the mask pitch, and k is the wave-vector amplitude. The x axis is parallel to the phase mask and perpendicular to the grooves, and the y axis is normal to the phase mask. The wavelength λ was set at 800 nm. The refractive index was assumed to be 1.45. The order amplitudes were determined from measurements of the order energy.[5] Patterns that contained fewer orders were generated by eliminating higher orders in the superposition. To display the modeled pattern we chose a level curve to simulate the grating threshold.[5]

Figure 1 demonstrates the concept of order walk-off. The images in the figure were generated by superimposing Gaussian intensity profiles traveling at angles set by the grating equation. Each order travels at the speed of light. The pulse widths of 60 μm in the y direction and 5000 μm in the x direction are comparable with experimental values. Near the mask the orders will overlap completely, and typical multiple-beam interference patterns will be observed.[6] In Fig. 1(a) the 0 order has propagated approximately 3000 μm beyond a 4.28-μm mask. The 0 and ± 1 orders still partially overlap, but the remaining orders lag behind. The 0 order leads ± 1 orders by ~60 μm, and the interference will be strongest at $x = 0$. Toward the edges of the pattern the ± 1 orders dominate the smaller contribution from the 0 order. Interference between the 0 and ± 1 orders results in an interference pattern pitch of 4.28 μm, so a transition to the two-beam pitch of 2.14 μm should be observed toward the edge of the grating pattern. At a larger distance of 5000 μm, the 0 order leads the ± 1 orders by 90 μm, and they clearly no longer overlap. Since the ± 1 orders contain most of the energy, they will be the dominant orders producing the interference pattern. The grating pattern would resemble straight lines separated by 2.14 μm, or half the pitch of the phase mask. The reason that the dominant walk-off effect is in the y direction is clearly that the spatial profile of the pulse is much smaller in this direction. For longer pulses this is no longer true, as the spatial extent in the y direction becomes very large. For example, a 30-ns source will have a spatial width of ~9 m in the y direction.

Figure 2 illustrates the observed grating pattern along the length of a grating produced at a phase-mask–fiber distance of 2.5 mm. Typical grating lengths of ~2 mm were fabricated with the 5-mm beam. Figures 2(a) and 2(c) are images of the profile at either end of the grating. The grating pitch of 2.14 μm corresponds to interference between the ± 1 orders. As in the case of Fig. 1(a) the 0 order is centered on $x = 0$ and will interfere with the ± 1 orders in this region, resulting in a pitch of 4.28 μm. This is illustrated in Fig. 2(b). Away from the center the much more energetic ± 1 orders dominate the pattern.

Figure 3 demonstrates the effect of increasing the phase-mask–fiber distance. Figures 3(a)–3(c) show the modeled five-, three-, and two-beam interference patterns for a 4.28-μm pitch mask. Figures 3(d), 3(e), and 3(f) are microscope images of the grating structures written at phase-mask–fiber distances of 200, 500, and 5000 μm, respectively. These images are of the center of the grating. At 200 μm the structure resembles the five-beam interference pattern. Further from the mask at 500 μm the pattern resembles that of the three-beam interference between the 0 and ± 1 orders. Finally, for the larger distance of 5 mm the pattern results from interference between the ± 1 orders. Two-beam interference is observed along the complete length of the grating. Although the ± 2 orders still overlap at this distance, the energy contained in them is small and the peak intensity will be below the threshold necessary to achieve a significant index change.

Two-beam interference patterns with a pitch of half that of the mask can be fabricated by exploiting the short pulse duration of a femtosecond laser source and

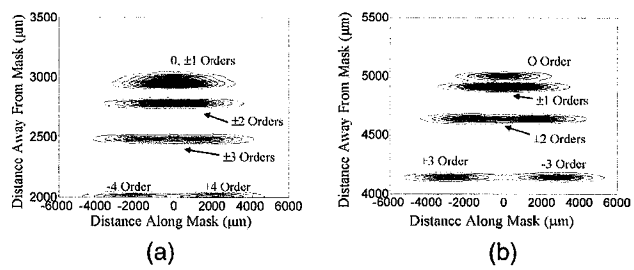

Fig. 1. Order propagation through space: (a) propagation of the phase-mask orders after the 0 order has traveled 3000 μm. Here the ± 2 orders lag behind the 0 and the ± 1 orders. The 0 and ± 1 orders will still interfere at this distance, but the interference pattern will vary along the x direction. (b) Case where the 0 order has propagated 5000 μm. The 0 order no longer overlaps the ± 1 order, resulting in two-beam interference. In these images a $1/e$ beam width of 5 mm and a temporal pulse length of approximately 60 fs were chosen, as those values are similar to the experimental parameters. The phase-mask position is $y = 0$.

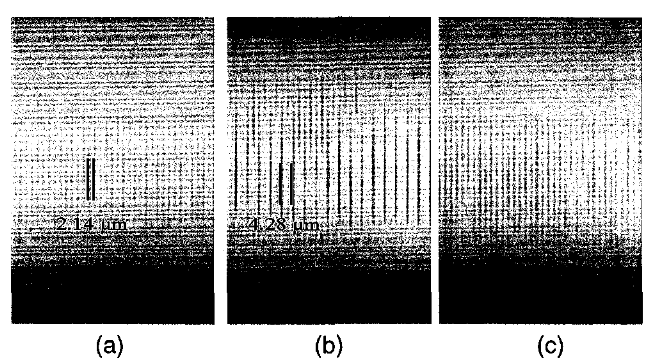

Fig. 2. (a) and (c) Microscope images of the structure at the ± 1-mm edge of a 2-mm-long grating, (b) structure in the middle of the grating ($x = 0$ mm). The grating was written with a 4.28-μm mask at a distance of 2.5 mm. The pattern has a pitch of 2.14 μm, or half that of the mask at the edges of the grating, while in the middle region the pitch is 4.28 μm, or the same as the mask. This suggests that there is strong three-beam interference in the center of the grating, whereas the interference between the more energetic ± 1 orders dominates toward the edge.

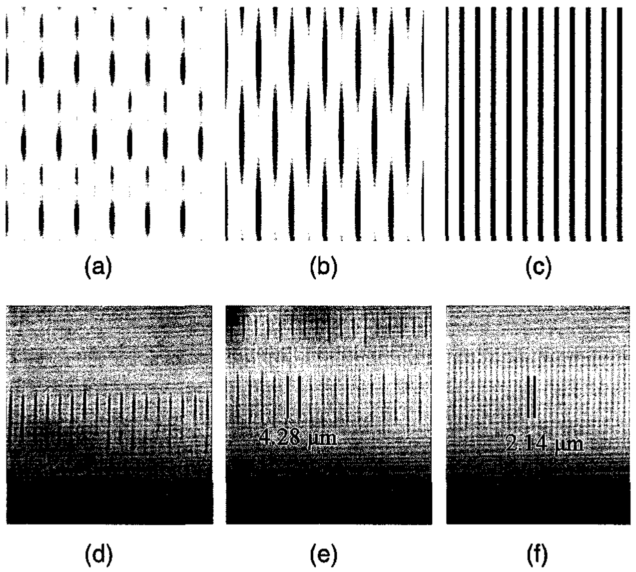

Fig. 3. Comparison of the modeled five-, three-, and two-beam interference patterns with the observed structure in the fiber at progressively larger distance from the phase mask. (a)–(c) Modeled five-, three-, and two-beam interference patterns. For comparison, (d)–(f) depict the observed grating structures at 200, 500, and 5000 μm. At 5000 μm only two-beam interference is present.

the walk-off of the diffracted phase-mask orders along an axis perpendicular to the phase mask. This is not possible for longer pulse sources, as the pulse duration is such that there would be much more order overlap at large distances from the phase mask. This effect is not restricted to the all-silica core fiber but is also present in SMF-28 fiber. The resulting interference patterns appear to be quite uniform and lack the phase jumps that are present in multiple-beam interference structures. As the structure is smooth and does not appear to be confined to the core region, one possible application of this technique is the fabrication of cladding-mode-suppressed gratings.

References

1. K. O. Hill, B. Malo, F. Bilodeau, D. C. Johnson, and J. Albert, Appl. Phys. Lett. **62,** 1035 (1993).
2. P. E. Dyer, R. J. Farley, and R. Giedl, Opt. Commun. **115,** 327 (1995).
3. J. D. Mills, C. W. J. Hillman, B. H. Blott, and W. S. Brocklesby, Appl. Opt. **39,** 6128 (2000).
4. S. J. Mihailov, C. W. Smelser, P. Lu, R. B. Walker, D. Grobnic, H. Ding, G. Henderson, and J. Unruh, Opt. Lett. **28,** 995 (2003).
5. S. J. Mihailov, C. W. Smelser, and D. Grobnic, in *Bragg Gratings, Photosensitivity, and Poling in Glass Waveguides*, Vol. 93 of OSA Trends in Optics and Photonics Series (Optical Society of America, Washington, D.C., 2003), paper TuB2.
6. C. W. Smelser, S. J. Mihailov, D. Grobnic, P. Lu, R. B. Walker, H. Ding, and X. Dai, Opt. Lett. **29,** 1458 (2004).

Article IV

C.W. Smelser, S. J. Mihailov, D. Grobnic: "*Hydrogen Loading for Fiber Grating Writing with a Femtosecond Laser and a Phase Mask*" Optics Letters 29 (18), p.2127-2129 (2004).

Hydrogen loading for fiber grating writing with a femtosecond laser and a phase mask

Christopher W. Smelser, Stephen J. Mihailov, and Dan Grobnic

Communications Research Centre Canada, 3701 Carling Avenue, P.O. Box 11490, Station H, Ottawa, Ontario K2H 8S2, Canada

Received June 25, 2004

The threshold for the fabrication of fiber Bragg gratings with ultrafast 800-nm radiation and a phase mask was studied in SMF-28 and all-silica core fiber by use of 125-fs pulses. High-pressure molecular hydrogen loading (H_2 loading) was observed to significantly lower the grating writing threshold in standard Ge-doped telecommunication fiber. No reduction was observed with all-silica core fiber. The index change appeared to be confined to the Ge-doped core region of the fiber. Gratings in H_2-loaded SMF-28 had thermal annealing behavior similar to UV-induced gratings. Unlike UV-induced H_2-loaded gratings, no absorption associated with Ge–OH defect formation was observed. © 2004 Optical Society of America

OCIS codes: 320.7140, 230.1480, 320.2250, 350.3390.

The study of induced index change in dielectrics by ultrafast processes for the fabrication of optical components has progressed significantly over the past decade. Research areas have included the application of ultrafast lasers to produce embedded waveguides, photonic crystal devices, and couplers.[1,2] Recently ultrafast femtosecond radiation was used to fabricate strong, high-spectral-quality fiber Bragg grating (FBG) structures in both all-silica core single-mode fibers and Corning SMF-28.[3,4] A significant amount of structural modification to the cladding region was observed. Two possible processes responsible for refractive-index change in transparent materials with femtosecond radiation are ionization and color center formation.

In the short-pulse regime (<10 ps) ionization in dielectrics such as silica is thought to result from the onset of avalanche photoionization triggered by multiphoton ionization (MPI).[5] For longer pulse durations (>10 ps) MPI is not the dominant mechanism in triggering the avalanche, and the threshold is probabilistic in nature. Because of the dominance of MPI for short pulses, the ionization threshold is deterministic; hence materials with only a modest dissimilarity in ionization thresholds can be distinguished. In the case of doped optical fiber, material modification would be predominant in the core if the MPI threshold was lower in the core than in the cladding.

GeE′ and germanium-oxygen-deficient centers have been observed in waveguide structures written in bulk Ge-doped silica glass with high-intensity femtosecond radiation.[1] For UV-induced index changes, increased photosensitivity as a result of H_2 loading of Ge-doped silica has been attributed to the much higher formation efficiency of GeE′ centers through photoinduced reactions of H_2 with Ge–SiO_2.[6,7]

In this Letter grating formation thresholds are studied in SMF-28 and all-silica core fiber in both H_2-loaded and unloaded samples. A significant reduction in the grating formation threshold is observed for the case of H_2-loaded SMF-28 fiber. These gratings exhibit material modification that is limited to the core region of the fiber. The grating formation occurs at intensities that are below the recognized threshold for ionization in bulk silica. Annealing curves of these gratings are comparable with annealing curves of UV gratings of the same strength. Evidence of absorption resulting from Ge–OH defect formation is absent.

SMF-28 and all-silica core fibers were loaded with hydrogen at 85 °C at 3000 psi for 24 h. Both the loaded and unloaded fibers were exposed to 125-fs 800-nm pulsed radiation from a regeneratively amplified Ti:sapphire laser at repetition rates of 1000 Hz. A 19-mm focal-length cylindrical lens was used to focus the pulse through a zeroth-order-nulled phase mask onto the fiber sample. The phase mask and fiber separation was set at 3 mm to avoid focusing near the phase mask and reduced the number of interfering orders to two.[8] This focusing arrangement resulted in a Rayleigh range of ~300 μm and a free-space spot size of ~4 $\mu m \times 5$ mm. The beam was scanned vertically to maximize coverage of the core region. The phase mask pitch used was 3.21 μm. The grating writing threshold is defined to be the pulse energy at which the first evidence of a grating is observed in reflection. This technique allows for the observation of refractive-index changes as small as 1×10^{-6}.

For an annealing comparison study, UV gratings were fabricated with a cw frequency-doubled argon-ion source with a phase mask optimized for 244-nm radiation. The average power was 200 mW, and the phase mask pitch was 1.07 μm. The grating length and reflectivity were the same as those of the femtosecond gratings.

Table 1 presents the femtosecond grating threshold energies for SMF-28 and all-silica core fiber. For SMF-28 fiber, hydrogen loading significantly reduced the grating writing threshold to 110 μJ, down from 330 μJ in unloaded fiber. The grating writing threshold for all-silica core fiber was 450 μJ and hydrogen loading did not reduce the threshold.

The threshold energies quoted in Table 1 can be related to the peak intensity. For a 19-mm focal-length cylindrical lens the linear focal spot area should be $\sim 2 \times 10^{-4}$ cm^2. Because of the interference of the

0146-9592/04/182127-03$15.00/0

Table 1. Ultrafast Grating Formation Thresholds

Fiber	Threshold for Grating Growth	
	Pulse Energy (μJ)	Intensity (W/cm^2)
SMF-28	330	2.1×10^{13}
H_2 SMF-28	110	7×10^{12}
All-silica core	450	2.9×10^{13}
H_2 all-silica core	450	2.9×10^{13}

mask orders, the interference peaks near the mask are significantly higher than the incident intensity. At a phase mask–fiber distance of 3-mm order, walk-off should reduce the peak intensity significantly.[8] If only the contribution of the ±1 orders, which contain ~80% of the incident energy, is considered, the interference of these two orders will result in a peak intensity that is ~160% that of the incident beam. For the case of H_2-loaded SMF-28 the grating threshold energy was 110 μJ. The threshold peak intensity is then calculated from

$$I_{\mathrm{th}} = \frac{E_{\mathrm{th}} \times 1.6}{\mathrm{Area} \times \tau} = \frac{110\ \mu\mathrm{J} \times 1.6}{2 \times 10^{-4}\ \mathrm{cm}^2 \times 125 fs}$$

$$= 7 \times 10^{12}\ \mathrm{W/cm}^2.$$

Here E_{th} is the energy threshold and τ is the FWHM temporal pulse length. Studies of the femtosecond-induced modification of silica have quoted energies consistent with threshold intensities of ~3×10^{13} W/cm^2. The intensity threshold in Table 1 for all-silica core fiber is comparable.[9] The calculated threshold intensities in SMF-28 fall below this value. The calculated intensity assumes a linear propagation of the pulse through the free space. It is possible that the fiber curvature or nonlinearity affect the focus. Consequently the threshold intensity quoted in Table 1 should be considered a lower limit.

Figure 1 shows optical microscope images of gratings written in both unloaded [Fig. 1(a)] and H_2-loaded [Fig. 1(b)] SMF-28 fiber. In the microscope images the writing beam is incident from the left side. In the unloaded case it is clear that the grating structure is not localized to the core region but extends into the cladding. At or above the grating threshold energy of 330 μJ, a cladding structure was always observed in unloaded fiber. It is clear that for H_2-loaded fibers the visible structural modification can be localized to the core. There is no observable material modification beyond the core–cladding interface.

The annealing behavior of gratings written in SMF-28 with the femtosecond and UV laser is presented in Fig. 2. The two lower curves present the annealing behavior of gratings with a refractive-index modulation (Δn) of ~1×10^{-5}. The index modulation for the femtosecond gratings was calculated from the strength of the resonance at 1550 nm. Because the mask pitch was 3.21 μm, the grating observed at 1550 nm is a third-order grating, and the actual index modulation in the medium may be higher. The normalized reflectivity of the low Δn H_2-loaded ultrafast grating (filled circles) is reduced to less than 0.4 at temperature of 300 °C in a manner similar to that observed with UV gratings (open circles). The upper two curves represent the annealing behavior of gratings with an initial index modulation of ~1×10^{-3}. Again the annealing behavior is similar for both the femtosecond (filled squares) and UV (open squares) gratings. Previous studies[4] with more energetic and intense (>5×10^{13} W/cm^2) ultrafast pulses exhibited temperature stability as high as 1000 °C.

It is clear that the presence of molecular hydrogen significantly reduces the threshold for femtosecond grating formation in SMF-28 fiber. No reduction in

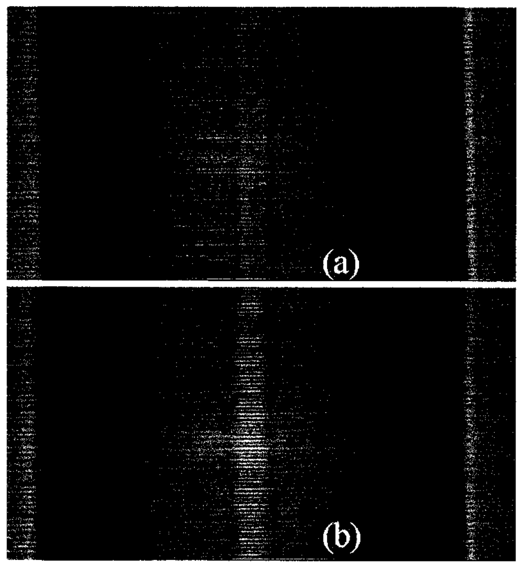

Fig. 1. Optical microscope images of ultrafast IR laser-induced gratings in SMF-28 fiber with a 3.21-μm pitch mask. The laser beam is incident from the left of the image. (a) Grating written in unloaded fiber with 400-μJ pulses. The grating structure clearly extends into the cladding region. (b) Grating structure in H_2-loaded fiber written with 220-μJ pulses. The structure in loaded fiber is clearly confined to the core region.

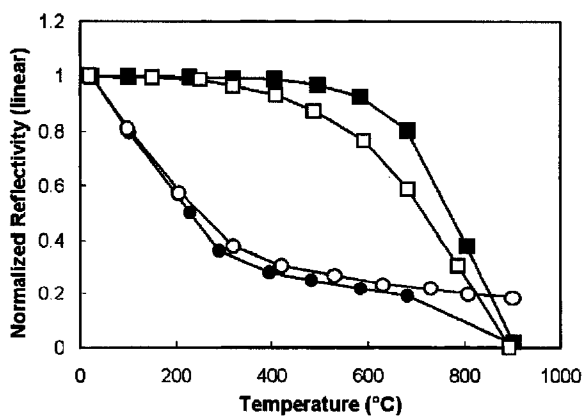

Fig. 2. Annealing data for femtosecond IR (filled circles and squares) and cw UV (open circles and squares) gratings. The lower annealing curves are for gratings with an initial refractive-index modulation of ~1×10^{-5}. The upper two curves are for gratings with an initial index modulation of ~1×10^{-3}. Clearly the annealing behavior is similar for both laser sources.

grating threshold was observed in all-silica core fiber. As demonstrated in Fig. 1, the modification is localized to the core region of the fiber. The annealing properties of the femtosecond gratings are similar to those observed in cw UV gratings of comparable strength. This suggests that the reduced threshold is related to color center formation in the Ge-doped core. In the case of the strong H_2-loaded UV gratings, UV-induced absorption associated with the formation of Ge–OH defects was observed. This was not the case for the strong gratings written with the femtosecond laser. The absence of Ge–OH formation renders the role of color center formation in the fabrication of gratings[4] with intense IR pulses unclear. It is possible that a small population of color centers could promote a resonant enhancement of MPI, resulting in an increased free-electron growth rate. The gratings in this study were written at intensities that are slightly above the threshold for grating growth. Clearly the temperature stability improves as the pulse intensity increases.[4] This could be a consequence of the generaion of stable structures that are formed in a strongly ionized medium. A small amount of third harmonic seemed to be generated within the fiber. The energy of the UV pulse generated was below our detection limit and thus was at most 1 μJ. It is unlikely that third-harmonic generation in the fiber was solely responsible for grating growth.

In conclusion, the introduction of high-pressure molecular hydrogen (H_2 loading) in SMF-28 fibers has significantly reduced the energy threshold for fiber grating fabrication by use of a 125-fs pulsed IR laser and a zeroth-order-nulled phase mask. No such reduction was observed for all-silica core fiber. For the case of H_2-loaded SMF-28 fiber, grating fabrication could be localized to the core and structural modification to the cladding could be avoided. The annealing behavior of ultrafast gratings is similar to that of gratings produced with UV sources. The reduction in threshold is likely related to enhanced color center formation in the presence of hydrogen; however, no evidence of Ge–OH defects was observed. The technique of hydrogen loading of bulk doped glasses could be used as a tool to facilitate femtosecond IR-induced index change, allowing for easier fabrication of ultrafast induced waveguide structures.

C. W. Smelser's e-mail address is christopher.smelser@crc.ca.

References

1. K. M. Davis, K. Miura, N Sugimoto, and K. Hirao, Opt. Lett. **21,** 1729 (1996).
2. K.-I. Kawamura, N. Sarukura, M. Hirano, and H. Hosono, Appl. Phys. Lett. **78,** 1038 (2001).
3. S. J. Mihailov, C. W. Smelser, P. Lu, R. B. Walker, D. Grobnic, H. Ding, G. Henderson, and J. Unruh, Opt. Lett. **28,** 995 (2003).
4. S. J Mihailov, C. W. Smelser, P. Lu, R. B. Walker, D. Grobnic, H. Ding, and J. Unruh, J. Lightwave Technol. **22,** 94 (2003).
5. B. C. Stuart, M. D. Feit, S. Herman, A. M. Rubenchik, B. W. Shore, and M. D. Perryt, J. Opt. Soc. Am. B **13,** 459 (1996).
6. T.-E. Tsai, G. M. Williams, and E. J. Friebele, Opt. Lett. **22,** 224 (1997).
7. T.-E. Tsai and E. J. Friebele, in *Bragg Gratings, Photosensitivity, and Poling in Glass Fibers and Waveguides: Applications and Fundamentals*, Vol. 17 of 1997 OSA Technical Digest Series (Optical Society of America, Washington, D.C., 1997), paper JMA4.
8. C. W. Smelser, D. Grobnic, and S. J. Mihailov, Opt. Lett. **29,** 1730 (2004).
9. C. B. Schaffer, A. Brodeur, J. F. Garcia, and E. Mazur, Opt. Lett. **26,** 93 (2001).

Article V

D. Grobnic, C. W. Smelser, S. J. Mihailov, R. B. Walker and P. Lu: "*Fiber Bragg Gratings with Suppressed Cladding Modes Made in SMF-28 with a Femtosecond IR Laser and a Phase Mask*" Photonics Technology Letters 16 (8), p. 1864-1866 (2004).

Fiber Bragg Gratings With Suppressed Cladding Modes Made in SMF-28 With a Femtosecond IR Laser and a Phase Mask

D. Grobnic, C. W. Smelser, S. J. Mihailov, *Member, IEEE*, R. B. Walker, and P. Lu

***Abstract*—High reflectivity fiber Bragg gratings (FBG) with strong cladding mode suppression were written in standard telecom fiber (SMF-28) with femtosecond 800-nm laser pulses and a phase mask. No special fiber photosensitization or fiber design was required. Induced index modulations were created by two-beam interference from the phase mask in both the core and cladding region, which resulted in cladding-mode coupling loss <0.1 dB for a high reflecting −30 dB in transmission FBG.**

***Index Terms*—Cladding-mode coupling, fiber Bragg gratings (FBGs), phase mask, ultrafast optics.**

I. Introduction

The ULTRAVIOLET (UV)-photoinduced fiber Bragg grating (FBG) has become a very popular technology for use in optical networks, wavelength-division-multiplexing (WDM) systems, and optical fiber sensor systems because of their high optical quality, relative ease of fabrication, fiber compatibility, and low cost. When the FBG is used as a high reflectivity narrow-band filter however, strong coupling from the forward-propagating fundamental core mode (LP_{01}) into discrete backward-propagating cladding modes can result in large out-of-band losses on the short wavelength side of the main reflection band [1]. This out-of-band loss is undesirable especially for dense WDM (DWDM) applications. Much effort has been directed into the development of specialty fibers to address this problem: high core–cladding refractive index difference fiber (high Δ) [2], depressed cladding fiber [3], and UV-photosensitive inner cladding fibers [4]. The UV-sensitive cladding fibers are the most effective in reducing cladding mode coupling losses since the LP_{01} and the cladding modes are orthogonal when the induced index grating is uniform across the core and cladding region of the fiber cross section where the LP_{01} has nonzero power [5]. These fibers are often costly to produce, however, as close matching of the photosensitivity of the core and inner cladding is required. These specialty fibers can also suffer from high splice loss when coupled to standard telecom fiber such as SMF-28. In order to achieve the required high index modulations for many DWDM applications, these fibers often need an additional processing step of photosensitization by H_2-loading [6].

Recently, high-quality FBG structures with high index modulation (Δn_m) were made in standard Ge-doped telecom fiber (SMF-28) [7] and all-silica core single-mode fiber [8] with a high power femtosecond infrared (IR) source and a phase mask without H_2-loading. Since high induced index change principally relies upon multiphoton ionization and need not depend on color-center formation or Ge-dopant concentration, grating structures were easily induced in both the fiber core and cladding [8]. In this work, we present for the first time a method of producing high-quality high-Δn_m FBGs with strong cladding mode suppression that were fabricated in standard SMF-28 without H_2-loading. Induced index modulation was localized to the core and surrounding cladding in a controlled fashion with a high-powered femtosecond laser and a phase mask.

II. Experimental Setup

High-order retro-reflective FBGs were fabricated in SMF-28 fiber with multiple pulses from a femtosecond source. The 800-nm output of a regeneratively amplified Ti : Sapphire laser was focused with a cylindrical lens of focal length $f = 19$ mm through a zeroth-order-nulled silica phase mask with pitch $\Lambda = 3.213$ μm onto the fiber sample. The fiber was positioned near the beam focus, either next to or 3 mm behind the phase mask. The Fourier transform-limited pulse duration was 125 fs as measured with an autocorrelator. The $1/e$ Gaussian beam radius w_o was measured by the knife-edge technique to be 2.45 mm. In the Gaussian beam approximation, the radius of the focal spot size is $w \approx \lambda f/\pi w_o$, where λ is the wavelength resulting in a focal line width of ~4 μm and a length of 4.9 mm. The fiber was exposed to 125 fs, 600-μJ laser pulses at 125 Hz for 1 min. The entire incident beam was centered onto the fiber core and then scanned across the fiber cross section using a piezo-actuated translation stage with a $\pm$10-μm travel and driven with a 20-s duty cycle. Structural modifications to the core and cladding were inspected using a high-power optical microscope. High-resolution transmission and reflection spectra of the FBGs were taken using a swept tunable laser system.

III. Results and Discussion

The phase mask used in this work had zeroth- and $\pm$1-order transmission at 800 nm, each with 1.9% and 38.8%, respectively [7]. The spectral response of a grating device written with the fiber in near-to-contact with the phase mask is shown in Fig. 1. In spite of the low zeroth-order energy, when the fiber

Manuscript received March 24, 2004; revised April 26, 2004.
The authors are with the Communications Research Centre Canada, Ottawa, ON K2H 8S2, Canada (e-mail: stephen.mihailov@crc.ca).
Digital Object Identifier 10.1109/LPT.2004.831239

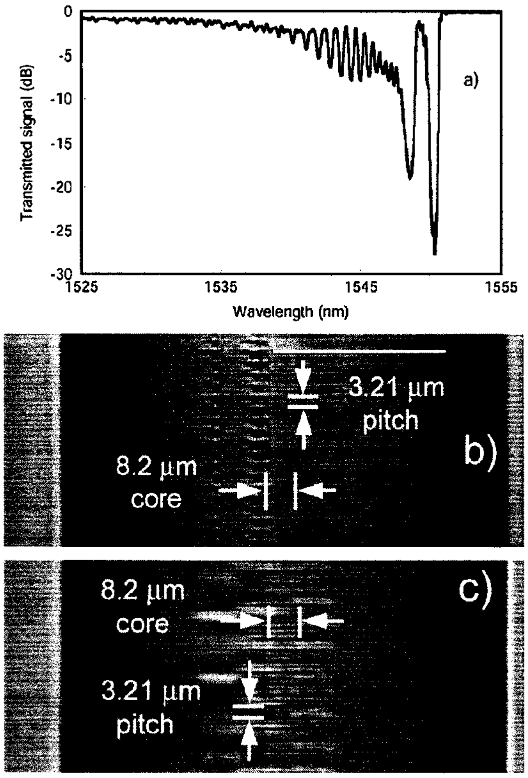

Fig. 1. (a) Transmission spectrum and microscope images of the grating structure written in SMF-28 fiber with 125 fs, 800-nm laser pulses with the 3.213-μm phase mask in near-contact to the fiber. (b) Fiber is imaged near the core and viewed normal to the beam axis, (c) Fiber is rotated 90° and is viewed along the beam axis.

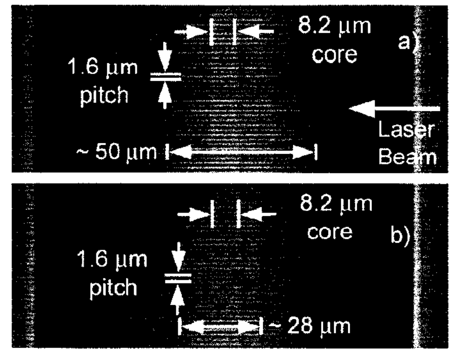

Fig. 2. Microscope images of photoinduced index modulation in SMF-28 produced with 125 fs, 800-nm laser pulses, with the fiber 3 mm from the 3.213-μm phase mask. (a) Fiber is imaged near the core and is viewed normal to the beam axis. (b) Fiber is rotated 90° and is viewed along the beam axis.

was placed near the phase mask, multiple beam interference resulted in the creation of complex index modulation patterns in the core and cladding with phase jumps along the beam axis. With the aid of the horizontal line drawn at the top of Fig. 1(b), a π-shift in the grating planes on either side of the core is visible. Such phase jumps have been associated with Talbot imaging of the mask [9]. The discontinuities in the index modulation across the cross section of the fiber contribute to cladding mode coupling especially, if they occur at the core–cladding interface. In Fig. 1(b), it can be seen that there is a large index modulation on only one side of the core resulting in a large gradient in the induced index change across the core of the fiber. Such a gradient in photosensitive cladding fiber has been associated with the coupling into asymmetrical cladding modes [5], such as the LP_{11} "ghost mode" which is most prominent in tilted gratings written in depressed-cladding fiber [3]. Strong coupling to the LP_{11} mode is clearly visible in Fig. 1(a), 1.5 nm below the Bragg resonance λ_{Bragg} at 1550 nm.

For a femtosecond pulse normally incident on the phase mask, the generated diffracted orders propagate at the speed of light at angles θ_i defined by the grating equation $\sin\theta_i = i\lambda/\Lambda$, where i is the diffracted order. When projected onto the zeroth-order beam axis normal to the phase mask, the pulse envelopes due to each order pair (± 1, ± 2, etc.) appear to travel with different group velocities from the zeroth order. With the fiber several millimeters behind the mask, the time of arrival at the fiber of each order pair is different causing a spatial separation of the order pairs. This has been defined as group velocity walkoff [10]. A pure two-beam interference pattern is generated by the ± 1 orders only, as these orders alone have sufficient intensity to induce an index change. For $\Lambda = 3.213$ μm and a 125-fs pulse, the spatial separation of the ± 1 order from the zeroth and ± 2 orders would occur at fiber-mask distances >1.3 mm. By using this technique, uniform periodic patterns without phase jumps were induced in the core and cladding region of the fiber, as shown in the optical microscope images presented in Fig. 2. Fig. 2(a) shows the grating structure viewed from the top of the fiber, which is normal to the femtosecond beam axis. The index modulation has a period half the pitch of the mask, which is consistent with two-beam interference, propagates ~50 μm in length, and is roughly centered about the core. The displacement of the pattern from the center depicts the accuracy with which the fiber is placed within the beam focus. Fig. 2(b) presents the grating structure viewed in line with the femtosecond beam axis with the fiber rotated 90° around the core, with respect to Fig. 2(a). The piezo-beam scanning resulted in ~28-μm-wide uniform modulation that is centered on the core. At its minimum, the grating extends from the core into the cladding region at least 8 μm.

The FBG in Fig. 2 displays excellent optical performance and cladding mode suppression. The transmission spectrum and the cladding mode loss spectrum are presented in Fig. 3(a) and (b), respectively. Fig. 3(b) presents the short wavelength side of the measured transmission spectrum corrected for sidebands in the grating reflection spectrum. Fig. 3(c) presents the reflection spectrum of the device. At λ_{Bragg}, the pitch of the grating structure in the fiber Λ_g is defined by $M\lambda_{\text{Bragg}} = 2n_{\text{eff}}\Lambda_g$, where M is the order number and n_{eff} is the effective index of the fiber resulting in a third-order retro-reflecting grating. The grating device has a −30-dB transmission at λ_{Bragg} with cladding mode coupling-induced loss ~0.1 dB [Fig. 3(b)]. With no explicit apodization process implemented, the grating is partially apodized due to the Gaussian profile of the incident beam and low average induced index change [7]. The apodized spectrum was modeled with a truncated Gaussian function [8] corresponding to a $\Delta n_m = 1.7 \times 10^{-3}$. The out-of-band insertion loss measured on the long wavelength side of the grating was <0.05 dB.

From the images presented in Fig. 2, it appears that there is good matching of the induced index change in the core and inner

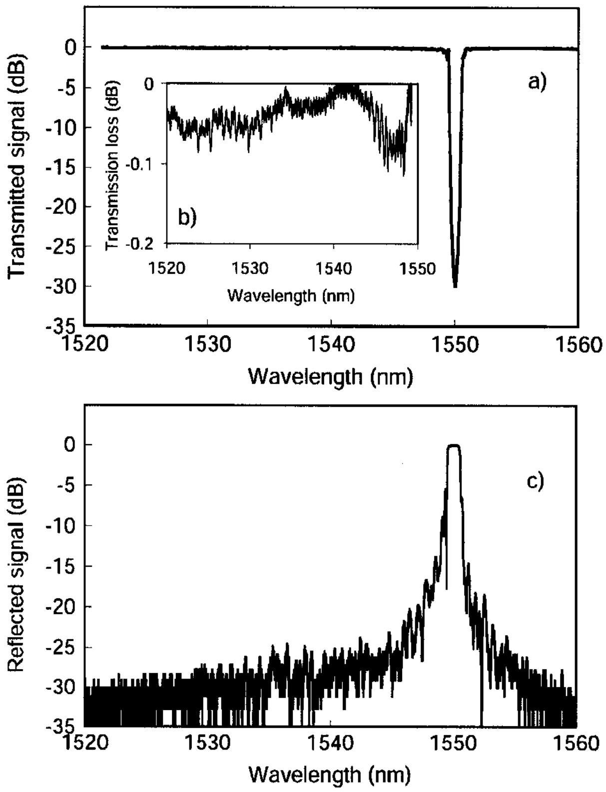

Fig. 3. (a) Transmission of cladding mode suppressed grating in SMF-28 shown in Fig. 2. (b) Cladding mode loss expressed as difference between the transmission spectrum and 1% reflectivity reflection spectrum. (c) Reflection spectrum.

cladding. This close matching is required in order to achieve the high-performance cladding mode suppression [5]. As well, the absence of the asymmetrical LP_{11} cladding mode in Fig. 3(b) implies that there is little gradient in the induced index change across the cross section of the core and cladding.

IV. Conclusion

Higher order retro-reflective FBGs with high reflectivity, high spectral quality, and extremely low cladding-mode coupling and insertion losses were written in off-the-shelf standard telecom SMF-28 fiber with a high-powered femtosecond IR laser and a phase mask. Through proper positioning of the irradiating beam and phase mask, pure two-beam interference patterns were generated by the mask at the fiber. Index modulations in specific regions of the core and cladding were induced resulting in excellent suppression of the cladding mode resonances. These devices are straightforward and economical to produce and easily integrable into DWDM network systems since no fiber photosensitization (H_2 loading) or special fiber designs (high Δ, depressed or UV-photosensitive cladding) are required.

References

[1] T. Erdogan, "Fiber grating spectra," *J. Lightwave Technol.*, vol. 15, pp. 1277–1294, Aug. 1997.

[2] V. Mizrahi, T. Erdogan, D. J. DiGiovanni, P. J. Lemaire, W. M. MacDonald, S. G. Kosinski, S. Cabot, and J. E. Sipe, "Four channel fiber grating demultiplexer," *Electron. Lett.*, vol. 30, no. 10, pp. 780–781, May 1994.

[3] S. J. Hewlett, J. D. Love, G. Meltz, T. J. Bailey, and W. W. Morey, "Coupling characteristics of photo-induced Bragg gratings in depressed- and matched-cladding fiber," *Opt. Quant. Electron.*, vol. 28, pp. 1641–1654, 1996.

[4] E. Delevaque, S. Boj, J. F. Bayon, H. Poignat, J. L. Mellot, M. Monerie, P. Niay, and P. Bernage, "Optical fiber design for strong gratings photoimprinting with radiation mode suppression," in *OSA Tech. Dig., Conf. Optical Fiber Communications*, vol. 8, San Diego, CA, 1995, pp. 343–346.

[5] L. Dong, G. Qi, M. Marro, V. Bhatia, L. L. Hepbrunt, M. Swan, A. Collier, and D. Weidman, "Suppression of cladding mode coupling loss in fiber Bragg gratings," *J. Lightwave Technol.*, vol. 18, pp. 1583–1590, Nov. 2000.

[6] P. J. Lemaire, R. M. Atkins, V. Mizrahi, and W. A. Reed, "High pressure H_2 loading as a technique for achieving ultrahigh UV photosensitivity and thermal sensitivity in GeO_2 doped optical fibers," *Electron. Lett.*, vol. 29, no. 13, pp. 1191–1193, June 1993.

[7] S. J. Mihailov, C. W. Smelser, P. Lu, R. B. Walker, D. Grobnic, H. Ding, G. Henderson, and J. Unruh, "Fiber Bragg gratings made with a phase mask and 800-nm femtosecond radiation," *Opt. Lett.*, vol. 28, no. 12, pp. 995–997, June 2003.

[8] S. J. Mihailov, C. W. Smelser, D. Grobnic, R. B. Walker, P. Lu, H. Ding, and J. Unruh, "Bragg gratings written in all-SiO_2 and Ge-doped core fibers with 800-nm femtosecond radiation and a phase mask," *J. Lightwave Technol.*, vol. 22, pp. 94–100, Jan. 2004.

[9] J. D. Mills, C. W. J. Hillman, B. H. Blott, and W. S. Brocklesby, "Imaging of free-space interference pattern used to manufacture fiber Bragg gratings," *Appl. Opt.*, vol. 39, no. 33, pp. 6128–6135, Nov. 2000.

[10] C. W. Smelser, S. J. Mihailov, D. Grobnic, P. Lu, R. B. Walker, H. Ding, and X. Dai, "Multiple beam interference patterns in optical fiber generated with ultrafast pulses and a phase mask," *Opt. Lett.*, vol. 29, no. 13, pp. 1458–1460, July 2004, to be published.

Article VI

C. W. Smelser, S. J. Mihailov, D. Grobnic, *"Formation of Type I-IR and Type II-IR gratings with an ultrafast IR laser and a phase mask"* Opt. Express 13, 5377-5386 (2005)

Formation of Type I-IR and Type II-IR gratings with an ultrafast IR laser and a phase mask

Christopher W. Smelser, Stephen J. Mihailov, and Dan Grobnic
Communications Research Centre Canada, 3701 Carling Ave., P.O. Box 11490, Station H, Ottawa, Ontario Canada K2H 8S2

christopher.smelser@crc.ca

Abstract: The formation of two grating types in SMF-28 fiber by focusing 125 fs, 0.5-2 mJ pulses through a phase mask onto a fiber sample is studied. The first type, specified as type I-IR, occurs below the damage threshold of the medium. The scaling behavior of the type I-IR gratings with field intensity and annealing properties suggests that their formation is related to nonlinear absorption processes, possibly resulting in color center formation. The second type, denoted as type II-IR, occurs coincidentally with white light generation within the fiber. These type II-IR gratings are stable at temperatures in excess of 1000 °C and are most likely a consequence of damage to the medium following ionization.

OCIS Codes: (230.1480) Bragg reflectors, (050.0050) Diffraction and Gratings, (320.7140) Ultrafast processes in fibers, (350.3390) Laser Materials Processing

---

References and Links

1. K. M. Davis, K. Miura, N. Sugimoto, and K. Hirao, "Writing waveguides in glass with a femtosecond laser," Opt. Lett. **21**, 1729-1731 (1996).
2. L. Sudrie, M. Franco, B. Prade, and A. Mysyrowicz, "Study of damage in fused silica induced by ultra-short IR laser pulses," Opt. Comm. **191**, 333-339 (2001).
3. Y. Kondo, K. Nouchi, T. Mitsuyy, M. Watanabe, P. G. Kanansky, and K. Hirao, "Fabrication of long-period fiber gratings by focused irradiation of infrared femtosecond laser pulses," Opt. Lett. **24**, 646-649 (1999).
4. S. J. Mihailov, C. W. Smelser, D. Grobnic, R. B. Walker, P. Lu, H. Ding, and J. Unruh, "Bragg Gratings Written in All-SiO2 and Ge-Doped Core Fibers With 800-nm Femtosecond Radiation and a Phase Mask," J. Lightwave Tech. **22**, 94-100 (2004).
5. S. J. Mihailov, C. W. Smelser, P. Lu, R. B. Walker, D. Grobnic, H. Ding, G. Henderson, and J. Unruh, "Fiber Bragg gratings made with a phase mask and 800-nm femtosecond radiation," Opt. Lett. **28**, 995-997 (2003).
6. Stephen A. Slattery, David N. Nikogosyan, Gilberto Brambilla, "Fiber Bragg grating inscription by high-intensity femtosecond UV laser light: comparison with other existing methods of fabrication", J. Opt. Soc. Am. B, **22**, pp. 354-361 (2005)
7. A. Dragomir, D. N. Nikogosyan, K. A. Zagorulko, P. G. Kryukov, and E. M. Dianov, "Inscription of fiber Bragg gratings by ultraviolet femtosecond radiation," Opt. Lett. **28**, 2171-2173 (2003).
8. K. A. Zagorulko, P. G. Kryukov, Yu. V. Larionov, A. A. Rybaltovsky, and E. M. Dianov, S. V. Chekalin, Yu. A. Matveets, and V. O. Kompanets, "Fabrication of fiber Bragg gratings with 267 nm femtosecond radiation" Opt. Express, **12**, 5996-6001 (2004)
9. A. Martinez, M. Dubov, I. Khrushchev, and I. Bennion, "Direct writing of fibre Bragg gratings by femtosecond laser," Electron. Lett. **40**, 1170-1172 (2004).
10. D. Grobnic, C. W. Smelser, S. J. Mihailov, R. B. Walker, and P. Lu, "Fiber Bragg Gratings With Suppressed Cladding Modes Made in SMF-28 With a Femtosecond IR Laser and a Phase Mask," IEEE Photon. Tech. Lett. **16**, 1864-1866 (2004).
11. C. W. Smelser, D. Grobnic, and S. J. Mihailov, "Generation of pure two-beam interference grating structures in an optical fiber with a femtosecond infrared source and a phase mask," Opt. Lett. **29**, 1730-1732 (2004).
12. C. W. Smelser, S. J. Mihailov, and D. Grobnic, "Hydrogen loading for fiber grating writing with a femtosecond laser and a phase mask," Opt. Lett. **29**, 2127-2129 (2004).

#7428 - $15.00 USD Received 10 May 2005; revised 8 June 2005; accepted 28 June 2005

13. C. W. Smelser, S. J. Mihailov, D. Grobnic, P. Lu, R. B. Walker, H. Ding, and X. Dai, "Multiple-beam interference patterns in optical fiber generated with ultrafast pulses and a phase mask," Opt. Lett. **29**, 1458-1460 (2004).
14. J. L. Archambault, L. Reekie, and P. S. J. Russell, "High Reflectivity and Narrow Bandwidth Fibre Gratings Written by Single Excimer Pulse," Electron. Lett. **29**, 28-29 (1993).
15. R. Kashyap, *Fiber Bragg Gratings*, (Academic Press, New York, 1999)
16. D. K. W. Lam, Brian K. Garside., "Characterization of single-mode optical fiber filters", Appl. Opt., **20**, 440-445 (1981)
17. G. Meltz, W. W. Morey, W. H. Glenn, "Formation of Bragg gratings in optical fibers by a transverse holographic method", Optics Letters, **14**, 823-825 (1989)
18. Junji Nishii, Naoyuki Kitamura, Hiroshi Yamanaka, Hideo Hosono, Hiroshi Kawazoe, "Ultraviolet-raditation-induced chemical reactions through one- and two- photon absorption processes in GeO2-SiO2 glasses", Opt. Lett., **20**, 1184-1186 (1995)
19. B. Malo, J. Albert, K.O. Hill, F. Bilodeau, D.C. Johnson, and S. Theriault., "Enhanced photosensitivity in lightly doped standard telecommunications fiber exposed to high fluence ArF excimer laser light", Electronic Letters, **31**, pp. 879-880 (1995)

---

1. Introduction

Femtosecond pulse duration (fs) IR lasers have proven themselves to be useful sources for non-linear laser-material processing for photonic device fabrication. Direct-write imbedded waveguides with large induced index changes (Δn) were made in bulk and Ge-doped silica using these sources [1]. Recently two regimes of ultrafast IR induced Δn in bulk silica were identified, which in terms of their magnitude and annealing properties, were similar to the Δn for UV induced Type I and II fiber Bragg gratings (FBG) [2]. Two power thresholds were established, one for a reversible index change that could be annealed out at 900 °C (referred to in [2] as Type I damage). The second higher power threshold was the self-focusing threshold above which the induced index change was likely a result of multiphoton and avalanche ionization causing plasma formation. The resultant index change, referred to in [2] as Type II damage, would not anneal out at 900 °C.

Ultrafast IR pulses have been used to induce index changes in existing waveguides. Long-period grating structures were fabricated in optical fiber [3]. More recently several groups have made retro-reflective FBGs with both IR and UV femtosecond sources and a phase mask [4-8] or via a point-by-point exposure with a femtosecond IR source[9]. When ultrafast IR laser exposures were made with the optical fiber in close proximity to the phase mask (within a fiber diameter), good quality high index modulation FBGs ($\Delta n_{mod} > 10^{-3}$) were easily achieved in SMF-28 and single mode silica core fibers without special photosensitization such as H_2 loading [4]. The resultant FBG structures were retro-reflective higher order gratings that had resonances in the telecommunication band and were stable at temperatures in excess of 1000 °C. White light emission was observed visually during the formation of these gratings. More recently high quality cladding mode suppressed gratings were made with 125 fs pulses and the SMF-28 fiber placed remotely from the phase mask (> 3 mm distance) in order to have a pure two-beam interference pattern [10, 11]. In this instance however, no white light generation was observed during the grating formation and when the Ge-doped fiber was loaded with Hydrogen [12] the FBG had annealing properties similar to standard UV gratings.

In this work, the properties of fiber gratings written with a 125 femtosecond IR laser, a phase mask and different peak intensities at the fiber are presented. Two intensity dependent regimes of induced index change, separated by an intensity value that generates white light, are observed and using a variation of the nomenclature given in [2] are here referred to as Type I-IR and Type II-IR induced index change. The annealing properties of these two types of gratings are then investigated. Finally, the Type I-IR gratings are shown to scale nonlinearly with the incident field intensity suggesting that the Type I-IR index change

Received 10 May 2005; revised 8 June 2005; accepted 28 June 2005

process is related to a multiphoton absorption process, possibly resulting in color center generation.

2. Threshold Study

FBGs were written in Ge-doped *Corning SMF-28* using 800 nm 125 fs pulses from an amplified Ti:sapphire system with a 1/e Gaussian beam radius, w_o, of 3.2 mm and a maximum output energy of ~2 mJ. This system has a maximum repetition rate of 1 kHz. The beam was focused using a cylindrical lens with a focal length f = 30 mm through a silica zero-order-nulled phase mask with a period Λ_m = 3.213 μm onto the fiber. The entire incident beam was centered onto the fiber core and then scanned vertically over the fiber cross-section using a piezo-actuated translation stage with a ±10 μm travel and a 20 s period. This ensured maximum coverage of the core region. The focus was always adjusted so that it remained at the fiber core. Transmission spectra were obtained using an Erbium source and a spectrum analyzer.

The fiber was placed at a fixed distance of 5 mm from the phase mask such that diffracted order walk-off from the mask would generate a 2-beam interference pattern from only the ± 1 orders [11]. For the determination of the Type I-IR threshold, the beam energy was increased until a multiple pulse exposure of ~ 100,000 pulses produced an index modulation that could be observed by monitoring the grating response in reflection. The pulse energy threshold at which grating formation could be observed was 500 μJ.

Because of the complex nature of the multiple beam interference field that is generated near the mask [13], it is difficult to obtain a quantitative estimate of the peak intensity in this region. In previous work [4, 5] the peak intensity seen at the fiber was solely based on the Gaussian beam approximation of the focal spot size. In [5] the beam diameter was mistakenly treated as the beam radius in the calculation. Considering only the focal spot size underestimates the peak intensity seen at the fiber, as the interference between phase mask orders should cause an increase in peak intensity [13]. Improved understanding of the multiple beam interference patterns generated through the interaction of the incident pulse and the phase mask as well as the discovery of order walk off effects has allowed for a much more accurate determination of the field intensity impinging on the fiber. Phase mask order walk off can be exploited to produce an interference pattern comprised of only the ±1 phase mask orders [11]. Considering that the 2-beam interference field produces a less complicated sinusoidal intensity modulation along the fiber length the peak intensity of the field is more easily calculated. The intensity threshold of index change in all-silica core fiber measured with this technique was consistent with studies in bulk media [12]. In this instance transverse walk-off of the diffracted beams was not considered. It is considered in the treatment presented here.

The ± 1 orders contained 77.6 % of the beam energy incident on the mask [4]. 5 mm from a 3.21 μm mask, the diffraction angle $\theta_{\pm 1}$ = 14.4° produces a lateral separation of 2.6 mm between the peaks of the +1 and −1 order Gaussian beams. In this location (red) the magnitude of the envelope of the ±1 interference field is reduced by a factor of 0.86 as shown in Fig. 1. Also, shown is the envelope after 10 mm (blue). There is a significant reduction in peak intensity. There should also be a reduction in fringe visibility towards the edge of the profile due to incomplete overlap of the orders.

#7428 - $15.00 USD

Received 10 May 2005; revised 8 June 2005; accepted 28 June 2005

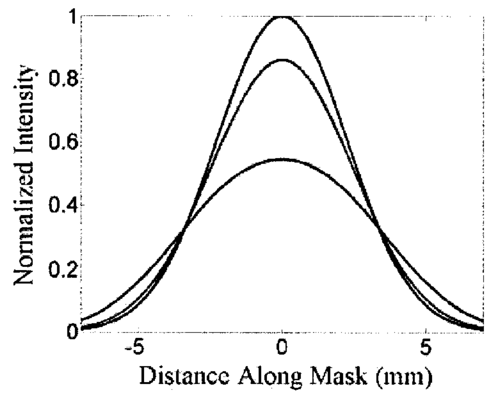

Fig. 1 Walk off of the ±1 orders reduces the peak field intensity. After 5 mm (red) the peak intensity is reduced by a factor of 0.86 compared to the peak at the phase mask (black). Also shown is the profile after 10 mm (blue).

Considering free space Gaussian beam optics, a 30 mm focal length cylindrical lens and an input beam diameter of 6.4 mm results in a focal area of 4.8 μm x 6.4 mm=3x10^{-4} cm^2. Due to the tight focusing geometry the impact of the fiber on the spot size is reduced. The error in the pulse energy, focal area and pulse duration was estimated to be ±10%, 6% and 8% respectively. The spot size used here is consistent with observations under a microscope. The intensity threshold for Type I-IR grating formation is then estimated to be:

$$I_{th} = \frac{pulse\ energy \times 2 \times \%\ energy \pm 1\ orders \times 0.86}{area \times pulse\ duration} = \frac{500\ \mu J \times 2 \times 0.776 \times 0.86}{3 \times 10^{-4} cm^2 \times 125 fs} = 1.8 \pm 0.4 \times 10^{13}\ W/cm^2 \quad (1)$$

With the same exposure conditions and set up, only the pulse energy was increased until white light generation occurred coincident with Type II-IR grating formation. The white light generation threshold pulse energy was 1.3 mJ which when using Equation (1) yielded the intensity threshold for Type II-IR grating formation of 4.6 ±1.1× 10^{13} W/cm^2.

In bulk silica, the Gaussian beam peak power threshold levels for Type I and Type II damage observed by Sudrie et al. were 0.6 MW and 1.9 MW respectively [2]. To compare these peak powers with the peak intensities obtained here, one can determine the peak power of the interference field. The peak power of the interference field is the energy contained in the central peak of the interference field divided by the temporal pulse length. The energy contained in the central peak can be determined by comparing the area under the central interference peak to the area under whole interference field. By integrating the field intensity for the central peak, and dividing by the area under the whole curve for ±1 orders that have traveled 5 mm away from the phase mask, it is found that the central peak contains ~1/4100th of the total energy. The peak power is now determined by:

$$P_{peak} = \frac{Energy \times 0.776}{4100 \times \tau} = \frac{500 \mu J \times 0.776}{4100 \times 125 \times 10^{-15} s} = 0.76 \pm 0.14 MW \quad (2)$$

The energy here is the total input energy and τ is the temporal pulse length. The factor of 0.776 determines the total energy contained in the ±1 orders. For an input energy of 1.3 mJ the peak power is 2±0.4 MW. These peak powers compare favorably to the thresholds for Type I and Type II index change found by Sudrie et al.

3. Annealing Study

The next study involved long term annealing of gratings written with and without coincident white light generation. Using a lower power amplifier system (maximum energy of 1 mJ) and the 19 mm focusing lens (beam diameter of 4.9 mm), gratings were fabricated either in close proximity to the mask or at 5 mm distance where two-beam interference would occur. For 125 fs pulses, the complex interference field near the phase mask had high peak intensities. It was therefore possible to create Type II-IR gratings using pulse energies lower than that required to produce Type II-IR gratings in the two-beam interference region. Interestingly this was also the case if an order of magnitude lower intensity Fourier transform-limited 1.6 ps pulse was used. To investigate the annealing characteristics of the Type I and Type II-IR gratings, three grating structures were fabricated. For the Type I-IR grating, the two-beam interference pattern was used with an estimated peak intensity of 3×10^{13} W/cm^2. After several thousand 125 fs pulses the grating with the transmission spectrum shown in Fig. 2 (a) was produced. Using a commercial software package the index modulation corresponding to the –25 dB transmission at λ_{Bragg} is $\Delta n_{\mathrm{mod}} = 1.1 \times 10^{-3}$. Some assumptions have been made when calculating the index modulation. Firstly the Bragg resonance λ_{Bragg} is assumed to be a fundamental resonance rather than higher order, and secondly the index modulation is to be a pure sinusoid with a 50/50 duty cycle.

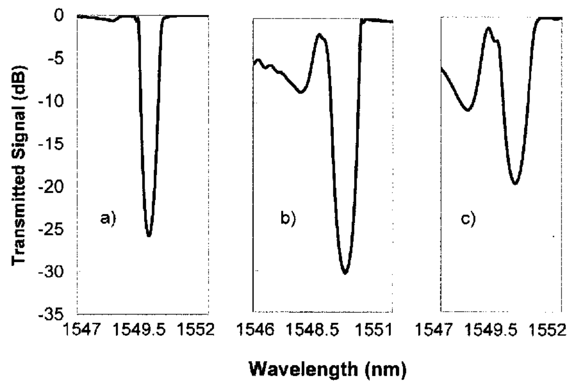

Fig. 2 Transmission spectra of gratings that were used in the annealing study. a) is the Type I-IR grating written with 125 fs pulses and 2-beam interference, b), c) Type II-IR grating written near the phase mask with 125 fs and 1.6 ps pulses repectively.

With fibers placed within a fiber diameter of the mask, two Type II-IR FBGs were fabricated with 125 fs and 1.6 ps pulses each with incident pulse energies on the mask of 1 mJ. Transmission spectra for the 125 fs and 1.6 ps gratings are shown in Fig 2 (b) and 2 (c) respectively. The Δn_{mod} were determined to be 1.5×10^{-3} and 1.7×10^{-3} respectively. In both cases the gratings were written after exposure to only a few dozen pulses. Considering the spectra presented in Fig. 2 (a), (b) and (c) it should be noted that the observed bandwidth respectively increases. This increase in bandwidth results from a reduction in the effective length of the grating. The strong cladding mode structures are a result of the non-uniform index change across the core as is seen in the observed optical microscope images of the index modulation in the fiber (see Fig 3). The fs and ps Type II-IR gratings shown in Fig. 3 (b) and (c) generally have an irregular structure in regions where the Gaussian beam profile tapers to zero, often resulting in missing grating lines. These missing fringes are a result of the threshold behavior of the Type II-IR induced index change. Being a damage-like process, fiber inhomogeneities or slight variations in beam uniformity can result in certain fringe lines being above threshold while others are not.

#7428 - $15.00 USD
Received 10 May 2005; revised 8 June 2005; accepted 28 June 2005

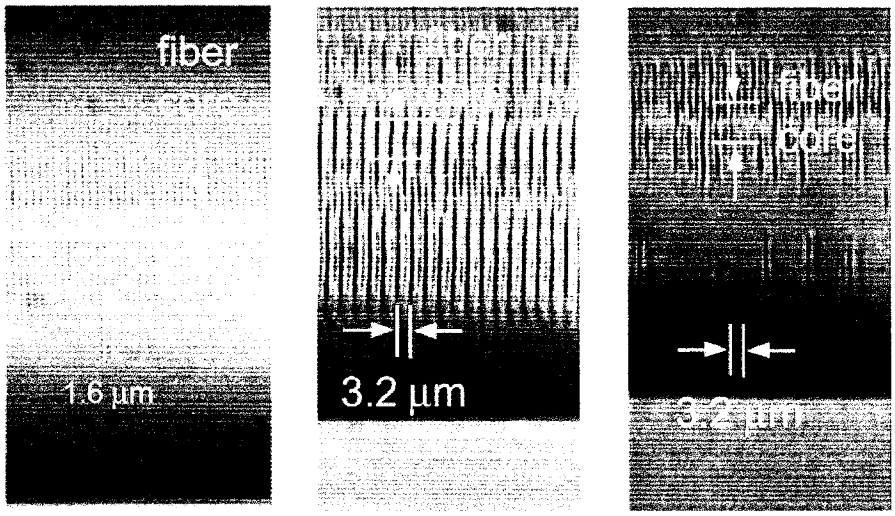

(a) (b) (c)

Fig. 3. Optical microscope images of the Type I and Type II-IR gratings that were used in the annealing study: a) is the Type I-IR 125 fs grating, b) is the Type II-IR 125 fs grating and c) is the Type II-IR 1.6 ps grating.

The grating growth rate for Type II-IR FBGs using both femtosecond and picosecond pulse durations is extremely rapid. A 30 dB loss at the Bragg wavelength could be achieved with as few as 20 shots. Type I-IR FBGs written with 125 fs pulses at large phase mask-fiber distances (>5 mm) exhibited regular monotonic growth and required several thousands of shots to produce a 30 dB loss at the Bragg wavelength. For picosecond pulses, only extremely small index changes ($<10^{-6}$) could be produced with phase mask fiber separations in excess of 1 mm.

The annealing curves of the three FBGs are presented in Fig 4. For comparison a Type I-UV FBG was inscribed in H_2-loaded SMF-28 fiber (3000 psi, 85 °C, 24 hr) using a frequency doubled Argon ion laser and a phase mask which produced a $\Delta n_{mod} = 5 \times 10^{-4}$. In Fig. 4 (a) the initial Δn_{mod} of each of the FBGs are normalized to 1. For increasing temperature the Δn_{mod} of the UV grating, denoted by the white circles, is seen to decrease and completely disappear when the grating temperature approaches 1000 °C. As well, the Type I-IR grating (denoted by black squares in Fig.4 (a)) undergoes an order of magnitude reduction in its Δn_{mod} with a final value after 1 hour at 1000 °C of 1×10^{-4}.

For the Type II-IR gratings, some interesting effects are observed. For the Type II-IR device written with 125 fs pulses, denoted by white squares in Fig.4 (a), the Δn_{mod} is seen to increase as the temperature increases. This increase may be a result of the two kinds of index change being written simultaneously. In the peaks of the complex interference pattern, sufficient intensity exists to ultimately ionize the glass in the fiber producing an index change that is durable with temperature. In the valleys of the interference pattern the power is below the Type II-IR threshold however some Type I-IR index change may occur. As the device is annealed the Type II-IR index change remains fixed while the Type I-IR component is erased resulting in a higher Δn_{mod}. For the Type II-IR grating written with the 1.6 ps pulse (denoted by black circles) the initial reduction and then stabilization of the Δn_{mod} is likely due to a component of the initial total index change coming from a Type I-IR index change.

#7428 - $15.00 USD
Received 10 May 2005; revised 8 June 2005; accepted 28 June 2005

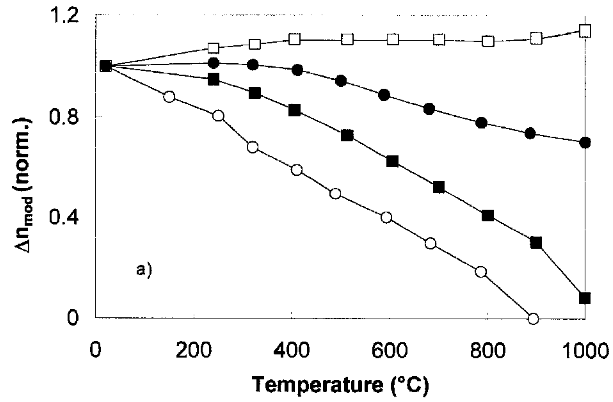

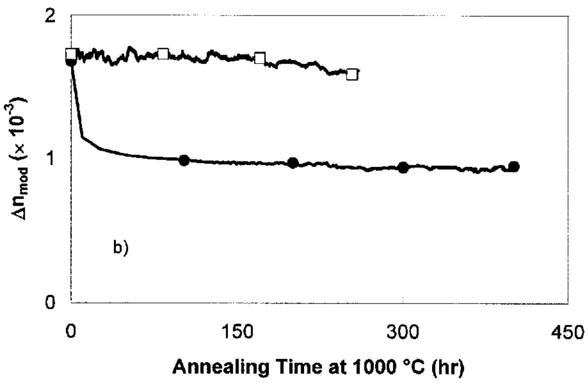

Fig. 4. a) Short term annealing study of Type I-IR (black square), Type II fs (white square) and ps (black circle) IR and Type I UV (white circle) gratings. Grating temperatures were raised in 100 °C increments and stabilized for one hour. Index modulations are normalized to their room temperature values.b) Long term annealing at 1000 °C of Type II fs IR (white square) and Type II ps IR (black circle) gratings.

In Fig. 4 (b), long term annealing tests at 1000 °C were performed on the 125 fs and 1.6 ps Type II-IR gratings. The calculated $\Delta n_{\rm mod}$ determined from the transmission spectra are plotted versus annealing time. After 260 hours there is only a slight reduction in the $\Delta n_{\rm mod}$ of the fs FBG from its peak value to 1.6×10^{-3} while for the ps FBG, after an initial erasure during the first 50 hours, the $\Delta n_{\rm mod}$ stabilized to a value of 1×10^{-3}.

From the intensity threshold measurements and the annealing study it is clear that there are two regimes of ultrafast IR induced index change that appear similar in properties to Type I-UV and Type II-UV induced index change. As no white light generation (self focusing/ionization) is observed for the Type I-IR induced index change, it is likely that the index change is a result of highly nonlinear defect formation resulting from a multi-photon absorption process. These defects, like those associated with Type I-UV exposures, can be annealed out below the t_g of the fiber. The Type II-IR gratings appear similar to the Type II-UV "damage" gratings. The white light generation that occurs concurrently with Type II-IR grating formation suggests that these gratings likely result from an ionization process, perhaps triggered by self focusing. Because of the ultrafast nature of the beam however, multiple pulse exposures can result in high index modulation within the fiber without the collateral damage to the interstitial material between high intensity zones. In the single pulse Type II-UV process, which utilizes longer time duration high peak power UV irradiation, there is material disruption around the high intensity portions of the beam producing laser-induced

Received 10 May 2005; revised 8 June 2005; accepted 28 June 2005

damage at the core-cladding interface [14]. Subsequent UV-irradiation of such damage sites would result in catastrophic failure of the glass.

4. Scaling behavior of Type I-IR gratings.

The mechanism associated with formation of type I-UV fiber Bragg gratings (FBG) in standard telecommunications fiber is the photoexcitation of free electrons, by dissociating the GeO defect, that are subsequently trapped at defect sites[15]. The resulting change in absorption would manifest in a change in the index of refraction via the Kramers-Kronig relations. The original Hill gratings were shown to result from the absorption of two 488 nm photons by the 242 nm GeO absorption band[16]. Later, gratings were commonly written by UV excimer, doubled Argon ion or quadrupled YAG sources. With these lasers the index change is related to the linear absorption of UV photons[17]. For fibers with low Ge dopant concentration the index change produced with an ArF 193 nm excimer source was shown to be the result of a two photon process. It was thought that this was the result of the absorption of two photons to bridge the band gap of silica[18]. The Type I-IR gratings exhibit grating growth and annealing behavior similar to that observed with Type I-UV gratings. It would seem reasonable that the mechanism for fabrication of Type I-IR gratings may result from color center formation as well. The 800 nm wavelength or 1.55 eV photon energy is far removed from the typical bandgap of Ge doped silica or silica, thought to be 7.1 and 9.3 eV, respectively[18,19]. It is important to question whether the formation of Type I-IR Bragg gratings with ultrafast sources results from a highly nonlinear absorption process. This can be determined through a study of the growth of the index modulation as a function of interference field intensity. If a nonlinear absorption process is involved in the index growth, the growth rate should scale with intensity as I^c, where I is the peak interference field intensity and c is a real constant >1.

The exposure conditions are the same as described in the threshold study except that the repetition rate of the laser was maintained at 100 Hz. The transmission loss at the Bragg wavelength was measured continuously (>1 Hz) for input energies of 850, 900, 950, 1000, 1100 and 1200 μJ. Several spectra were taken at each energy increment and the spectral response of the grating was then modeled with a commercial FBG software package. A typical spectrum for a 1200 μJ input energy is shown in Fig. 5.

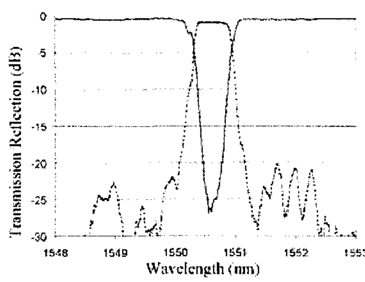

(a)

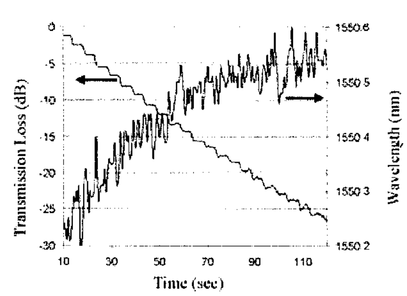

(b)

Fig. 5. Typical transmission and reflection spectra near 1550 nm for a Type I-IR grating written with a 1200 μJ input pulse and a 3.21 μm phase mask is shown in (a). The cladding mode is significantly reduced as compared with Type I-UV gratings. (b) depicts the transmission loss and peak wavelength shift as a function of time. The wavelength shift is smaller than would be expected for a Type I UV grating. The noise in. (b) is the result of the laser scanning across the core.

#7428 - $15.00 USD
Received 10 May 2005; revised 8 June 2005; accepted 28 June 2005

The grating length typically becomes larger as a function of incident intensity and has been considered in all simulations.

The index modulation growth curves for gratings written with a 3.21 μm mask are shown in Fig. 6 (a) along with the scaling behavior of the growth rate as a function of energy in Fig. 6 (b).

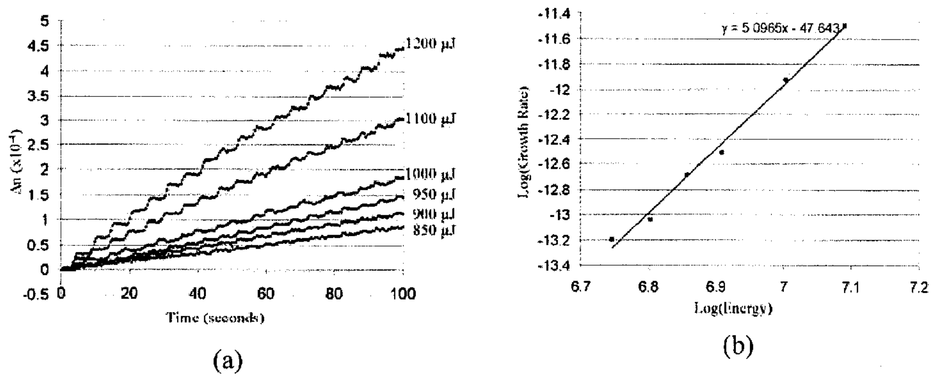

Fig 6. Growth rate curves for various pulse energies are shown in (a). (b) shows the scaling behavior of the index modulation growh rate as a function of energy. The slope of 5 indicates a highly nonlinear process is involved in the grating growth.

The ripple observed in the growth curves is a result of scanning the beam across the fiber core. The total number of pulses for each sweep is constant. The slope of ~5 in Fig. 6 (b) suggests that the growth rate scales with I^5. This suggests a 5 photon absorption process. This behavior seems reasonable in Ge doped silica as 5 photons would bridge a gap of 7.75 eV, comparable to that of Ge doped silica[19]. It is possible, considering the scaling behavior and annealing properties, that this process is similar to that observed during the formation of Type I-UV gratings.

There are some interesting features of the spectrum in Fig. 5 (a) that are important. As has been reported previously there is commonly a significant reduction in the cladding modes on the short wavelength side of the transmission spectrum[10]. If the 1/e beam diameter of the Gaussian writing beam is 6.4 mm then a modeled 3 dB bandwidth of ~450 pm and an index modulation of ~$4.1\text{x}10^{-4}$ would be expected for the transmission loss of 27 dB shown in Fig. 5. The wavelength shift would then be ~280 pm for this index change, similar to the actual shift in Fig 5 (b). The actual 3 dB bandwidth in Fig. 5 (a) is ~600 pm, a difference of 150 pm. To model this bandwidth it was necessary to reduce the width of the Gaussian by a factor of 1.4 and increase the index modulation to ~$5.7\text{x}10^{-4}$ for the same transmission loss. As the wavelength shift should scale linearly with the index modulation a wavelength shift of ~400 pm should be expected. Clearly in Fig. 5 (b) the wavelength shift for Type I-IR gratings is only about 300 pm.

The nonlinear dependence of the index change on the input field intensity provides a possible explanation for the observed bandwidth and wavelength shift of Type I-IR gratings. In Fig. 7 (a) there is a comparison between the interference field intensity for the same parameters as Fig. 1 (blue) and the same field raised to the power of 5 (red). The pitch of the grating has been greatly exaggerated in Fig. 7 (a) for clarity. Fig. 7 (b) illustrates the relative area under the central peak for a grating that depends on I (blue) and a grating that depends on I^5 (red).

#7428 - $15.00 USD Received 10 May 2005; revised 8 June 2005; accepted 28 June 2005
(C) 2005 OSA 11 July 2005 / Vol. 13, No. 14 / OPTICS EXPRESS 5385

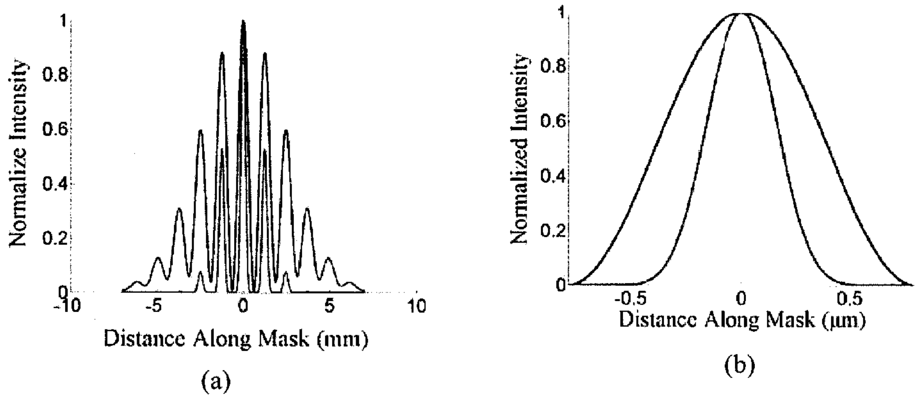

Fig. 7. A comparison of the intensity profile for ±1 orders 1.5 mm away from a 3.21 μm mask in red with the profile of I^5 in blue. The differences in these profiles offer a possible explanation for the unique spectral properties of Type I-IR gratings. (b) illustrates the reduced area under each peak of the nonlinear grating (red) compared to the linear grating (blue).

There are two main differences between the profiles in Fig. 7 (a). The width of the profile becomes considerably narrower and the area under each interference peak (Fig. 7 (b)) becomes smaller. The smaller contribution these peaks would have to the average index would cause a reduction in wavelength shift and minimize the impact of the apodization profile on the spectral response. The narrower profile would result in an increase in spectral bandwidth. The nonlinear profile appears to be consistent with the spectral observations. As mentioned earlier the grating profiles appeared to become larger as a function of energy. This observation is not consistent with the nonlinear dependence of the index on the intensity field as the effective length of the grating should remain the same. A threshold effect could also mimic some of the spectral properties of Type I-IR gratings such as the observed wavelength shift. However, the scaling behavior does not seem to be consistent with such a model. It is possible that the grating growth is both nonlinear and threshold like. A direct measurement of the index profile of Type I-IR gratings will help determine the relative contribution of each effect to the structure of the index profile.

5. Conclusion

Two types of grating structure have been fabricated with an ultrafast laser and a phase mask. These gratings, referred to as Type I-IR and Type II-IR, exhibit different intensity thresholds, annealing behavior and grating structure. White light generation delineates the two grating types. The intensity thresholds and annealing behavior appear to be consistent with previous studies in bulk media [2] where self focusing triggered the transition. Type I-IR gratings are shown to scale highly nonlinearly with the input field intensity. This coupled with annealing behavior suggests that the grating growth mechanism is related to some form of color center formation. The white light and high temperature stability of Type II-IR gratings suggest that the dominant index change mechanism is that of ionization and damage.

#7428 - $15.00 USD
Received 10 May 2005; revised 8 June 2005; accepted 28 June 2005

Article VII

C. W. Smelser, S. J. Mihailov, and D. Grobnic, "Rouard's method modeling of type I-IR fiber Bragg gratings made using an ultrafast IR laser and a phase mask," J. Opt. Soc. Am. B **23**, 2011-2017 (2006)

Rouard's method modeling of type I-IR fiber Bragg gratings made using an ultrafast IR laser and a phase mask

Christopher W. Smelser, Stephen J. Mihailov, and Dan Grobnic

Communications Research Centre Canada, 3701 Carling Avenue, P.O. Box 11490, Station H, Ottawa, Ontario, Canada K2H 8S2

Received January 26, 2006; revised April 28, 2006; accepted May 28, 2006; posted June 30, 2006 (Doc. ID 67453)

Rouard's method is used to model the spectral response of type I-IR gratings. Type I-IR gratings are shown to have a broader bandwidth and larger sideband suppression than would be expected from standard type I UV-written gratings. These properties are related to the nonlinear dependence of the index change on intensity. At higher intensities the spectral response indicates saturation of the index change growth rate. © 2006 Optical Society of America

OCIS codes: 230.1480, 050.0050, 320.7140, 350.3390.

1. INTRODUCTION

The spectral response characteristics of type I UV-written color-center gratings are well known.[1] For a given index profile and grating strength, one can expect a well-defined bandwidth and sideband structure. Coupled-mode theory, matrix methods, and Rouard's method have all been used successfully to model the spectral response of type I UV-written gratings.[2] Recently, fiber Bragg grating fabrication with an ultrafast Ti:sapphire laser and a phase mask has been demonstrated.[3,4] Ultrafast gratings have also been produced using UV sources and a point-by-point exposure technique.[5,6]

Two distinct types of ultrafast phase-mask-written grating have been observed.[7] The first to be reported, type II-IR gratings, was formed in standard telecom fiber through an ionization process and was stable at temperatures up to 1000 °C. The spectral response often included large sidebands and a large cladding mode loss. These gratings formed in a thresholdlike manner, and large index changes ($>10^{-3}$) could be achieved after a few laser shots.

The second variety, type I-IR gratings, is formed at lower intensities and exhibits smooth grating growth similar to that observed with type I UV-written gratings. Type I-IR gratings have also been shown to anneal out at temperatures less than 1000 °C. These gratings exhibit a different spectral bandwidth and sideband structure than would be expected from the writing-beam spot size, assuming they result from a single photon process. Type I-IR gratings are fabricated using a remote writing technique that involves increasing the separation between the phase mask and the fiber to produce a two-beam interference pattern through order walk-off.[8,9] As a consequence of this, the visibility of the interference profile varies along the length of the grating. Type I-IR grating growth has also been shown to scale nonlinearly with the interference field intensity.[7] This nonlinear dependence causes a narrowing of the index change profile relative to that expected for UV gratings and nonsinusoidal interference fringes. Rouard's method is an effective technique for modeling an arbitrary index profile.[10–12] Variations in the duty cycle of the index modulation can easily be taken into account, making this method ideally suited for modeling of gratings written with ultrafast laser pulses.

In this paper the spectral properties of type I-IR and type I UV-written gratings are compared and modeled using Rouard's method. Particular attention is paid to the spectral bandwidth, roll-off, and sideband structure of both grating types. Type I-IR grating properties are shown to be consistent with a narrower Gaussian index profile with a smaller contribution to the average index than would be the case for UV-written color-center gratings. These properties are related to the fact that the index change results from a nonlinear absorption process. The varying overlap of the index change with the core along the length of the grating also affects the grating length. At higher intensities, the spectral properties of type I-IR gratings indicate saturation in the grating growth rate. Limiting behavior and intensity clamping are common in highly nonlinear absorption processes and may be responsible for the observed saturation effect.[13]

2. ROUARD'S METHOD

The reflectivity for a series of three thin films shown in Fig. 1 can be determined with the Airy equation[10–12]:

$$\rho_2 = \frac{r_1 + r_2 \exp(-i\delta)}{1 + r_1 r_2 \exp(-i\delta)}. \qquad (1)$$

Here ρ_2 is a complex reflectivity, and r_1 and r_2 are the Fresnel reflection coefficients of the first and second interfaces. δ is the accumulated phase by a double pass through layer 2:

0740-3224/06/102011-7/$15.00

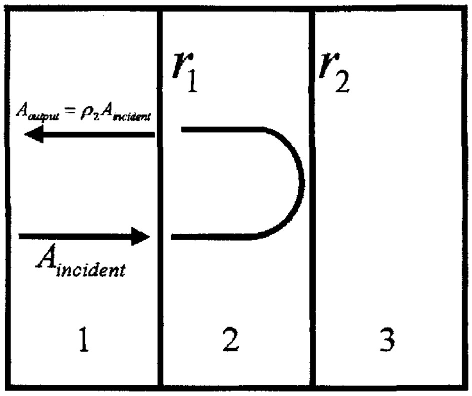

Fig. 1. Reflection from three planes. The incident amplitude A_{inc} undergoes reflections from the surfaces r_1 and r_2. These two reflections can be treated as one reflection with a complex reflectivity ρ_2.

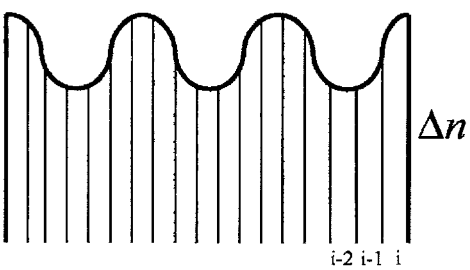

Fig. 2. Grating can be subdivided into a series of Fresnel reflections. The total complex reflectivity can be determined through an iterative process.

$$\delta = |\mathbf{k}|2d = \frac{4\pi n_2}{\lambda_o} d, \tag{2}$$

where n_2 is the index of refraction of layer 2, λ_o is the free-space wavelength, and d is the thickness of layer 2.

As shown in Fig. 2, a grating can be divided into a long series of i segments.

Starting at the extreme end of a series of thin films, one can determine the complex reflectivity for the last three segments:

$$\rho_{i-1} = \frac{r_{i-2} + r_{i-1}\exp(-i\delta)}{1 + r_{i-2}r_{i-1}\exp(-i\delta)}. \tag{3}$$

The reflectivity is then calculated for the layers $i-3$, $i-2$, and $i-1$ where the reflectivity between the $i-1$ and the $i-2$ segments is the complex reflectivity ρ_{i-1}. The index of refraction can be taken as the average within the segment. This iterative procedure can be carried out for the entire series of segments to determine the reflectivity for the entire grating.

Typically, for modeling UV-written gratings, each segment is one grating pitch. The complex reflectivity for each segment is determined through coupled-mode theory, and then the iterative procedure is used to determine the reflectivity for the entire grating.[10,11] For modeling type I-IR gratings, however, a more classical approach has been employed where the grating is further subdivided into a large series of thin-film reflections. This approach allows for modeling of essentially any arbitrary index profile. To correctly model the steep grating peaks, a section width of 50 nm was required to accurately model type I-IR gratings.

3. TYPE I-IR GRATINGS

Ultrafast fiber Bragg gratings are formed in SMF-28 fiber by one's focusing ultrafast laser pulses through a phase mask onto a fiber sample as shown in Fig. 3.

The diffracted phase-mask orders interfere behind the phase mask, and the interference pattern is imprinted onto the fiber core. The distance between the phase mask and fiber, d, can be varied. The gratings considered in this study are type I-IR gratings formed with a two-beam interference method that exploits the phase-mask-order walk-off effect to eliminate the zeroth and higher orders in the interference field impinging on the fiber.[8,14] The resulting interference field, owing to the interference of only the ±1 phase-mask orders, is a sinusoidal pattern with a periodicity half that of the phase mask and a Gaussian envelope. As shown in Fig. 4, the order walk-off effect causes both a reduction of the visibility of the interference fringes and a reduction in peak intensity at extended distances at a distance of $d=1.5$ mm from the phase mask. In Fig. 4 phase-mask pitch is 1.07 μm (corresponding to

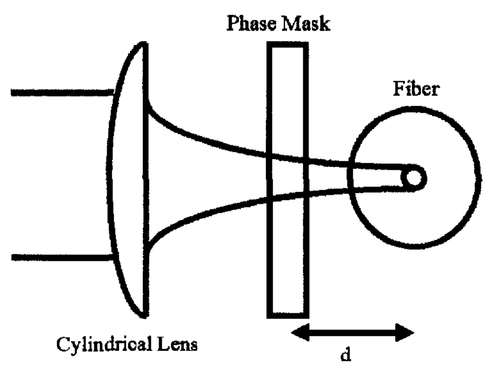

Fig. 3. Schematic of the focusing arrangement. A cylindrical lens focuses the ultrafast beam through a phase mask, and the distance between the fiber and phase mask, d, can be adjusted to reduce the number of interfering phase-mask orders.

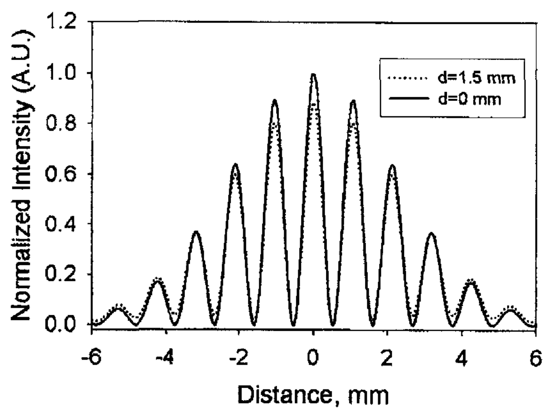

Fig. 4. Two-beam intensity patterns as a function of phase-mask fiber distance. The peak amplitude, the width of the interference region, and the edge visibility are all reduced as the phase-mask fiber separation, d, is increased. The grating pitch is exaggerated for clarity.

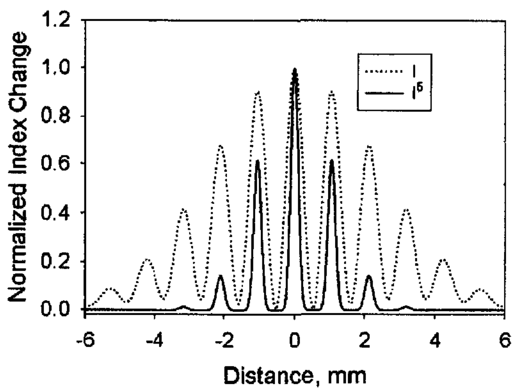

Fig. 5. Comparison between the linear (dotted curve) and the nonlinear (solid curve) index modulation profiles. If the index change in the medium depends nonlinearly on the interference field, then the grating effective length and the area under each peak become smaller. The grating pitches of the index modulation profile are exaggerated for clarity.

±1-order angles of ~48°), and the beam's $1/e$ intensity radius is 3.2 mm. The grating pitch is exaggerated in the figures.

Recently, it has been demonstrated that the growth rate of the index change during the fabrication of these gratings is not linear with the interference field intensity.[7] It was estimated that the index modulation scaled with intensity to the power of 5. Figure 5 compares an index modulation profile that depends linearly on the incident field intensity (dotted curve), as would be the case for standard UV-written gratings, and the profile that would be expected if the index change in the fiber depended on I^5 (solid curve). As shown, the nonlinear profile exhibits a reduced grating length and a narrower interference fringe peak. The reduced visibility due to order walk-off is no longer evident, but the index profile now deviates from a sinusoidal pattern. The reduced grating length results in a broader spectrum, and the narrower interference peak results in a reduced contribution of the grating to the average index.[7] Owing to the nonsinusoidal nature of the resulting pattern, higher-order components in the grating spectrum should be present and have been observed.[15] Rouard's method is attractive for modeling these gratings as the higher-order Bragg resonances are easily modeled by the calculation.

4. COMPARISON OF TYPE I-IR AND TYPE I UV-WRITTEN GRATINGS

Type I UV-written gratings fabricated using ~240 nm light in hydrogen-loaded SMF-28 fiber are known to result from a linear absorption mechanism.[2] The resulting index change profile scales linearly with the interference field. For comparison with type I-IR gratings, type I UV gratings were spot written in hydrogen-loaded SMF-28 with a frequency-doubled argon-ion laser and a 150 mm focal-length lens. The fiber was placed flush with the zero-order nulled, 1.07 μm pitch standard UV phase mask. The $1/e$ radius of the laser beam was measured using a knife-edge technique to be approximately 2.8±0.1 mm. Figure 6(a) shows the measured grating spectrum for a type I UV-written grating (dashed curve). Superposed with this spectrum is the modeled spectrum (solid curve) generated using a sinusoidal index modulation pattern with a Gaussian envelope set by the knife-edge measurement. The index change used in the simulation must be corrected for the confinement factor of the field in the core. The coupled-mode index change, assumed to be confined to the core, relates to the Rouard method refractive index through[12] $\Delta n_{\mathrm{Rouard}} = 0.73\Delta n_{\mathrm{core}}$. The peak index modulation of this grating was $\Delta n_{\mathrm{core}} = 1.05 \times 10^{-3}$. A commercial software package produced the same spectrum. Figure 6(b) displays the index profile that was used to model the grating. The grating pitch has been exaggerated for clarity. The $1/e$ spot radius that fits the data in the simulation was 2.6 mm. This value is slightly smaller than the knife-edge measurement. There are two important features that should be mentioned with regard to the spectrum. First, for a given transmission loss at the Bragg wavelength, the width of the spectral profile is governed by the width of the writing beam. Second, the strong sidebands on the short-wavelength side of the spectrum are a consequence of the contribution of the Gaussian beam profile to the effective index. The central portion of the grating tends to be redshifted compared with the wings owing to the larger average effective index near the Gaussian peak. The modulation on the short-wavelength side of the spectrum is a consequence of the effective Fabry–Perot set up by the wings of the grating, which are less redshifted than the center.

The same analysis can be applied to the type I-IR gratings. Type I-IR gratings were fabricated in SMF-28 fiber with a Ti:sapphire 125 fs 800 nm laser source without hydrogen loading. The ultrafast laser beam was focused

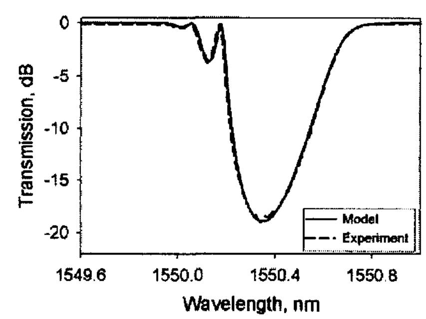

(a)

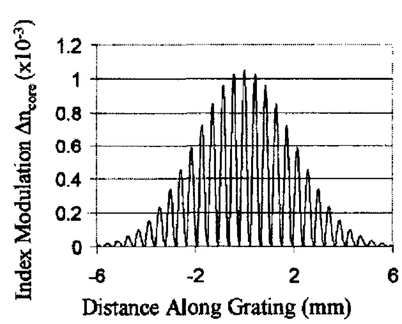

(b)

Fig. 6. Rouard's method used to model a UV-written grating. (a) A comparison between the experimental (dashed curve) and modeled (solid curve) curve for the UV-written grating. (b) The linear intensity profile that was used to model the grating response.

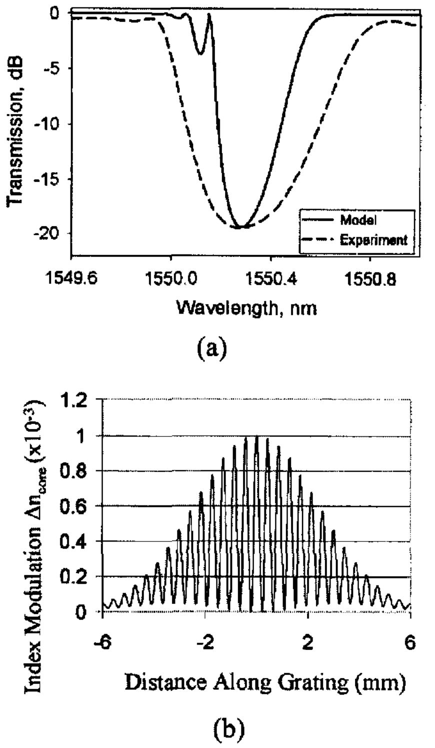

Fig. 7. (a) Comparison between the experimentally observed type I-IR grating spectrum (dashed curve) and the modeled grating spectrum, assuming that the index change in the fiber depends linearly on the interference field intensity (solid curve). (b) Index modulation profile used in the modeled spectrum.

with a 30 mm cylindrical lens through a 1.07 μm pitch phase mask optimized for 800 nm onto the fiber sample. The distance between the phase mask and fiber was kept at 1.5 mm to allow for the generation of a two-beam interference pattern. The focus was kept at the core of the fiber. The $1/e$ intensity radius was measured, with a knife-edge technique, to be 3.2±0.1 mm. The measured spectrum (dashed curve) obtained for a type I-IR grating written with 800 μJ pulses is shown in Fig. 7(a). The modeled spectrum (solid curve), assuming that the grating growth is linear, is shown also. The index modulation profile used in the modeled profile is shown in Fig. 7(b). The modeled index modulation to achieve a 20 dB transmission loss was $\Delta n_{\mathrm{core}} \sim 8 \times 10^{-4}$. Clearly, the measured spectrum differs from the modeled spectrum significantly.

The pulse energy can be directly related to the intensity through[7]

$$I = \frac{\text{pulse energy}(2)(\%\text{energy} \pm 1\text{orders})0.86}{\text{area(pulse duration)}}$$

$$= \frac{800\ \mu\mathrm{J}(2)(0.728)(0.86)}{3 \times 10^{-4}\ \mathrm{cm}^2(125\ \mathrm{fs})} = 2.7 \times 10^{13}\ \mathrm{W/cm}^2. \qquad (4)$$

Here the factor of 0.86 is the reduction in the peak intensity due to order walk-off, and 0.728 is the percentage of energy in the ±1 orders. This intensity is below the type I-IR–Type II-IR transition.[7]

In Figs. 8(a) and 8(b) the modeled index change has been assumed to scale nonlinearly with intensity to the power of 5, as had been previously observed.[7] Raising the intensity pattern to a higher power causes a reduction in resultant grating length of $\sim w/\sqrt{p}$, where w is the initial beam width and p is the order to which the profile is raised. In Fig. 8(b) this means that the actual $1/e$ grating diameter in the fiber will be ~2.8 mm. The modeled index modulation required to achieve a 20 dB transmission loss was $\Delta n_{\mathrm{core}} \sim 2 \times 10^{-3}$.

The comparison with the experimental spectrum is clearly improved. The bandwidth of the modeled grating is still slightly narrower than the experimental spectrum. The reduction of the sidebands on the short-wavelength side of the spectrum is evident. In the calculation of this spectrum, the previously observed fifth-order dependence of the index change on intensity has been strictly adhered to. It was suggested in a previous publication that the order of the effect could be as high as 6.[16] With a sixth-order effect the $1/e$ grating diameter would be ~2.6 mm. In Fig. 9 the index change has been assumed to scale with intensity to the power of 6. Clearly, the fit is much improved. The grating profile used to model the spectrum is shown in Fig. 9(b). The index modulation used to model the spectrum was $\Delta n_{\mathrm{core}} \sim 2 \times 10^{-3}$.

If an apodization profile is imposed, type I-IR gratings would exhibit apodization properties similar to those of UV-written gratings. The main difference, and the reason for the reduced sidebands above, is that the contribution to the average index change is diminished owing to the smaller duty cycle of type I-IR gratings.

5. GRATING SPECTRUM RESULTING FROM HIGH INPUT PULSE INTENSITIES

The spectrum for a grating written with a pulse energy of 1200 μJ is shown in Fig. 10(a) (solid curve). Also shown is

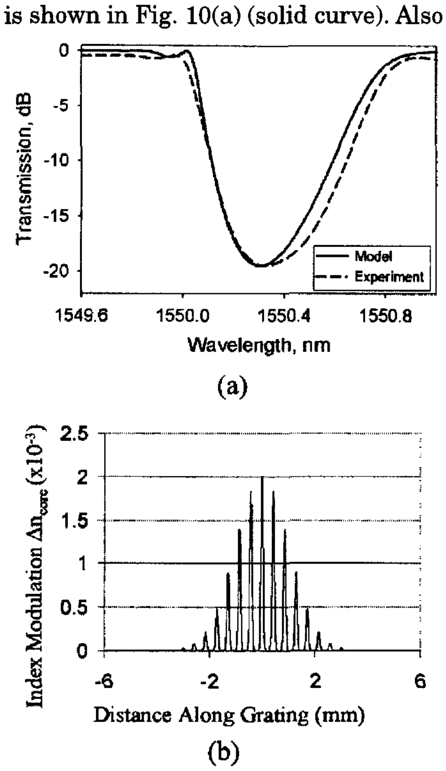

Fig. 8. (a) Comparison between the experimentally observed (dashed curve) and the modeled spectra, assuming that the index change scales with intensity to the power of 5 (solid curve). (b) The index modulation profile used to model the spectrum.

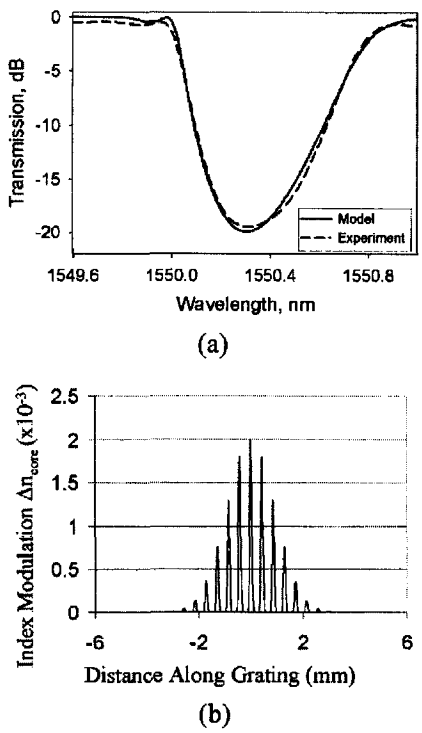

Fig. 9. (a) Comparison between the experimentally observed (dashed curve) and the modeled spectra, assuming that the index change scales with intensity to the power of 6 (solid curve). (b) The index modulation profile used to model the spectrum.

the modeled spectral profile for a grating that scales with intensity to the power of 6 (dashed curve). It is clear from this comparison that at higher pulse energies the grating profile deviates significantly from the I^6 scaling.

The grating profile that best models the 1200 μJ grating [Fig. 10(b)] was generated by normalizing the linear interference profile in Fig. 7(b) and substituting it into the empirical saturation function,

$$\Delta n_{\text{norm}} = \frac{I^6}{C + I^6}. \tag{5}$$

The constant in this case was set at 0.05. Equation (5) has the feature that it scales highly nonlinearly for low intensities and saturates abruptly. The index change in the material had not saturated (typically, $\Delta n_{\text{core}} \sim 5 \times 10^{-3}$); therefore the top-hat profile results from a saturation in the rate of index change in the material. The mechanism responsible for the production of these gratings must also have this feature. It was also beneficial to truncate the profile in Eq. (5) at $\Delta_{\text{norm}} = 0.4$. This was then normalized again [as shown on the left axis in Fig. 10(b)] and multiplied by Δn_{core} to set the transmission loss at the experimental value of 20 dB. The modeled spectrum for the 1200 μJ grating is displayed as the dashed–dotted curve in Fig. 10(a). As the modeled grating profile for the 1200 μJ grating has a larger effective length [as seen when comparing Figs. 9(b) and 10(b)], a smaller index change modulation is required to achieve a 20 dB loss than with the 800 μJ grating. An index modulation of $\Delta n_{\text{core}} \sim 1.2 \times 10^{-3}$ [shown on the right axis of Fig. 10(b)] was required to achieve a 20 dB loss at the Bragg wavelength for the 1200 μJ grating.

Not included in the nonlinear model, and perhaps the reason for the truncation, is any consideration of the impact of incomplete overlap of grating fringes with the guided core mode. It has been demonstrated that ultrafast gratings are not confined to the core region of the fiber but are present in both the core and the cladding layer.[3,14] In Fig. 11, optical microscope images of a grating formed with a 3.21 μm mask are presented that illustrate that the coverage of the core and surrounding cladding region in the center of the grating is greater than that toward the edges. The reflection from a grating plane is governed by both the magnitude of the index change and the overlap of the grating fringe with the core mode. Only index change that overlaps with the core mode will contribute to the observed grating spectrum. The overlap of the grating fringe with the core is also not considered in Rouard's method and will instead be interpreted as a variation in the magnitude of the index change.

Some combination of a saturationlike mechanism and the overlap of the index change with the core is responsible for the modeled profile in the right-hand side of Fig. 11. Intensity dependence in the grating spectrum is unique to ultrafast fiber Bragg gratings and has not been observed, to our knowledge, in UV-written gratings. Previously, it was reported that the effective grating length of type-I-IR gratings increases as a function of energy.[7] This observation is consistent with a saturable growth rate as the effective length of the resulting grating increases with input intensity. Side scan measurements were performed on the 800 and 1200 μJ gratings,[17] and the grating lengths were found to be consistent with the profiles in Figs. 9 and 10, respectively.

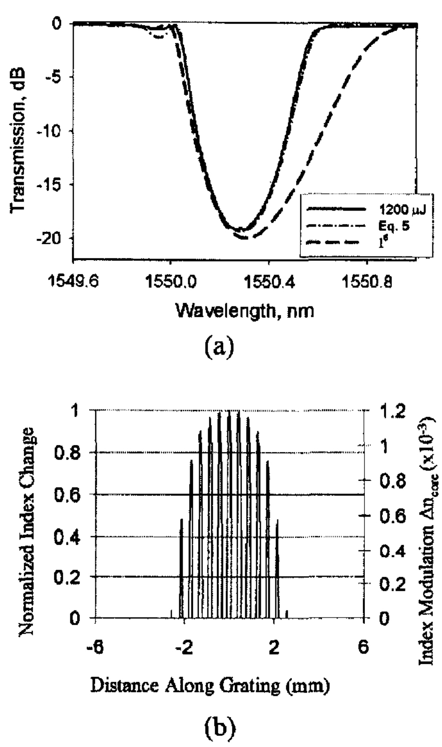

Fig. 10. (a) Comparison of the spectrum of a grating written with an input energy of 1200 μJ (solid curve) and the modeled spectrum for a grating that depends on I^6 (dashed curve) and one based on Eq. (5) (dashed–dotted curve). (b) The spectral profile that best fits the 1200 μJ data.

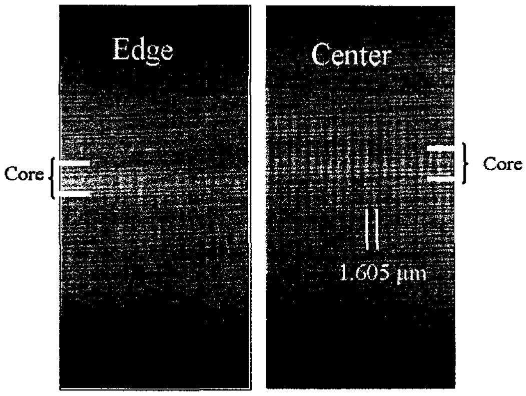

Fig. 11. Comparison of the coverage of the core at the edge of the grating structure to that at the center. The phase-mask pitch used here was 3.21 μm to allow for a visible two-beam interference pattern under an optical microscope.

6. DISCUSSION

Rouard's method provides the opportunity to model the observed grating spectra and, from the resulting grating profiles, suggests mechanisms responsible for their fabrication. The excellent agreement between the model results and the observed low-intensity spectra suggests that the nonlinear model explains most of the low-intensity behavior of ultrafast type I-IR gratings. At higher intensities the modeled profiles based on the observed spectra exhibit a significant deviation from the profiles observed at low intensities. The grating profile that agrees with the high-energy grating is consistent with a grating growth rate that saturates at high intensities.

A consideration of the peak field intensities may elucidate the possible mechanisms responsible for the saturationlike behavior. Equation (4) can be used to show that the 800 and 1200 μJ pulse energies are consistent with intensities of 2.7×10^{13} and 4×10^{13} W/cm^2, respectively. Fiber geometry is not taken into account. The type II-IR grating transition was observed to occur at approximately 1300 μJ or at an intensity of 4.3×10^{13} W/cm^2. These intensities are the same as those used to achieve similar index changes in previous studies[18] and are above or near the multiphoton ionization threshold (MPI) for dielectrics.[13]

Recently, limiting[13] and intensity clamping[19] effects have been observed during the irradiation of bulk media with ultrafast pulses. The saturation of type I-IR gratings near the type II-IR threshold is likely related as both effects would cause saturationlike behavior. This will be the subject of future research. Fiber Bragg gratings conceivably offer increased sensitivity with which to investigate index change in dielectrics at intensities near the MPI threshold.

7. CONCLUSION

The spectra of type I-IR gratings differ from the traditional UV-written type I gratings significantly. Rouard's method has been utilized to model the spectra and show that many of the observed differences can be related to the nonlinear dependence of the index change on intensity. In addition, type I-IR gratings demonstrate an intensity-dependent self-apodization effect not observed with type I UV-written gratings. The modeled index profiles that fit the type I-IR grating spectra indicate saturation in the index change growth rate at intensities approaching the type II-IR grating transition. It is possible that limiting behavior or intensity clamping could be responsible for this observation.

ACKNOWLEDGMENTS

C. W. Smelser thanks Ping Lu for several helpful discussions.

C. W. Smelser, the corresponding author, can be reached by phone, 1 613 998 2183; fax, 1 613 993 7139; or e-mail, christopher.smelser@crc.ca.

REFERENCES

1. T. Erdogan, "Fiber grating spectra," J. Lightwave Technol. **15**, 1277–1294 (1997).
2. R. Kashyap, *Fiber Bragg Gratings* (Academic, 1999).
3. S. J. Mihailov, C. W. Smelser, D. Grobnic, R. B. Walker, P. Lu, H. Ding, and J. Unruh, "Bragg gratings written in all-SiO_2 and Ge-doped core fibers with 800-nm femtosecond radiation and a phase mask," J. Lightwave Technol. **22**, 94–100 (2004).
4. S. J. Mihailov, C. W. Smelser, P. Lu, R. B. Walker, D. Grobnic, H. Ding, G. Henderson, and J. Unruh, "Fiber Bragg gratings made with a phase mask and 800-nm femtosecond radiation," Opt. Lett. **28**, 995–997 (2003).
5. A. Dragomir, D. N. Nikogosyan, K. A. Zagorulko, P. G. Kryukov, and E. M. Dianov, "Inscription of fiber Bragg gratings by ultraviolet femtosecond radiation," Opt. Lett. **28**, 2171–2173 (2003).
6. A. Martinez, M. Dubov, I. Khrushchev, and I. Bennion, "Direct writing of fibre Bragg gratings by femtosecond laser," Electron. Lett. **40**, 1170–1172 (2004).
7. C. W. Smelser, S. J. Mihailov, and D. Grobnic, "Formation of Type I-IR and Type II-IR gratings with an ultrafast IR laser and a phase mask," Opt. Express **13**, 5377–5386 (2005).
8. C. W. Smelser, D. Grobnic, and S. J. Mihailov, "Generation of pure two-beam interference grating structures in an optical fiber with a femtosecond infrared source and a phase mask," Opt. Lett. **29**, 1730–1732 (2004).
9. C. W. Smelser, S. J. Mihailov, D. Grobnic, P. Lu, R. B. Walker, H. Ding, and X. Dai, "Multiple-beam interference patterns in optical fiber generated with ultrafast pulses and a phase mask," Opt. Lett. **29**, 1458–1460 (2004).
10. L. A. Weller-Brophy and D. G. Hall, "Analysis of waveguide gratings: application of Rouard's method," J. Opt. Soc. Am. A **2**, 863–871 (1985).
11. L. A. Weller-Brophy and D. G. Hall, "Analysis of waveguide gratings: a comparison of the results of Rouard's method and coupled-mode theory," J. Opt. Soc. Am. A **4**, 60–65 (1987).
12. Z. Wang, G. Peng, and P. Chu, "Improved Rouard's method for fiber and waveguide gratings," Opt. Commun. **177**, 245–250 (2000).
13. D. M. Rayner, A. Naumov, and P. B. Corkum, "Ultrashort pulse non-linear optical absorption in transparent media," Opt. Express **13**, 3208–3217 (2005).
14. D. Grobnic, C. W. Smelser, S. J. Mihailov, R. B. Walker, and P. Lu, "Fiber Bragg gratings with suppressed cladding modes made in SMF-28 with a femtosecond IR laser and a phase Mask," IEEE Photon. Technol. Lett. **16**, 1864–1866 (2004).
15. D. Grobnic, S. J. Mihailov, and C. W. Smelser, "Higher

order spectral response characteristics of fiber Bragg gratings made with ultrafast IR radiation and a phase mask," in *Proceedings of Bragg Grating, Photosensitivity and Poling Topical Meeting* (BGPP/ACOFT, 2005), P43.

16. C. W. Smelser, S. J. Mihailov, and D. Grobnic, "Intensity dependence of the index modulation growth rate of type I-IR ultrafast fiber Bragg gratings," in *Proceedings of Bragg Grating, Photosensitivity and Poling Topical Meeting* (BGPP/ACOFT, 2005), W1445.
17. P. A. Krug, R. Stolte, and R. Ulrich, "Measurement of index modulation along an optical fiber Bragg grating," Opt. Lett. **20**, 1767–1769 (1995).
18. L. Sudrie, M. Franco, B. Prade, and A. Mysyrowicz, "Study of damage in fused silica induced by ultra-short IR laser pulses," Opt. Commun. **191**, 333–339 (2001).
19. W. Liu, S. Petit, A. Becker, N. Aközbek, C. M. Bowden, and S. L. Chin, "Intensity clamping of a femtosecond laser pulse in condensed matter," Opt. Commun. **202**, 189–197 (2002).

Article VIII

D. Grobnic, S. J. Mihailov, **C. W. Smelser**, H. Ding: "*Sapphire Fiber Bragg Grating Sensor Made Using Femtosecond Laser Radiation for Ultra High Temperature Applications*" Photonics Technology Letters **16** (11), p. 2505-2507 (2004).

Sapphire Fiber Bragg Grating Sensor Made Using Femtosecond Laser Radiation for Ultrahigh Temperature Applications

Dan Grobnic, Stephen J. Mihailov, *Member, IEEE*, Christopher W. Smelser, and Huimin Ding

***Abstract*—We report for the first time the inscription of retro-reflective Bragg gratings in multimode crystalline sapphire fiber. The gratings were fabricated using 800-nm femtosecond laser radiation and a phase mask. The grating behavior was investigated up to 1500 °C with no detectable reduction in the grating reflectivity or hysteresis in the Bragg resonance. Measurements of the change in the effective index of the fiber as a function of temperature are reported and the performance of the grating as a temperature sensor is evaluated.**

***Index Terms*—Fiber Bragg gratings (FBGs), fiber sensors, sapphire fiber, ultrafast optics.**

I. Introduction

FIBER Bragg grating (FBG) sensors are highly versatile, simple, intrinsic sensing elements. For sensing applications involving temperature and strain, variation in the spectral response of the grating can be directly correlated to strain and temperature on the grating structure [1]. The retro-reflective Bragg resonance or wavelength $\lambda_{\rm Bragg}$ of the FBG is dependent upon the periodicity of the grating within the fiber and the effective refractive index of the fiber. Typically, FBGs are generated by exposing the ultraviolet (UV)-photosensitive core of a germanium-doped silica core optical fiber to a spatially modulated UV laser beam in order to create permanent refractive index changes in the fiber core. A limitation of the UV-induced FBGs, especially for high-temperature sensor applications, is that operation of the sensor at elevated temperatures results in the erasure of the UV-induced index modulation of the grating. In fact, at temperatures approaching the glass transition temperature of the fiber, which for silica is approximately 1050 °C, total erasure of the induced index modulation results.

One approach to fiber-based measurements at high temperatures is to use sensor elements fabricated in sapphire fiber, which has a very high melting temperature (~2050 °C). Sapphire fiber-based sensors often employ Fabry–Pérot etalons fabricated on the fiber tip which generate broad-band interference fringe pattern that can be monitored as a function of temperature [2]. Although this type of device maybe effective as a point sensor, the sensor structure is often complex and the generated fringe pattern cannot be addressed in a multiplexed fashion. The sensor is, therefore, inappropriate for distributed sensor arrays. Unlike conventional silica-based optical fiber, sapphire fibers are only made in the form of rods that lack a cladding. With fiber diameters of 150 μm commercially available, beam propagation within the fiber is highly multimode at the 1550-nm telecommunication wavelengths and does not support single-mode propagation that is often needed for FBG sensors. Recently, long-period Bragg grating structures have been fabricated in sapphire fiber through a photolithographic process [3]. Grating responses for such structures are only observable in transmission.

Recently, high-quality FBG structures with high index modulation (Δn_m) were made in standard Ge-doped telecom fiber (SMF-28) and all-silica core single-mode fiber with a high-power femtosecond infrared source and a phase mask [4]. Since high induced index change principally relies upon multiphoton ionization, grating structures could be induced in many transparent materials, such as sapphire. Reflective FBG sensors in sapphire fiber would have definite advantages over Fabry–Pérot etalon-based sapphire fiber sensors as FBG sensors with their discrete resonant wavelength could be used potentially as distributed optical sensor arrays up to 2000 °C. The FBG sensors can also be used as probes to determine the behavior of the sapphire fiber itself in the same temperature range. In this letter, we report the fabrication, for the first time, of a retro-reflective FBG in multimode sapphire fiber. The device was tested up to 1500 °C and could potentially operate up to 2000 °C.

II. Experiment

High-order retro-reflective FBGs were fabricated near one end of 25-cm-long 150-μm diameter single crystal sapphire fibers supplied by Photran Inc. The fiber was grown along the crystallographic c axis (0, 0, 1) of the sapphire crystal. Multiple pulses from an 800-nm regeneratively amplified Ti : Sapphire laser were focused with a cylindrical lens of focal length $f = 19$ mm through a silica phase mask that was zeroth-order-nulled at 800 nm, with pitch $\Lambda = 4.284$ μm onto the fiber sample. The fiber was positioned near the beam focus, several millimeters behind the phase mask in order to produce pure two-beam interference [5]. No adverse dispersion effects from or optical damage to the phase mask were observed. The Fourier transform-limited pulse duration was 125 fs as measured with an autocorrelator. The 1/e Gaussian beam radius w_o was measured by the knife-edge technique to be 2.45 mm. In the Gaussian beam approximation, the radius of the focal spot size is $w \approx \lambda f/\pi w_o$, where λ is the wavelength resulting in a focal line width of ~4 μm and a length of 4.9 mm. The fiber was exposed to 500-μJ laser pulses at 100 Hz for 1 min. The resulting fluence within the fiber is above the threshold

Manuscript received June 7, 2004; revised June 30, 2004.

The authors are with the Communications Research Centre Canada, Ottawa, ON K2H 8S2 Canada (e-mail: stephen.mihailov@crc.ca).

Digital Object Identifier 10.1109/LPT.2004.834920

1041-1135/04$20.00 © 2004 IEEE

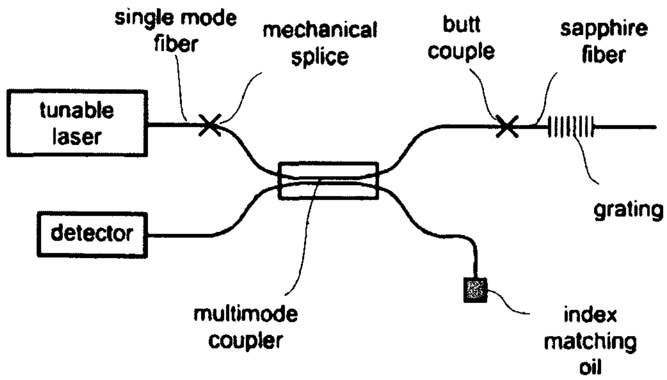

Fig. 1. Diagnostic setup for monitoring spectral response of the sapphire fiber grating.

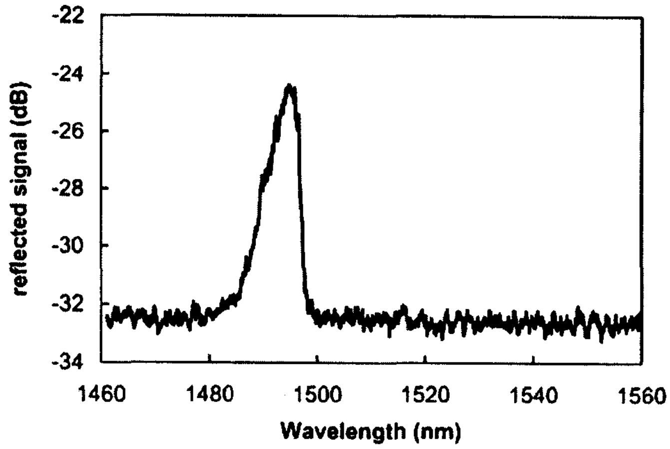

Fig. 2. Reflection spectrum of the sapphire FBG device at room temperature.

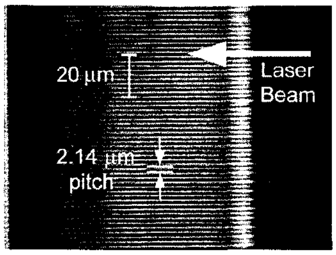

Fig. 3. Microscope images of the grating structure written in 150-μm diameter sapphire fiber with 125-fs 800-nm laser pulses with the 4.28-μm phase mask.

for multishot surface damage observed in sapphire [6]. Using a piezo-actuator, the beam was translated and scanned across the cross section of the fiber in a step-and-repeat fashion in order to widen the grating cross section across the fiber. In this way, a good overlap between the grating and supported propagating modes results.

After exposure, the sapphire fiber with grating was butt-coupled using a mechanical fiber alignment jig to a four-port coupler made of multimode silica core fiber of 100-μm core diameter and 125-μm cladding diameter, as shown in Fig. 1. The signal from an Agilent 81680A tunable laser (1460–1580-nm range), which was stepped with 20-pm increments, was launched through a single-mode fiber into the input port of the coupler and the detector at the output port collected the reflected signal from the grating. The end of the sapphire fiber that contained the Bragg grating was then inserted into a high-temperature ceramic microfurnace (NTT model CMH-7022). In order to position the Bragg grating within the microfurnace, a He–Ne laser was connected to the input port of the multimode coupler. The red light scattered by the Bragg grating was then used to position the grating accurately within the center of the furnace where the temperature distribution was at its maximum. The microfurnace temperature was monitored at its center using a platinum–rhodium thermocouple with a measurement range up 1700 °C. A gradient with a 20% decrease in the temperature from the center to edge of the 20-mm-long microfurnace was observed.

In addition to spectral measurements, fiber elongation was measured at various temperatures with the micromechanical actuators of the translation stages and a microscope.

III. Results and Discussion

The spectral response of the sapphire FBG in reflection at room temperature is presented in Fig. 2. The measured spectral profile looks very similar in shape to the reflection spectrum of UV-induced grating made in the Ge-doped silica multimode fiber [7], which is also consistent with the spectral response for lower order mode excitation [8]. A standard optical microscope without phase contrast was used to obtain an image of the sapphire fiber grating as presented in Fig. 3. The high image contrast is indicative of large induced index changes which in bulk Ge-doped glass can be as high as 0.035 [9]. The grating structure displays a 2.14-μm periodicity and covers roughly 60% of the fiber cross-sectional area. The periodicity in the fiber is half that of the mask and is a result of pure two-beam interference generated by the mask [5].

For higher order Bragg gratings, at λ_{Bragg}, the pitch of the grating structure in the fiber Λ_g is defined by

$$M\lambda_{\text{Bragg}} = 2n_{\text{eff}}\Lambda_g \tag{1}$$

where M is the order number and n_{eff} is the effective index of the fiber. λ_{Bragg}, which is taken to be at the long wavelength edge of the -3-dB bandwidth, is 1495.8 nm. With $\Lambda_g = 2.14$ μm, the grating is a fifth-order retro-reflecting grating with $n_{\text{eff}} = 1.746$. This value for n_{eff} is consistent with the ordinary refractive index of sapphire (electric field perpendicular to the c axis) quoted in the literature in the 1550-nm range [10].

The temperature of the microfurnace was varied between 22 °C and 1530 °C. The Bragg grating spectrum as well as the elongation of the fiber were measured after the fiber had stabilized at a given temperature for 1 h. From 22 °C to 1530 °C, the total fiber elongation was 320 ± 20 μm. The variation of λ_{Bragg} with temperature is denoted by the black squares in Fig. 4. There was no obvious reduction of the grating reflectivity with temperature, nor was any spectral variation or distortion of the reflected signal observed implying that launching conditions into the sapphire fiber were stable with temperature. There was no hysteresis in the Bragg resonance when the device was cycled back to room temperature three times. Any change to the mechanical strength of the grating after cycling was not evaluated. The wavelength thermal sensitivity of the sapphire

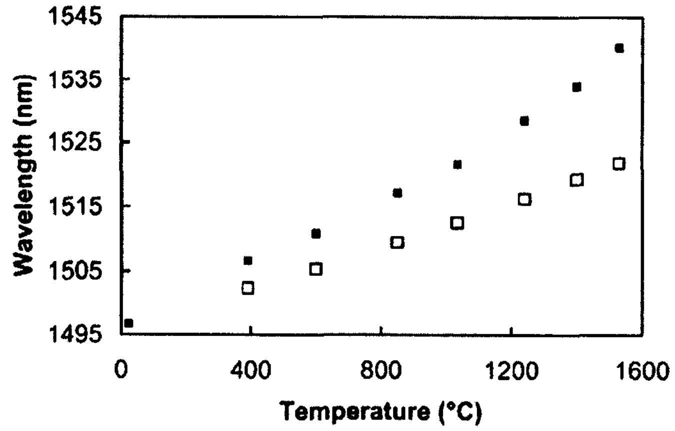

Fig. 4. Variation of Bragg resonance in sapphire fiber grating with temperature. Black squares are the measured λ_{Bragg} as a function of temperature while the white squares are the calculated λ_{Bragg} based on pitch variation resulting from fiber elongation.

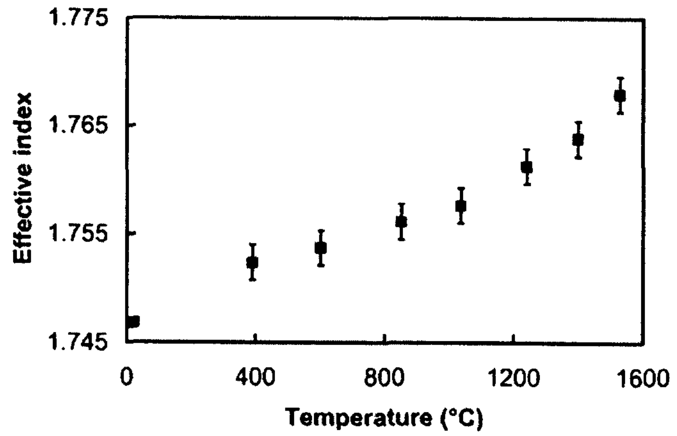

Fig. 5. Variation of effective index of the sapphire fiber grating with temperature. Error bars reflect propagation of measurement errors of the elongation length.

grating was evaluated to be ~25 pm/°C up to 1200 °C with the tendency to increase at higher temperatures.

The characteristic wavelength λ_{Bragg} of the FBG is dependent upon both Λ_g of the grating and n_{eff} of the fiber. Utilizing the Bragg grating, changes to the n_{eff} of the sapphire fiber with temperature could be investigated. By taking into consideration the expansion of the heated fiber, the increase in Λ_g due to fiber elongation could be estimated. For the calculation of Λ_g variation with temperature, we have taken into account the temperature distribution of the microfurnace. Using the n_{eff} measured at room temperature and (1), the variation in λ_{Bragg} resulting only from the grating elongation is denoted by white squares in Fig. 4. Alone, the elongation of the grating pitch could not account for the increase in λ_{Bragg} with temperature. With the grating elongation and the measured λ_{Bragg} incorporated into (1), the increase in the n_{eff} of the fiber with temperature is presented in Fig. 5 and was evaluated to be $\sim 1.1 \times 10^{-5}$/°C up to 1200 °C.

IV. Conclusion

Using femtosecond laser radiation and a phase mask, retro-reflective FBGs have been successfully fabricated in sapphire fiber for the first time. The variation with temperature of the Bragg resonant wavelength was evaluated up to 1500 °C with no observed degradation of the grating strength at high temperature. By using the spectral response and measured expansion of the fiber, the variation in effective index of the fiber with temperature was estimated. Such gratings would be suitable for distributed optical sensor arrays up to 2000 °C.

References

[1] A. D. Kersey, M. A. Davis, H. J. Patrick, M. LeBlanc, K. P. Koo, C. G. Askins, M. A. Putnam, and E. J. Friebele, "Fiber grating sensors," *J. Lightwave Technol.*, vol. 15, pp. 1442–1463, Aug. 1997.

[2] A. Wang, S. Gollapudi, R. G. May, K. A. Murphy, and R. O. Claus, "Sapphire optical fiber-based interferometer for high temperature environmental applications," *Smart Mat. Struct.*, vol. 4, no. 2, pp. 147–151, June 1995.

[3] S. Yin, S.-H. Nam, J. Chavez, Z. Chun, and C. Luo, "Innovative long period gratings: Principles and applications," *Proc. SPIE*, vol. 5206, pp. 30–44, Oct. 2003.

[4] S. J. Mihailov, C. W. Smelser, D. Grobnic, R. B. Walker, P. Lu, H. Ding, and J. Unruh, "Bragg gratings written in all-SiO_2 and Ge-doped core fibers with 800-nm femtosecond radiation and a phase mask," *J. Lightwave Technol.*, vol. 22, pp. 94–100, Jan. 2004.

[5] C. W. Smelser, S. J. Mihailov, D. Grobnic, P. Lu, R. B. Walker, H. Ding, and X. Dai, "Multiple beam interference patterns in optical fiber generated with ultrafast pulses and a phase mask," *Opt. Lett.*, vol. 29, no. 13, pp. 1458–1460, July 2004.

[6] D. Ashkenasi, R. Stoian, and A. Rosenfeld, "Single and multiple ultrashort laser pulse ablation threshold of Al_2O_3 (corundum) at different etch phases," *Appl Surf. Sci.*, vol. 154–155, pp. 40–46, Feb. 2000.

[7] W. Zhao and R. O. Claus, "Optical fiber grating sensors in multimode fibers," *Smart Mater. Struct.*, vol. 9, no. 2, pp. 212–214, Apr. 2000.

[8] T. Mizunami, T. V. Djambova, T. Niiho, and S. Gupta, "Bragg gratings in multimode and few-mode optical fibers," *J. Lightwave Technol.*, vol. 18, pp. 230–235, Feb. 2000.

[9] D. Homoelle, S. Wielandy, A. L. Gaeta, N. F. Borrelli, and C. Smith, "Infrared photosensitivity in silica glasses exposed to femtosecond laser pulses," *Opt. Lett.*, vol. 24, no. 18, pp. 1311–1313, Sept. 1999.

[10] F. Gervais, "Aluminum Oxide (Al_2O_3)," in *Handbook of Optical Constants of Solids*, E. D. Palik, Ed. San Diego, CA: Academic, 1991, vol. 2, pp. 761–775.

Chapter 3: Conclusion and future Research

This thesis represents the first studies of phase mask assisted fabrication of fiber Bragg gratings with an ultrafast laser source. The research has covered three important areas of grating design. First, the behavior of the material itself has been studied and different grating types have been identified. It has also been shown that various other materials, outside of Ge-doped silica, can be modified with ultrafast radiation. Second, the interaction of an ultrafast pulse with a phase mask has been investigated. These studies have greatly improved the achievable spectral quality of ultrafast gratings through the use of pure two-beam interference resulting from order walk-off. Finally, an attempt has been made to model the gratings and develop accurate models for ultrafast grating spectra. Future research in ultrafast fiber Bragg gratings will likely focus on these three areas.

I. Dielectric Materials

It will be critical to continue to understand the interaction of intense radiation with not only Ge-doped silica, which has found application in the telecommunications industry, but other materials as well.

Sapphire possesses very high temperature stability (as high as 2000 °C) which makes this material attractive for high temperature sensor applications. As demonstrated in this thesis, ultrafast gratings have been formed in multi-mode sapphire fiber [64]. The grating has been shown to be stable to temperatures of at least 1500 °C. Typically, sapphire temperature sensors employ a Fabry-Perot cavity design [69,70]. Bragg gratings offer an advantage as they can be used to make a distributed sensor. There are some complications that arise from the sapphire fiber itself. It is currently not possible to produce single mode sapphire crystal fiber. This means that the grating sensor spectral response is very broad with a - 3 dB bandwidth of ~20nm. The broad spectral profile of the grating complicates the temperature dependent wavelength measurement. It would be preferable to develop a sensor with a single mode response [71]. This would either require the fabrication of a single mode sapphire fiber or possibly increasing the input beam size to couple only one mode to the multi-mode sapphire fiber.

Photonic crystal fibers (PCF) are used in switching, index of refraction measurements, high power light transmission amongst other applications [72-74]. The standard index guided PCF is typically composed of a hole filled cladding layer and a pure silica core. As there is often no Ge-doping, fabrication of photonic components such as a Bragg grating with an UV source is not possible. Ultrafast lasers, as they have been shown to modify pure silica core fiber should be able to inscribe fiber Bragg gratings in these fibers [48]. The major complication that arises with the fabrication of fiber Bragg gratings in PCF is that the cladding layer scatters the incident beam. As the interaction of the material with the incident intensity field is so highly nonlinear even a small amount of scattering reduces that interference field intensity enough to reduce the induced index change significantly. The use of different fiber geometries, which contain few scattering holes or tapering of the fiber has shown promise [67].

Other materials of interests are Lithium Niobate [65], for use in nonlinear frequency generation and switching, and Fluoride [68] fiber as a gain medium in fiber laser applications. Fiber gratings have been written directly into Er-doped fiber for fiber laser applications. Ultrafast lasers have the advantage in that they can directly modify the gain media and eliminate undesirable splice losses [75,76].

Ultrafast modification of dielectric materials is a field that is in its relative infancy. In addition to engineering reliable photonic devices, the physical processes involved in the material modification are not well understood. With the advent of more powerful solid-state Ti:sapphire laser sources it will be possible to produce very energetic ultrafast pulses with a wide range of wavelengths. As laser technology advances so, hopefully, will our ability to modify a wide range of materials.

II. Phase Mask-Pulse interaction

Turning to the interaction of the phase mask with the incident laser pulse, it is important to note that the theory is not complete as the transverse profile of the incident beam has not yet been taken into consideration. If the transverse profile is not considered the calculated peak intensity is likely not correct due to angular dispersion, which has not been considered in the plane wave model. Precise knowledge of the incident beam profile may also be critical for successfully tailoring the grating profile, such as with apodisation, to achieve a desired spectrum.

III. Fiber Bragg grating simulation

In addition to a better understanding of the interference pattern produced by the ultrafast pulse it will be necessary to develop a theory that correctly predicts the spectral profile of a grating. It is still unclear what role absorption in the cladding layer of the material plays in the interference profile impinging on the core region. It is possible that a model that includes cladding layer absorption would explain some of the small discrepancies between theory and experiment at low energies and the saturation-like behavior when gratings are fabricated with high pulse energies. It is also well known that ultrafast gratings possess higher order resonances. It is important to understand the implications of the nonsinusoidal nature of ultrafast gratings on grating simulation and grating fabrication.

References

[1] K.O.Hill, Y. Fujii, D.C.Johnson, and B. S. Kawasaki, “Photosensitiviy in optical fiber waveguides: Application to reflection filter fabrication”, Appl. Phys. Lett., **32**, 647-649 (1978)

[2] B. S. Kawasaki, K.O. Hill, D. C. Johnson, and Y. Fujii, “Narrow-band Bragg reflectors in optical fibers”, Opt. Lett, **3**, 66-68 (1978)

[3] D. K. W. Lam and B. K. Garside, “Characterization of single-mode optical fiber filters”, Applied Optics, **20**, 440-445 (1981)

[4] G. Meltz, W. W. Morey, and W. H. Glenn, “Formation of Bragg gratings in optical fibers by a transverse holographic method”, Opt. Lett. , **14**, 823-825 (1989)

[5] K. O. Hill, B. Malo, F. Bilodeau, D. C. Johnson, J. Albert, “Bragg gratings fabricated in monomode photosensitive optical fiber by UV exposure through a phase mask”, Appl. Phys. Lett., **62**, 1035-1037 (1993)

[6] H. Hosono et al. “Nature and origin of the 5-eV band in SiO_2:GeO_2 glasses”, Phys. Rev. B, **46**, 11445-11451 (1992)

[7] T. E. Tsai et al. “Structural origin of the 5.16 eV optical absorption band in silica and Ge-doped silica”, Appl. Phys. Lett., **64**, 1481-1483 (1994)

[8] J. D. Jackson, *Classical Electrodynamics* (Wiley, New York, 1975)

[9] T.E. Tsai, D.L. Griscom, E. J. Friebele, and J. W. Fleming, “Radiation induced defect centers in high-purity GeO_2 glass” J. Appl. Phys., **62**, 2264-2268 (1987)

[10] E. J. Friebele, D. L. Griscom, and G. H. Sigel Jr., “Defect centers in germanium-doped silica-core optical fiber”, J. Applied Phys., **45**, 3424-3428 (1974)

[11] M. Essid, J.L. Bebner, J. Albert, K. Awazu, “Difference in behavior of oxygen defects in Ge-doped silica optical fiber preforms under ArF and KrF excimer laser irradiation”, J. Appl. Phys., **84**, 4193-4197 (1998)

[12] J. Nishii, “Permanent index changes in Ge-SiO_2 glasses by excimer laser irradiation”, Materials Science and Technology, **B54**, 1-10 (1998)

[13] M. Gallagher and U. Österberg, “Time resolved 3.1 eV luminescence in germanium-doped silica glass”, Appl. Phys. Lett, **63** , 2987-2989 (1993)

[14] R. M. Atkins, V. Mizrahi, and T. Erdogan, "248 nm induced vacuum UV spectral changes in optical fiber preform cores: support for a colour centre model of photosensitivity", Elec. Lett., **29**, 385-387 (1993)

[15] J. Albert, M. Fokine, and W. Margulis, "Grating formation in pure silica-core fibers", Opt. Lett., **27**, 809-811 (2002)

[16] P. J. Lemaire, R. M. Atkins, V. Mizrahi, and W.A. Reed, "High pressure H_2 loading as a technique for achieving ultrahigh UV photosensitivity and thermal sensitivity in GeO_2 doped optical fiber", Elec. Lett., **29**, 1191-1193 (1993)

[17] F. Bilodeau et al., "Photosensitization of optical fiber and silica-on-solicon/silica waveguides", Opt. Lett., **18**, 953-955 (1993)

[18] V. Grubsky, D. S. Starodubov, and J. Feinberg, "Photochemical reaction of hydrogen with gemanosiliate glass initiated by 3.4-5.4-eV ultraviolet light", Opt. Lett., **24**, 729-731 (1999)

[19] J. Albert et al.,"Photosensitivity in Ge-doped silica optical waveguides and fibers with 193-nm light from an ArF excimer laser", Opt. Lett., **19**, 387-389 (1994)

[20] B. Poumellec, P. Niay, M. Douay, and J. F. Bayon, "The UV-induced refractive index grating in Ge:SiO_2 preforms: additional CW experiments and the macroscopic origin of the change in index", J. Phys. D, **29**, 1842-1856 (1996)

[21] A. I. Gusarov, D. B. Doyle, "Contribution of photoinduced densification to refractive-index modulation in Bragg gratings written in Ge-doped silica fibers", Opt. Lett., **25**, 872-874 (2000)

[22] C. W. Smelser, Stephen. J. Mihailov, and Dan Grobnic, "Formation of Type I-IR and Type II-IR gratings with an ultrafast IR laser and a phase mask", Optics Express 13 (14), p.5377-5386 (2005)

[23] J.L. Archambault, L. Reekie, and P. St. J. Russell, "100% reflectivity Bragg reflectors produced in optical fibres by single excimer laser pulses", Elec. Lett., **29**, 453-455 (1993)

[24] B. Malo, J. Albert, D. C. Johnson, F. Bilodeau, K. O. Hill, "Elimination of photoinduced absorption in Ge-doped silica fibres by annealing of ultraviolet colour centres", Elec. Lett., **28**, 1598-1599 (1992)

[25] F. Piao, W. G. Oldham, E. E. Haller, "Ultraviolet-induced densification of fused silica", J. Appl. Phys., **87**, 3287-3293 (2000)

[26] T. Erdogan, and V. Mizrahi, "Characterization of UV-induced birefringence in photosensitive Ge-doped silica optical fibers", JOSA B, **11**, 2100-2105 (1994)

[27] R. W. Boyd, "Nonlinear Optics" (Academic Press, New York, 1992)

[28] D. Strickland, and G. Mourou, "Compression of amplified chirped optical pulses", Opt. Commun., **56**, 219-221 (1985)

[29] O.E. Martinez, J.P. Gordon, and R. L. Fork, "Negative group-velocity dispersion using refraction", J. Opt. Soc. Am. A., **1**, 1003 (1984)

[30] O. E. Martinez, "Grating and prism compressors in the case of finite beam size", J. Opt. Soc. Am. B, **3**, 929 (1986)

[31] D. Du, X. Liu, G. Korn, J. Squier, and G. Mourou, "Laser-induced breakdown by impact ionization in SiO_2 with pulse widths from 7 ns to 150 fs", Appl. Phys. Lett., **64**, 3701-3703 (1994)

[32] B. C. Stuart, M. D. Feit, A. M. Rubenchik, B. W. Shore, and M. D. Perry, "Laser-Induced Damage in dielectrics with Nanosecond to Subpicosecond Pulses", Phys. Rev. Lett., **74**, 2248-2250 (1995)

[33] K. M. Davis, K. Miura, N. Sugimoto, and K. Hirao, "Writing waveguides in glass with a femtosecond laser," Opt. Lett. **21**, 1729-1731 (1996)

[34] S. Nolte, M. Will, J. Burghoff, A. Tuennermann, "Femtosecond waveguide writing: a new avenue to three-dimensional integrated optics", Appl. Phys. A, **77**, 109-111 (2003)

[35] M. Lenzner, J. Krüger, S. Sartania, Z. Cheng, Ch. Spielman, G. Mourou, W. Kautek, and F. Krausz, "Femtosecond optical breakdown in dielectrics", Phys. Rev. Lett, **80**, 4076-4079 (1998)

[36] Junji Nishii, Naoyuki Kitamura, Hiroshi Yamanaka, Hideo Hosono, Hiroshi Kawazoe, "Ultraviolet-raditation-induced chemical reactions through one- and two-photon absorption processes in GeO2-SiO2 glasses", Opt. Lett., **20**, 1184-1186 (1995)

[37] B. Malo, J. Albert, K.O. Hill, F. Bilodeau, D.C. Johnson, and S. Theriault., "Enhanced photosensitivity in lightly doped standard telecommunications fiber exposed to high fluence ArF excimer laser light", Electronic Letters, **31**, pp. 879-880 (1995)

[38] X. Lu, D. Du, G. Mourou, "Laser Ablation and Micromachining with Ultrashort Laser Pulses", J. Quant. Elec., **33**, no. 10, 1706-1716 (1997)

[39] C. Hnatovsky, R. S. Taylor, P. P. Rajeev, E. Simova, V. R. Bhardwaj, D. M. Rayner and P. B. Corkum, "Pulse duration dependence of femtosecond-laser-fabricated nanogratings in fused silica" Appl. Phys. Lett. **87**, 014104 (2005)

[40] D. M. Rayner, A. Naumov and P.B. Corkum, ""Ultrashort pulse non-linear optical absorption in transparent media," Opt. Express **13**, 3208-3217 (2005)

[41] W. J. Reichman, D. M. Krol, C. W. Smelser and S. J. Mihailov, "Fluorescence spectroscopy of fiber gratings written with an ultrafast infrared laser and a phase mask" presented at CLEO 2005 May 23-26, 2005 Baltimore, Maryland, USA, paper CTuAA3.

[42] E. Hecht. *Optics*, (Addison-Wesley, New York, 1998)

[43] P. E. Dyer, R. J. Farley, and R. Giedl, "Analysis of grating formation with excimer-laser irradiated phase masks", Opt. Commun. **115**, 327 (1995).

[44] S. Kawata, I. Hikima, Y. Ichihara, and S. Watanabe, "Spatial Coherence of KrF excimer Lasers", Applied Optics, **31**, no.3, 387-396.

[45] K. Kawamura, T. Ogawa, N. Sarukura, M. Hirano, and H. Hosono, "Fabrication of surface relief gratings on transparent dielectric materials by two-beam holographic method using infrared femtosecond laser pulses," Appl. Phys. B, **71**, 119 - 121 (2000).

[46] C.W. Smelser, D. Grobnic, S. J. Mihailov: "Generation of Pure Two beam Interference Grating Structures in an Optical Fiber With a Femtosecond IR Source and a Phase Mask" Optics Letters 29 (15), p.1730-1732 (2004).

[47] D. Grobnic, C. W. Smelser, S. J. Mihailov, R. B. Walker and P. Lu: "Fiber Bragg Gratings with Suppressed Cladding Modes Made in SMF-28 with a Femtosecond IR Laser and a Phase Mask" Photonics Technology Letters 16 (8), p. 1864-1866 (2004).

[48] S.J. Mihailov, C. W. Smelser, D. Grobnic, R. B. Walker, P. Lu, H. Ding and J. Unruh: "Bragg Gratings Written in All-SiO_2 and Ge-doped Core Fibers with 800 nm Femtosecond Radiation and a Phase Mask "Journal of Lightwave Technology 22 (1), p. 94-100 (2004)

[49] C.W. Smelser, S. J. Mihailov, D. Grobnic, P. Lu, R. B. Walker, H. Ding and X. Dai: "Multiple Beam Interference Patterns in Optical Fiber Generated with Ultrafast Pulses and a Phase Mask" Optics Letters 29 (13), p.1458-1460 (2004).

[50] R. Kashyap, *Fiber Bragg Gratings* (Academic, New York, 1999)

[51] D. Marcuse, Theory of Dielectric Optical Waveguides (Academic, New York, 1974)

[52] T. Erdogan, "Fiber Grating Spectra" J. Lightwave Tech. **15**, 1277-1294 (1997)

[53] K. O. Hill, "Aperiodic distributed-parameter waveguides for integrated optics", Appl. Opt. **13**, 1853-1856 (1974)

[54] M. Yamada and K. Sakuda, "Analysis of almost-periodic distributed feedback slab waveguides via a fundamental matrix approach," Appl. Opt., **26**, 3474-3478 (1987)

[55] R. Zengerle and O. Leminger, "Phase-shifted Bragg gratings filters with improved transmission characteristics," J. Lightwave Tech., **13**, 2354 (1995)

[56] L. A. Weller-Brophy and D. G. Hall, "Analysis of waveguide gratings: application of Rouard's method," J. Opt. Soc. Am. A **2,** 863-871 (1985)

[57] L. A. Weller-Brophy and D. G. Hall, "Analysis of waveguide gratings: a comparison of the results of Rouard's method and coupled-mode theory," J. Opt. Soc. Am. A **4**, 60-65 (1987)

[58] Z. Wang, G. Peng, and P. Chu, "Improved Rouard's method for fiber and wavequide gratings," Opt. Commun. **177**, 245-250 (2000)

[59] C. W. Smelser, S. J. Mihailov, and D. Grobnic, "Rouard's method modeling of type I-IR fiber Bragg gratings made using an ultrafast IR laser and a phase mask," J. Opt. Soc. Am. B **23**, 2011-2017 (2006)

[60] G. A. Miller, C. G. Askins, and E. J. Friebele, "Modified F-Matrix Calculation of Bragg Grating Spectra and Its Use With a Novel Nonlinear Index Growth Law," J. Lightwave Tech., **24** , 2416-2427 (2006).

[61] W. X. Xie, M. Douay, P. Bernage, P. Niay, J. F. Bayon, and T. Georges, "Second order diffraction efficiency of Bragg gratings written within germanosilicate fibres," Opt. Comm., **101**, 85-91, (1993)

[62] D. Grobnic, S. J. Mihailov, C. W. Smelser, "Higher order spectral response characteristics of fiber Bragg gratings made with ultrafast IR radiation and a phase mask," *Proceedings of Bragg Grating, Photosensitivity and Poling Topical Meeting* (Sydney Australia, 2005), P43.

[63] L. Dong, G. Qi, M. Marro, V. Bhatia, L. L. Hepbrunt, M. Swan, A. Collier, and D. Weidman, "Suppression of cladding mode coupling loss in fiber Bragg gratings", J. Lightwave Tech. **18**, 1583 (2000)

[64] D. Grobnic, S. J. Mihailov, C. W. Smelser, H. Ding: "Sapphire Fiber Bragg Grating Sensor Made Using Femtosecond Laser Radiation for Ultra High Temperature Applications" Photonics Technology Letters 16 (11), p. 2505-2507 (2004).

[65] D. Grobnic, S. J. Mihailov, C. W. Smelser, F. Généreux, G. Baldenberger and R. Vallée "Bragg Gratings made in Reverse Proton Exchange Lithium Niobate Waveguides with a Femtosecond IR Laser and a Phase Mask" Phot. Tech. Lett.**17** ,1453-1455 (2005)

[66] D. Grobnic, S.J. Mihailov, C.W. Smelser, M. Becker and M.W. Rothhardt, "Femtosecond laser fabrication of Bragg Gratings in Borosilicate Ion-Exchange Waveguides" accepted for publication in Photonics Technology Letters (2006)

[67] S. J. Mihailov, D. Grobnic, H. Ding, C. W. Smelser, and J. Broeng, "Femtosecond IR Laser Fabrication of Bragg Gratings in Photonic Crystal Fibers and Tapers," Photon. Tech. Lett., **18**, 1837-1839 (2006).

[68] Dan Grobnic, Stephen J. Mihailov and Christopher W. Smelser, "Femtosecond IR inscription of Bragg gratings in Single- and Multi-mode Fluoride Fibers", Photon. Tec. Lett., **18**, 2686-2688 (2006)

[69] A. Wang, S. Gollapudi, R. G. May, K.A. Murphy, and R. O. Claus, "Sapphire optical fiber-based interferometer for high temperature environmental applications", Smart Materials and Structures, **4**, 147-151 (1995)

[70] H. Xiao, J. Deng, G. Pickrell, R. G. May and A. Wang, "Single-crystal sapphire fiber-based strain sensor for higher-temperature applications", J. Lightwave Tech., **22**, 94-100 (2003)

[71] D Grobnic, S J Mihailov, H Ding, F Bilodeau and C W Smelser, "Single and low order mode interrogation of a multimode sapphire fibre Bragg grating sensor with tapered fibres" Measurement Science and Technology 17 (5), p. 980-984 (2006)

[72] C. Kerbage, P. Steinvurzel, P. Reyes, P. S. Westbrook, R. S. Windeler, A. Hale, and B. J. Eggleton, "Highly tunable birefringent microstructured optical fiber ," Opt. Lett. **27**, 842-844 (2002)

[73] B. Eggleton, C. Kerbage, P. Westbrook, R. Windeler, and A. Hale, "Microstructured optical fiber devices," Opt. Express **9**, 698-713 (2001)

[74] P. St.J. Russell, "Photonic crystal fibers," Science 299, 358-362 (2003).

[75] Y. Lai, A. Martinez, I. Khrushchev, and I. Bennion, "Distributed Bragg reflector fiber laser fabricated by femtosecond laser inscription," Opt. Lett. **31**, 1672-1674 (2006)

[76] E. Wikszak, J. Thomas, J. Burghoff, B. Ortaç, J. Limpert, S. Nolte, U. Fuchs, and A. Tünnermann, "Erbium fiber laser based on intracore femtosecond-written fiber Bragg grating," Opt. Lett. **31**, 2390-2392 (2006)